# A CONSECUTIVE REACTION MODEL AND KINETICS OF $Cr_2O_3$ REDUCTION FROM SLAG BY CARBON DISSOLVED IN MOLTEN IRON

BY

STEPHEN SIMUKANGA, B.Min.Sc., M.Min.Sc.

THESIS SUBMITTED TO THE DEPARTMENT OF METALLURGY, UNIVERSITY OF STRATHCLYDE, IN ACCORDANCE WITH THE REGULATIONS GOVERNING THE AWARD OF THE DEGREE OF DOCTOR OF PHILOSOPHY



SEPTEMBER, 1990

## DEDICATION

This Thesis is dedicated to my wife, Agnes, and our two sons, Suwilanji and Chindikanji, for their love and tolerance

**ACKNOWLEDGEMENTS**

I wish to express my sincere gratitude to my supervisor, Dr. R.J. Pomfret for his guidance, interest and constructive criticism throughout the period of this study.

Thanks are due to the technical staff for their assistance with apparatus and materials. My sincere gratitude goes to Dr. A. Sutherland of the Department of Statistics for his assistance with construction of some of the computer programs. Special thanks are due to Mr. Leslie Thomson of Public Health Engineering for provision of an atomic absorption spectrophotometer.

My profound love and appreciation go to all members of my family, especially my parents for their encouragement and support.

Finally, I wish to extend my gratitude to The British Council and to my employers, The University of Zambia, for financial support.

## ABSTRACT

A first-order, consecutive, two-stage reaction model for the reduction of $Cr_2O_3$ from slag was developed. The model was applied to the results obtained by studying the effect of various parameters on the rate of reduction of $Cr_2O_3$ from a $CaO-SiO_2-Al_2O_3$ slag, by carbon dissolved in molten iron, at temperatures 1400-1550$^oC$. The parameters studied were: varying the furnace atmosphere; $Cr_2O_3$ concentration in slag; metal chromium content; the experimental temperature; slag and metal volume; the presence of the surface-active elements, S or Se and adding FeO and $CaF_2$ to the slag. The progress of the reactions was monitored by taking slag samples at predetermined time intervals, and analysing them for the relevant species.

The results showed that the reduction of $Cr_2O_3$ from slag takes place primarily at the slag/metal interface, and follows a first-order, consecutive, reversible, two-stage reaction scheme in which $(Cr^{2+})$ is the intermediary product. The rate of $(Cr^{3+})$ reduction remained the same in an argon or carbon monoxide atmosphere whilst an argon atmosphere increased the rate of $(Cr^{2+})$ reduction by a factor of about 1.4, compared to a carbon monoxide atmosphere. The rate of reduction of the chromium species increased with increase in temperature and

activation energies obtained were 54.16, 27.15 and 81.33 kcal/mol for ($Cr^{3+}$), ($Cr^{2+}$) and $Cr_2O_3$ reduction. Addition of S or Se to the system markedly increased the rates of reduction of all the chromium species, with an attendant increase in the FeO content of the slag. Metal emulsification, which is a consequence of reduced surface-tension of the metal, is thought to be responsible for the increase in rate of $Cr_2O_3$ reduction. Addition of FeO to slag decreased the reduction rates of all the chromium species whilst $CaF_2$ addition increased the rate of reduction of the chromium species. The reduction in slag viscosity due to $CaF_2$ addition is thought to be responsible for the increased rates of reduction.

# CONTENTS

## CONTENTS CONTD

## CONTENTS CONTD

## CONTENTS CONTD

## CONTENTS CONTD

## LIST OF FIGURES

## LIST OF FIGURES CONTD

## LIST OF FIGURES CONTD

## LIST OF FIGURES CONTD

## LIST OF FIGURES CONTD

## LIST OF FIGURES CONTD

## LIST OF FIGURES CONTD

## LIST OF FIGURES CONTD.

## LIST OF FIGURES CONTD.

## LIST OF FIGURES CONTD.

## LIST OF FIGURES CONTD.

## LIST OF FIGURES CONTD.



## LIST OF PLATES

## LIST OF SYMBOLS

| | |
|---|---|
| V | slag basicity expressed as $\%CaO/\%SiO_2$ |
| T | absolute temperature, $^{o}K$ |
| %X | weight percent X |
| t | time, mins |
| A | frequency factor as defined in equation (1.37) |
| K | equlibrium constant as defined in equation (1.6) |
| $\Delta G^{o}$ | standard gibbs energy, J/mol |
| $K'_{SiCr}$ | equilibrium constant as defined in equation (1.13) |
| $L_{Cr}$ | chromium distribution ratio between slag and liquid alloy as defined in equation (1.21) |
| $\gamma_i$ | activity coefficient of component i |
| $a_i$ | activity of component i |
| J | Flux, $mol.cm^{-2}.s^{-1}$ |
| D | Diffusion coefficient, $cm^2.s^{-1}$ |
| C | concentration |
| A | reaction area, $cm^2$ |
| $\delta$ | effective boundary layer thickness, cm |
| $k_m$ | mass transfer coefficient as defined in equation (1.31) |
| $k_i$ | rate constant for forward or reverse reaction (where i = 1,2.....6) |
| E | activation energy, kcal/mol |
| ( ) | component in slag phase |
| [ ] | component in metal phase |
| R | gas constant = 1.987 cal/degree K |

## LIST OF SYMBOLS CONTD

| | |
|---|---|
| P | pressure, atm |
| h | slag height, cm |
| absd. | observed |
| calcd. | calculated |

## SUBSCRIPTS

| | |
|---|---|
| e | equilibrium |
| tot | total |
| g | gaseous state |
| s | solid state |
| l | liquid state |
| i | interface |
| o | initial value at time, t = 0 |
| ads | adsorbed |

## LIST OF TABLES

## LIST OF TABLES CONTD

## LIST OF TABLES CONTD.

## LIST OF TABLES CONTD

# CHAPTER 1

# LITERATURE REVIEW

# INTRODUCTION

In the production of high-chromium and low-carbon ferro-chromium alloys and alloy steels, an important objective is the oxidation of carbon to very low levels without excessive simultaneous oxidation of chromium. From studies[1,2,3,4] on the decarburisation of stainless steel, it is presumed that in the process of decarburisation, oxidation of chromium occurs and the solid chromium oxide formed is subsequently reduced by carbon. The reduction of chromium oxide from slag can be represented as a two stage process:

$$Cr_2O_3 + C = 2CrO + CO(g) \quad (1.1)$$

$$2CrO + 2C = 2[Cr] + 2CO(g) \quad (1.2)$$

These reactions suggest that the reduction of $Cr_2O_3$ from slag follows a two-stage consecutive reaction mechanism, in which CrO is the intermediary product. This is evidenced by the change in colour of slag from light green to deep blue during the initial stages of reduction, suggesting that the chromium species changes from the $(Cr^{3+})$ to the $(Cr^{2+})$ ion[20,31,37].

In most studies of the reduction of chromium oxide from slag, the total chromium content of the slag is used when analysing the kinetics of the system. Robison and

Pehlke[31] and recently Anyakwo[37] managed to split the total chromium content in slag into ($Cr^{3+}$) and ($Cr^{2+}$) ions. They recognised the fact that the reduction of chromium oxide from slag takes place primarily in two stages, but considered the two reactions separately when analysing the kinetics of the system.

The objective of the present investigation has been to develop a first-order consecutive two-stage reaction model for the reduction of $Cr_2O_3$ from slag in which the two reactions above are considered to be taking place simultaneously and are combined in the kinetic analysis of the system. The model is applied to experimental data obtained by studying the effect of various parameters on the kinetics of reduction of $Cr_2O_3$ from slag by carbon dissolved in molten iron. The parameters studied are the effect of furnace atmosphere, the effect of chromium oxide concentration in slag, the effect of metal chromium content, the effect of temperature, the effect of melt geometry, the effect of sulphur additions to slag and metal, the effect of selenium additions to metal, the effect of FeO addition to slag and the effect of calcium fluoride additions to slag.

It is thereby hoped the model can be helpful in determining the kinetic types and rate constants of the reactions occurring during the reduction of chromium

oxide from slag as well as in understanding the events occurring in the AOD process of stainless steel refining and the smelting of chromium ore. It is also relevant to the use of chromium ore as a decarburising and chromium-supplying agent.

# CHAPTER 1

# LITERATURE REVIEW

## 1.1 Solubility of chromium in slags

The solubility of chromium oxides in acid and basic slags is limited and, although little is known concerning the solubility, it is generally conceded to be less than 10 wt per cent[5]. If this limit is exceeded very viscous, practically unworkable slags result, which are liable to produce very stable foams during periods of gas evolution from the metal bath.

There is a variation in the solubility limits determined by various investigators. Grant et al[6] estimated the solubility of chromite in slags of the type $CaO(MgO)-SiO_2-FeO-Cr_2O_3$ to be about 2 to 5 wt per cent $Cr_2O_3$ in the temperature range of 1550 to 1700°C. Pathy and Ward[7] showed that in simple $CaO-MgO-'FeO'-SiO_2$ slags the solubility of $Cr_2O_3$ is very limited, being less than 10 wt per cent at 1736°C. Glasser and Osborn[8] found a solubility limit of $Cr_2O_3$ in the system $CaO-Cr_2O_3-SiO_2$ to be 8wt per cent at 1700°C and a V ratio, (wt%CaO + wt%MgO ) / $wt\%SiO_2$, of 1.0.

McCoy and Langenberg[9] proposed an equation for estimating the chromium concentrations in slags of the ternary $CaO-SiO_2$-15 $Al_2O_3$ system in equilibrium with metal containing chromium and silicon in the range 11 to 18 % and 0.10 to 0.80% , respectively, for temperatures 1520 to 1720°C and slag basicity of 0.3 to 0.9 as:

$$\text{Log (\%Cr)} = 4.887 - \frac{8866}{T} + 0.340 \text{ Log [\%Cr]}$$

$$- 0.178 \text{ Log[\%Si]} - 1.721 \text{ Log V} \qquad (1.3)$$

where T = absolute temperature in degrees kelvin

[%Cr] = equilibrium weight per cent chromium in the metal

[%Si] = equilibrium weight per cent silicon in the metal

V = slag basicity expressed as wt%CaO/wt%$SiO_2$

Equation (1.3) was estimated from equilibrium concentrations of chromium in slag and metal by statistical methods using an expression for weight percent chromium in slag of the form:

$$\text{Log (\%Cr)} = A + \frac{B}{T} + C \text{ Log [\%Cr]}$$

$$+ D \text{ Log [\%Si]} + E \text{ Log V} \qquad (1.4)$$

where A, B, C, D and E are constants, T is the absolute temperature, and V the slag basicity. The constants in equation (1.4) were evaluated using the logarithm of the percent chromium in the slag as the dependent variable and the reciprocal of the absolute temperature, the logarithm of the metal chromium and silicon concentrations as the independent variables.

They found a good agreement between the actual experimental and the estimated values of chromium in slag predicted by equation (1.3), as shown in Fig. 1.1. A maximum solubility of chromium in the $CaO-SiO_2$-15%$Al_2O_3$ slag was found to be 19.8 %Cr. Furthermore, they concluded that the chromium solubility in slag decreases with increase in slag basicity (Fig. 1.2).

Recently, Morita et al[10] studied the solubility of $MgO.Cr_2O_3$ in $MgO-Al_2O_3-SiO_2-CaO$ melts at 1600°C as a function of oxygen partial pressure and slag composition. Their results show the solubility of $MgO.Cr_2O_3$ to be 1.1 to 4.5 wt% $Cr_2O_3$ for $MgO-SiO_2$ melts in air (broken lines-Fig. 1.3). For MgO-CaO melts the solubility substantially rises to as much as 40 to 55 wt% $CrO_x$ as shown in Fig. 1.4. Under reducing conditions, however, and for $MgO-SiO_2$ melts, they found that the solubility of $MgO-Cr_2O_3$ at $pO_2 = 2.73 \times 10^{-10}$ atm (shown in Fig. 1.3 as a solid line) increases. At $2MgO.SiO_2$ saturation, the

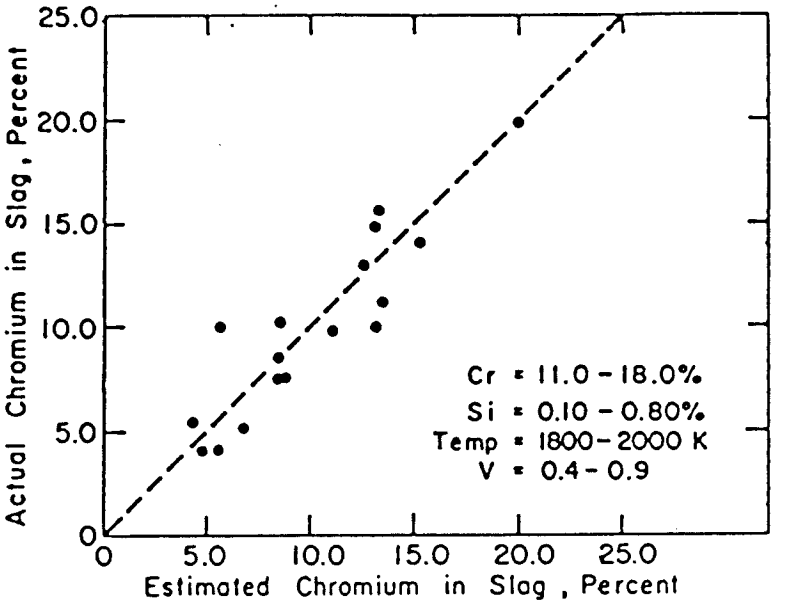


Fig. 1.1 Actual and estimated chromium contents of slags (9)

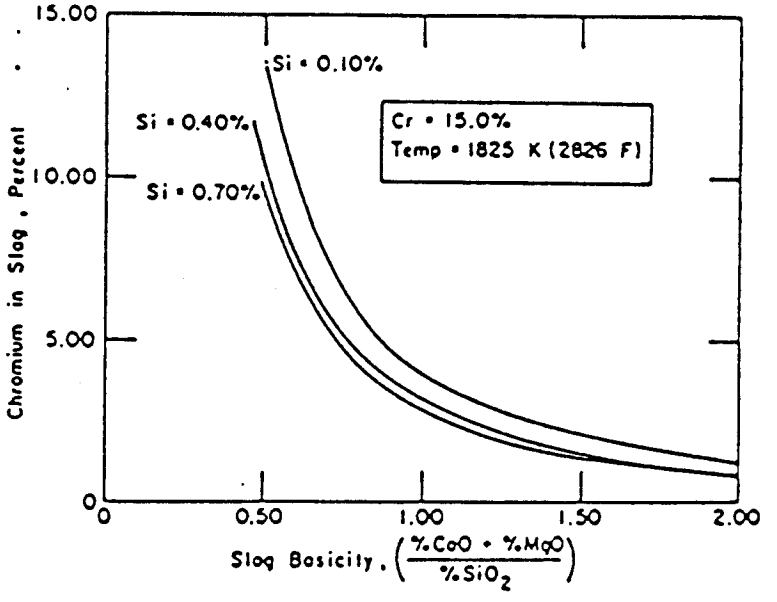


Fig. 1.2 Estimated equilibrium chromium content in slag vs basicity (9).

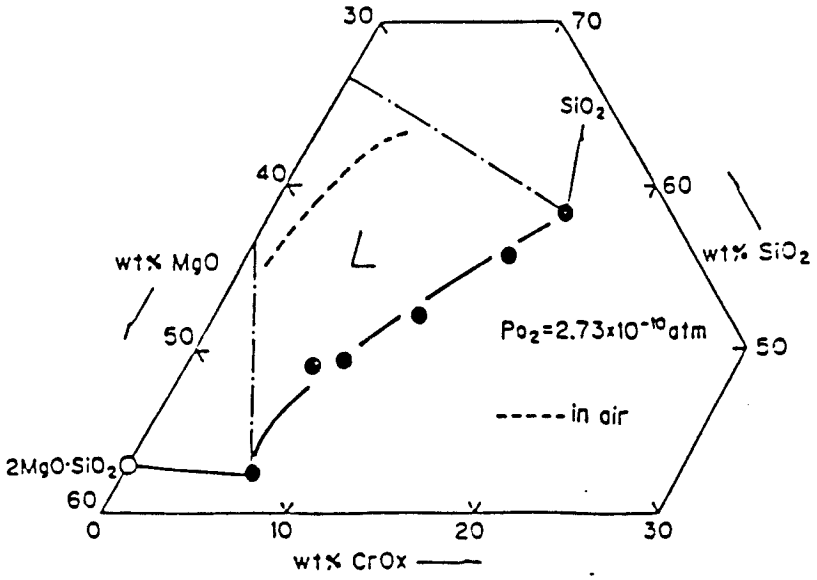


Fig. 1.3 Comparison of the solubility of $MgO-Cr_2O_3$ in the $MgO-SiO_2(-CrO_x)$ system at 1600°C under different oxygen partial pressures (10).

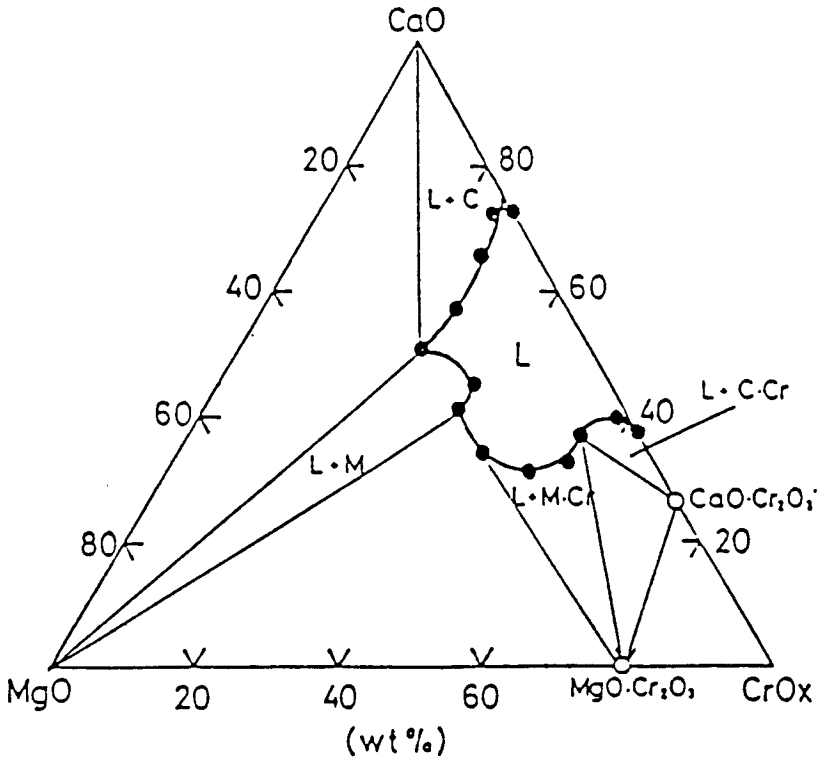


Fig. 1.4 Liquidus in the $MgO-CaO-CrO_x$ system at 1600°C in air. (L:liquid, M:MgO, C:CaO, Cr:$Cr_2O_3$) (10).

solubility increased from 0.7 to 8.2 wt% Cr by lowering the oxygen partial pressure from 0.21 to 3.6 x $10^{-13}$ atm, as shown in Fig. 1.5. They also found that addition of CaO to the $MgO-SiO_2$ slag under reducing conditions gives rise to a decrease in the solubility and also in the $Cr^{2+}/Cr^{3+}$ ratio. These results are shown in Fig. 1.6 and are in good accord with those of McCoy and Langenberg[9].

The scant data on the solubility of $Cr_2O_3$ and $FeCr_2O_4$ in rather arbitrary slag compositions are given in Tables 1.1 and 1.2[5].

**Table 1.1: Solubility limit of $Cr_2O_3$ in slags.**

| Slag type | $\frac{wt\%CaO + wt\%MgO}{wt\%SiO_2}$ | Temp. °C | wt% $Cr_2O_3$ | Ref. |
|---|---|---|---|---|
| $CaO-SiO_2-Cr_2O_3$ | 0.4 | 1700 | 2 | 8 |
| $CaO-SiO_2-Cr_2O_3$ | 1.0 | 1700 | 8 | 8 |
| Complex | 1.2-1.7 | 1660 | 6 | 13 |
| Complex | 1.2-1.7 | 1720 | 8 | 13 |
| $MgO-SiO_2-Cr_2O_3$ | 0.5-0.8 | 1600 | 4.5 | 10 |

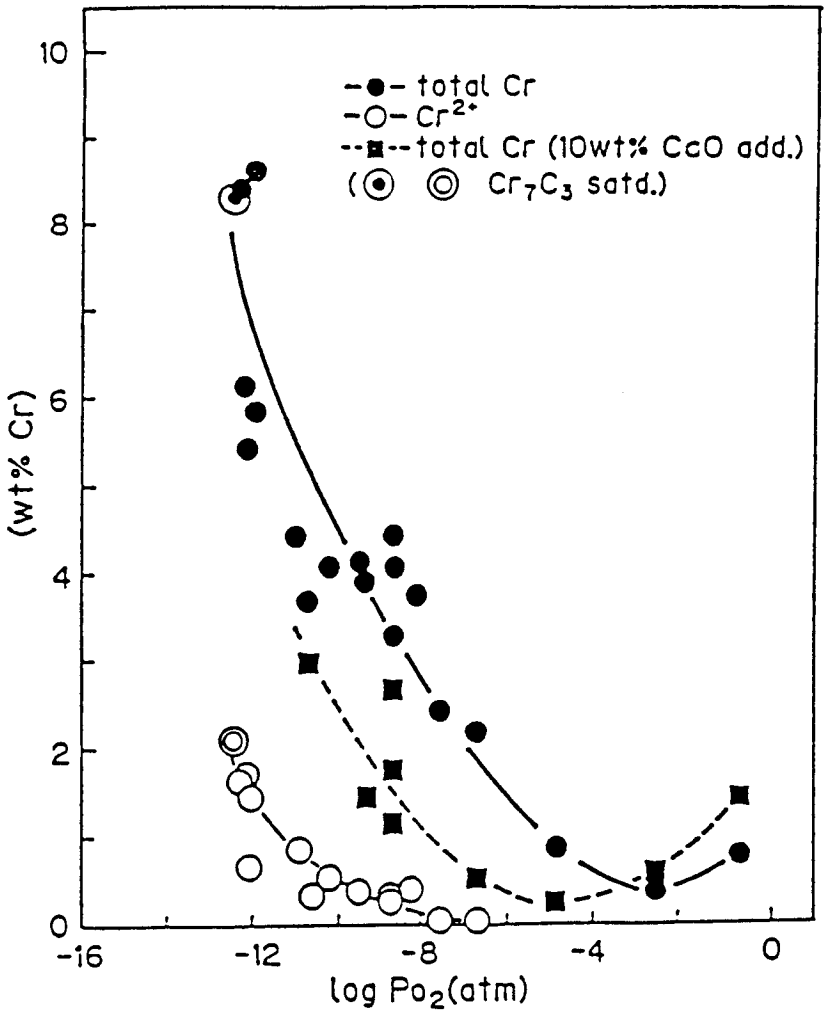


Fig. 1.5 Oxygen partial pressure dependence of the solubility of $MgO.Cr_2O_3$ in the $MgO-SiO_2$ (-CaO) system ($2MgO.SiO_2$ satd.) at 1600°C (10).

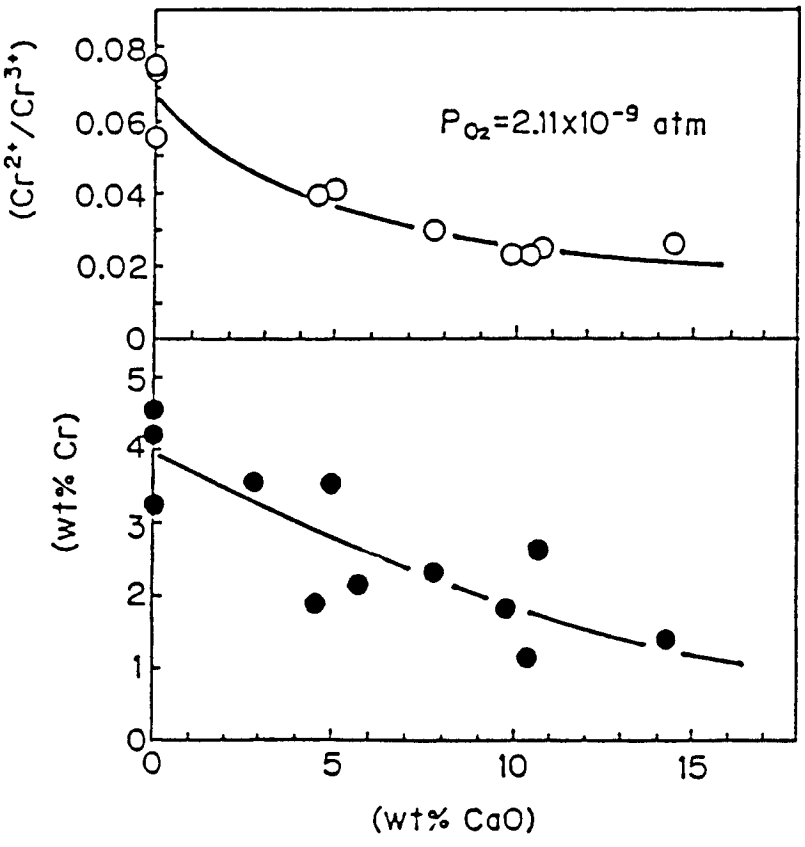


Fig. 1.6 Effect of CaO content on the solubility of $MgO.Cr_2O_3$ and $Cr^{2+}/Cr^{3+}$ ratio in the $MgO-SiO_2-CaO$ system ($2MgO.SiO_2$ satd.) at 1600°C (10).

**Table 1.2: Solubility limit of $FeCr_2O_4$ in slags.**

| Slag type | Temp. °C | wt%$Cr_2O_3$ | Ref. |
|---|---|---|---|
| Acid | 1600 | ~ 6 | 12 |
| | 1700 | ~ 10 | 12 |
| Intermediate $(CaO+MgO)/SiO_2$ = 1.3-2.2 | 1660 | 3 | 13 |
| | 1720 | 4 | 13 |
| Basic | 1600 | 3 | 8 |
| | 1700 | 5 | 8 |

## 1.2 Phase equilibria in slags containing chromium

The behaviour of chromium oxides in slag is complex as the nature of the equilibrium oxide appearing at saturation is dependent on the chromium content of the steel melt. For purposes of calculation it is commonly assumed that the oxide phases in equilibrium with molten Fe-Cr alloys are chromite ($FeO.Cr_2O_3$) and $Cr_2O_3$ [5]. A review of the literature, however, indicates that some investigators have considered this assumption inadequate to explain their observations and strongly suspect that other oxides of chromium may be involved.

Herasymenko [11], in his study of the reactions of chromium in the acid open-hearth furnace assumed the chromium in slag to be present as CrO based on the

postulation that this is the only oxide that can exist in acid slags in equilibrium with liquid steel.

Chen and Chipman[12] summarised their observations with the statement that at 1595°C chromite ($FeO.Cr_2O_3$) was the stable phase in equilibrium with melts containing less than 5.5 wt% Cr and at higher concentrations in the metal $Cr_2O_3$ became the stable phase.

Grant et al[6] carried out equilibrium studies on the distribution of chromium and oxygen between liquid iron, containing less than 1 wt%Cr, and simple slags of the $CaO(MgO)-SiO_2-FeO-Cr_2O_3$ type in the temperature range 1526-1734°C. Their results showed that the solubility of chromite in slags is estimated to correspond to about 2 to 5 wt%$Cr_2O_3$ at temperatures of 1500 and 1700°C. They represented the reaction of chromium with oxygen at low chromium contents in the presence of chromite-saturated slags as:

$$FeO.Cr_2O_3(s) = Fe(l) + 2[Cr] + 4[O] \qquad (1.5)$$

$$K = [Cr]^2 \times [O]^4 \qquad (1.6)$$

Their experimental data strongly supports the existence of $FeO.Cr_2O_3$ as the equilibrium phase at low metal

chromium levels thus confirming the results of Chen and Chipman[12].

Keith[13] studied phase equilibria in the system $MgO-Cr_2O_3-SiO_2$. He showed that there is an extensive two-phase-liquid region, and that the stability fields of periclase, pichromite and chromic oxide extend across most of the diagram. His results are shown in Fig. 1.7. The diagram shows that the three phases chromic oxide ($Cr_2O_3$), pichromite ($MgCr_2O_4$), and periclase (MgO) occupy almost the entire composition triangle, whereas the primary phase areas of the $SiO_2$-containing phases (cristobalite, $SiO_2$; forsterite, $Mg_2SiO_4$; and protoenstatite, $MgSiO_3$) are restricted to narrow strips adjacent to the $MgO-SiO_2$ join.

The studies of Glasser and Osborn[8] on the phase equilibrium in the system $CaO-Cr_2O_3-SiO_2$ show that for compositions above (higher in silica) the $Ca_2SiO_4-CaCr_2O_4$ join (Fig. 1.8) the chromium is virtually all in trivalent form. A huge primary-phase field for $Cr_2O_3$ dominates the diagram.

Pathy and Ward[7] summarised their results from the equilibrium studies between synthetic $CaO-MgO-'FeO'-SiO_2-Cr_2O_3$ slags of lime-silica ratios between 1.2 and 2.0 with iron-chromium alloys in the

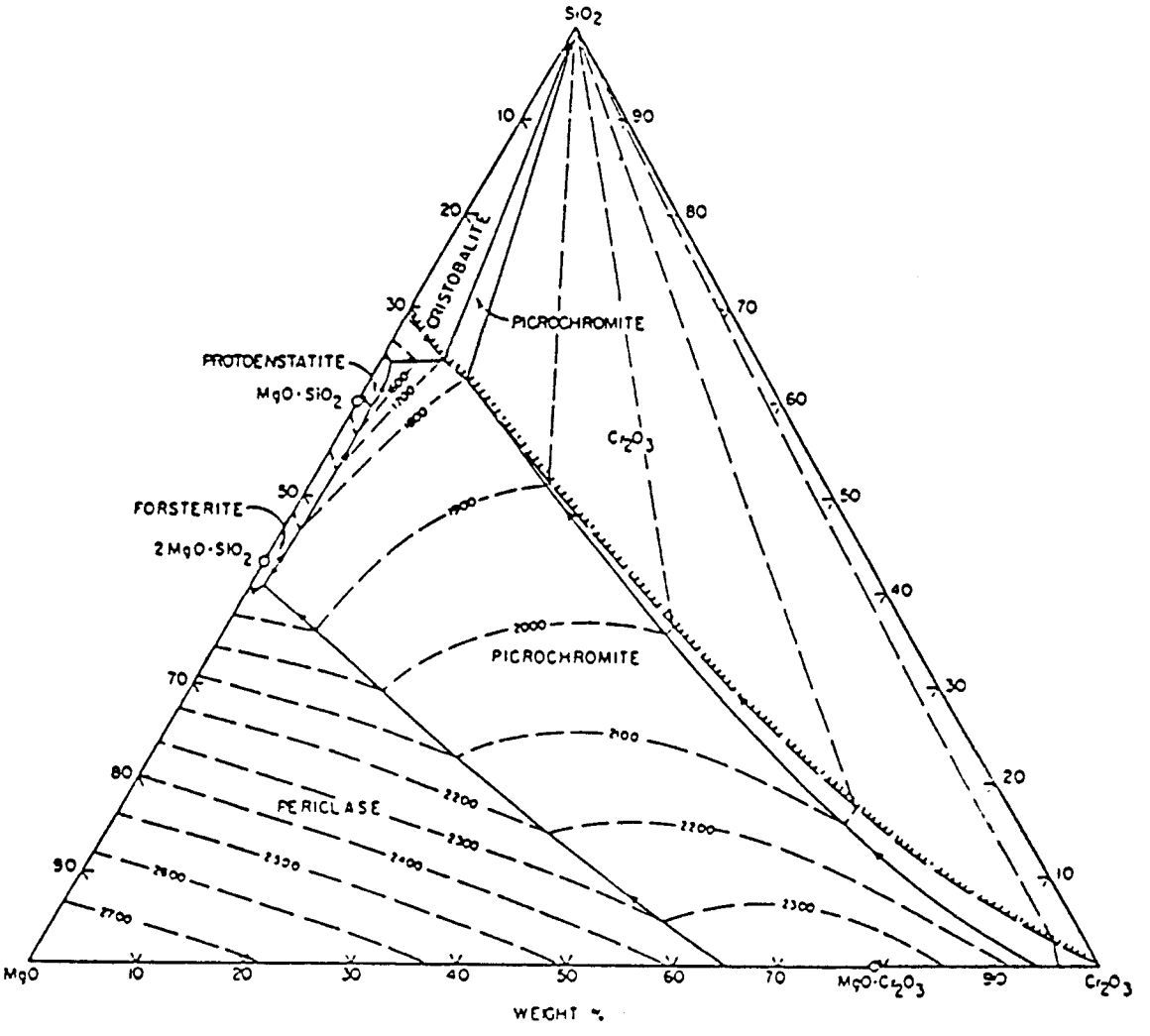


Fig. 1.7 Phase diagram for the system $MgO-Cr_2O_3-SiO_2$ (13).

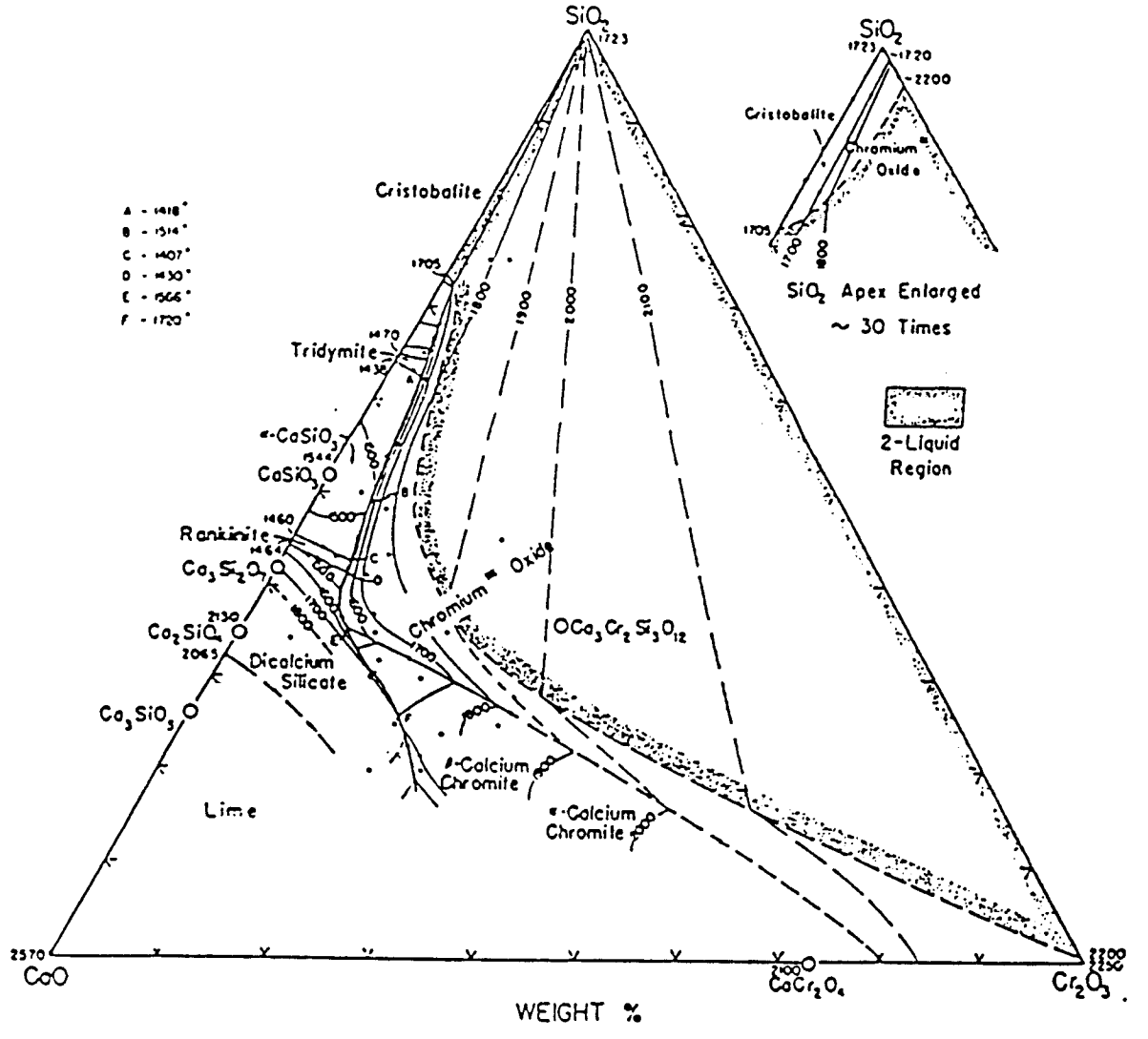


Fig. 1.8 Phase diagram for the ternary system CaO-$Cr_2O_3$-$SiO_2$. Dots represent compositions of mixtures studied (8).

range 0-2 wt% and 14-20 wt%Cr and at temperatures 1626, 1686 and 1736°C that chromite ($FeCr_2O_4$) is in equilibrium with low-chromium steels (0.1 to 1.0 %Cr) and that chromic oxide ($Cr_2O_3$) is in equilibrium with high-chromium steel (14-20 %Cr). This is in accord with the results of Grant et al[6] and Chen and Chipman[12].

Hook and Adair[14] subjected $Cr_2O_3$ and $Cr_3O_4$ to various heat treatments with arc-melted iodide chromium over the temperature range 1000 to 1750°C. With the help of X-ray diffraction, supplemented by optical metallography, they concluded that $Cr_3O_4$ is first observable in samples annealed at 1300°C and coexists with $Cr_2O_3$ (the low-temperature oxide) over a temperature range exceeding 200°C. Furthermore, heat treatment at low temperatures leads to the disproportionation of $Cr_3O_4$ and precipitation of $Cr_2O_3$.

Healy and Schottmiller[15] in their investigation of the chromium oxide-silica system at low oxygen pressures showed the existence of CrO in a silica saturated melt at low oxygen pressures. A deep blue chromous silicate, identified as $Cr_2SiO_4$, formed from the melt at about 1400 to 1500°C and was found to be unstable at room temperature, since on slow cooling it disproportionates in whole or in part to $Cr_2O_3$, Cr and $SiO_2$.

Maeda and Sano[16] determined the equilibrium concentrations of chromium in the molten $CaO-MgO-Al_2O_3-SiO_2$ system coexisting with $Cr_3C$, C and one atmosphere of CO at 1500 and 1650°C. They found chromium in the slag to exist as CrO. Fig. 1.9 shows some results from their study.

In their study of the behaviour of chromium in stainless-steelmaking, Rankin et al[17] equilibrated Fe-Cr-Si alloys and $SiO_2-CaO-Al_2O_3-FeO-CrO_x$ slags in alumina crucibles at 1600°C. Their results indicate that chromium in reduced slags is predominantly as $Cr^{2+}$ or CrO. They found the best average composition of Cr in the slags as $CrO_{1.07}$, which is equivalent to a mixture of 86% $Cr^{2+}$ and 14% $Cr^{3+}$.

## 1.3 Distribution of chromium between slag and metal.

Experimental studies of the partition of chromium between slag and metal under blast furnace and open hearth conditions have shown that the extent to which this element is reduced is related to the oxygen potential associated with silica reaction.

Korber and Oelsen[18] derived an expression for the dependence of the distribution ratio of chromium between metal and silica saturated slags on the iron oxide

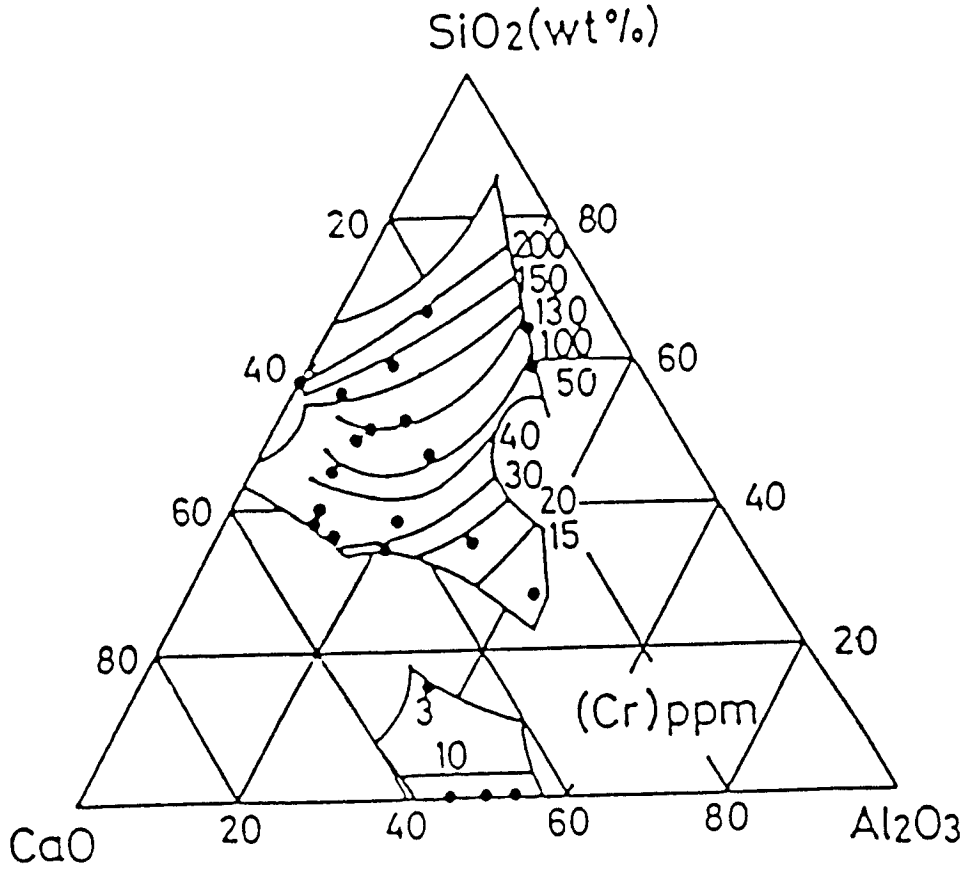


Fig. 1.9 The equilibrium concentration of chromium oxide in $CaO-Al_2O_3-SiO_2$ slags coexisting with chromium carbide, graphite and carbon monoxide at 1500°C (16).

content of the slags at 1600-1640°C. The equilibrium equation considered is

$$(CrO) + [Fe] = (FeO) + [Cr] \qquad (1.7)$$

from which the distribution ratio can be written assuming activities to obey Henry's law:

$$K^{-1} \times (wt\%FeO) = \frac{(wt\%Cr)}{[wt\%Cr]} \qquad (1.8)$$

The value of $K^{-1}$ was found to be 0.34 from the data shown in Fig. 1.10.

Pathy and Ward[7] carried out experiments to determine the free energies of the reactions

$$Fe + 2Cr_{(\%\text{ in Fe})} + 4O_{(\%\text{ in Fe})} = FeO.Cr_2O_3(s) \qquad (1.9)$$

$$\Delta G^\circ = -972100 + 415\,T \quad J/mol \qquad (1.10)$$

and

$$2Cr_{(\%\text{ in Fe})} + 3O_{(\%\text{ in Fe})} = Cr_2O_3(s) \qquad (1.11)$$

$$\Delta G^\circ = -887400 + 393\,T \quad J/mol \qquad (1.12)$$

From equations (1.9) and (1.11) it is evident that the partitioning of chromium between slag and metal should increase with increasing oxygen potential of the bath.

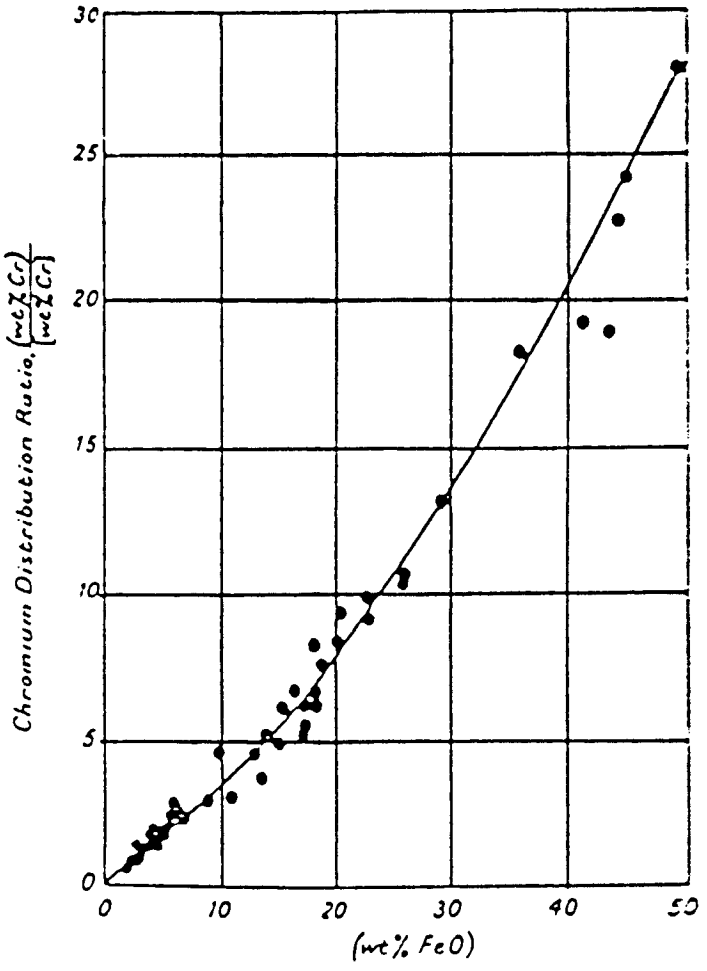


Fig. 1.10 The dependence of the chromium slag-metal distribution ratio on the oxide content of the slags (18).

Their results show iron oxide content of the slag to be an indicator of the state of oxidation of chromium as shown in Fig. 1.11. The chromium distribution ratio was also found to increase with decrease in temperature.

Herasymenko[11], in his investigation of the equilibrium between acid slags and steel containing small amounts of Cr in the acid open-hearth furnace, derived an expression for the equilibrium constant $K'_{SiCr}$ involving the partition of chromium between slag and metal and its dependence on the silicon content of the metal as:

$$K'_{SiCr} = \frac{(CrO)^2 \times [Si]}{[Cr]^2} \qquad (1.13)$$

which was found to increase with temperature.

Niinomi et al[19] conducted a study of the reduction equilibrium of chromium between molten pig iron ($Fe-C_{sat}-Cr[1\%]$) and molten slag of the type ($CaO-SiO_2-Al_2O_3-CrO$), in the temperature range of 1350-1500°C and slag basicity, $CaO/SiO_2$, of 0.6 to 1.4 under atmospheric pressure of CO. They concluded that the chromium oxide in slags was mainly present in the form of CrO. The partition ratio of chromium (%CrO)/[%Cr] between pig iron and slags decreased with increase in basicity up to about 1 (Fig. 1.12).

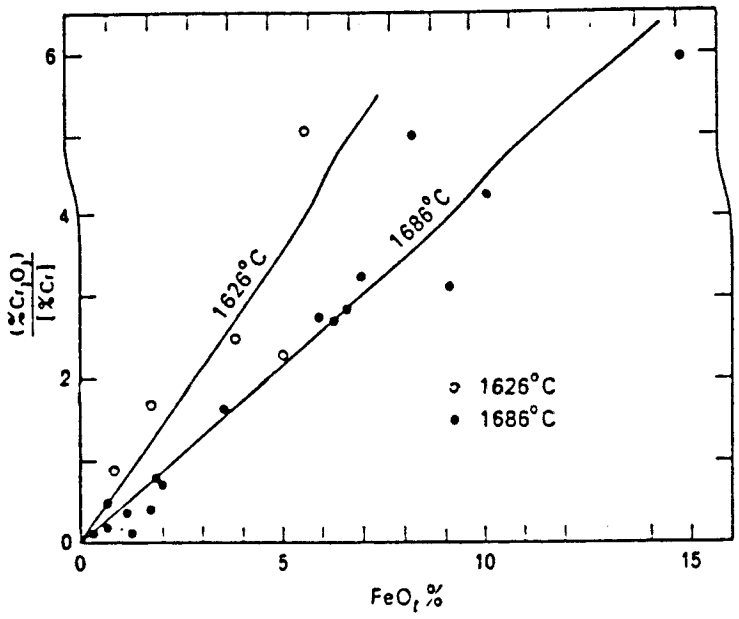


Fig. 1.11 Dependence of chromium distribution between slag and metal on the bath temperature and iron oxide content of slags unsaturated with chromium oxides (7).

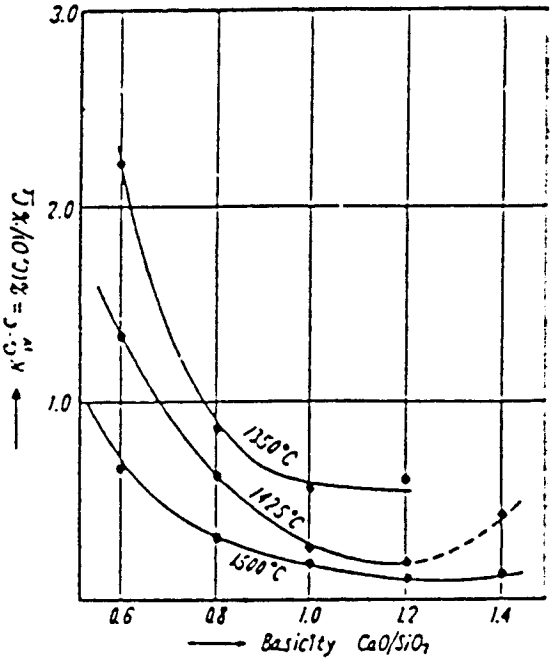


Fig. 1.12 Effects of basicity and temperature on chromium distribution (19).

In their studies of the reduction of chromous oxide from lime-silica-alumina slags, McCoy and Philbrook[20] observed that it was not possible to achieve a constant slag-metal distribution ratio for chromium due to simultaneous reduction of silica from the slag. The ratio (%Cr)/[%Cr] ranged from zero at lime-silica ratios above 1.2 to only 0.04 at a basicity ratio of 0.6 as shown in Fig. 1.13. They suggested the process of chromium distribution to be represented by the equation

$$2(CrO) = 2[Cr] + O_2(g) \quad (1.14)$$

$$K_{Cr} = \frac{a_{Cr}^2 \times pO_2}{a_{CrO}^2} \quad (1.15)$$

therefore

$$pO_2 = \frac{K_{Cr} \times a_{CrO}^2}{a_{Cr}^2} \quad (1.16)$$

An identical situation exists with respect to silica:

$$(SiO_2) = [Si] + O_2(g) \quad (1.17)$$

$$pO_2 = \frac{K_{Si} \times a_{SiO_2}}{a_{Si}} \quad (1.18)$$

The condition where the reduction of CrO and $SiO_2$ by carbon is proceeding simultaneously can be represented by

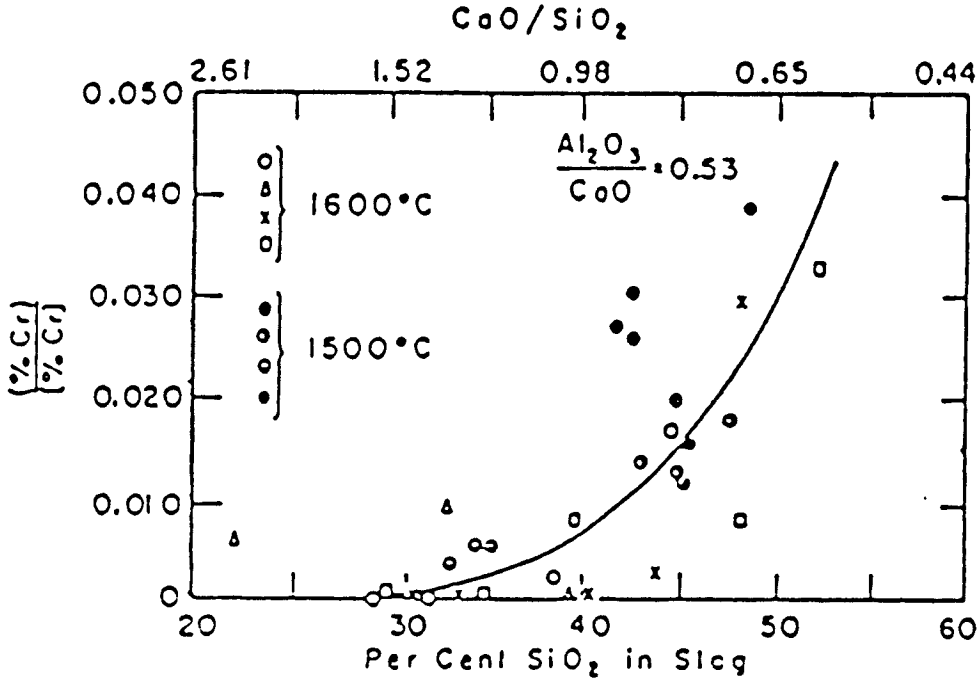


Fig. 1.13 Relation of chromium distribution to simultaneous silica content of slag (20).

setting equations (1.16) and (1.18) equal:

$$pO_2 = \frac{K_{Cr} \times a_{CrO}^2}{a_{Cr}^2} = \frac{K_{Si} \times a_{SiO_2}}{a_{Si}} \qquad (1.19)$$

rearranging and simplifying we have

$$\frac{(\%CrO)^2}{[\%Cr]^2} = \frac{K'_{SiCr} \times a_{SiO_2}}{[\%Si]} \qquad (1.20)$$

This equation predicts a variation of the chromium distribution ratio with silica in slag at a constant [%Si] shown in Fig. 1.13.

Recently, Katayama et al[21] carried out equilibrium experiments between Fe-Cr alloys and $CaO-MgO-Al_2O_3-SiO_2$ slags having compositions near the $CaO-Al_2O_3$ binary system at temperatures 1575, 1600 and 1650°C. They derived an expression for the chromium distribution ratio between liquid alloy and slags as

$$\text{Log } L_{Cr} = 2.04 \text{ Log}[wt\%O] - 0.048[wt\%Cr] + 0.292 K_i N_i + \frac{26805}{T} - 10.487 \qquad (1.21)$$

where

$$L_{Cr} = \frac{(wt\%Cr)}{[wt\%Cr]}$$

$$K_i N_i = N_{CaO} + 0.1 N_{MgO} - 0.8 N_{Al_2O_3} - N_{SiO_2}$$

A good correlation was found between the observed Log $L_{Cr}$ and the calculated values from the above equation as shown in Fig. 1.14.

## 1.4 The equilibrium controlling the decarburisation of iron-chromium-carbon melts.

In the production of low-carbon ferro-chrome and low-carbon chromium steels it is often necessary to remove carbon from the metal by oxidation during refining. This removal is made difficult by the strong affinity of chromium for carbon. Therefore, the extent to which carbon can be removed in normal practice without simultaneously oxidizing chromium is limited by the chromium content of the alloy.

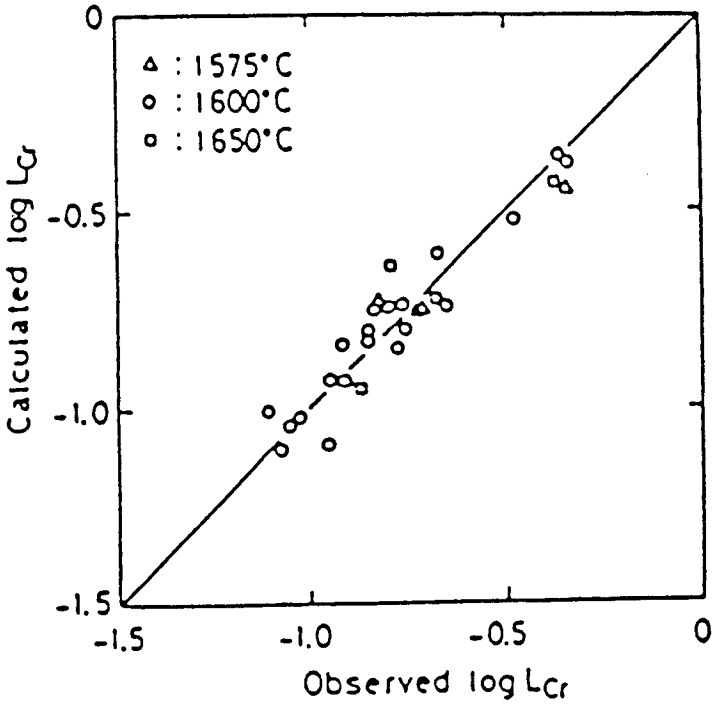


Fig. 1.14 Comparison of Log $L_{Cr}$ observed with Log $L_{Cr}$ calculated from equation (1.21) (21).

Hilty[22] studied the relationship between chromium and carbon in chromium steel refining by injecting oxygen through Fe-Cr-C melts containing approximately 0.06 %C and 8 %Cr to 0.4 %C and 30 %Cr and measuring the amounts of carbon and chromium that remained dissolved in molten iron after oxygen injection had produced a slag saturated with oxides of chromium. He observed that the ratio of chromium to carbon remained approximately constant (Fig. 1.15). He therefore suggested that the decarburisation equilibrium was

$$(CrO) + [C] = [Cr] + CO(g) \qquad (1.22)$$

for which

$$K_1 = \frac{[\%Cr]}{[\%C]} \qquad (1.23)$$

where pCO = 1 atm and the activity of CrO was unity in the slag.

Later Dennis and Richardson[23] investigated the state of equilibrium of iron-chromium-carbon melts saturated with solid $Cr_2O_3$, with gases of known CO and $CO_2$ potentials and suggested the decarburisation equilibrium to be given by the equation

$$(Cr_2O_3) + 3[C] = 2[Cr] + 3CO \qquad (1.24)$$

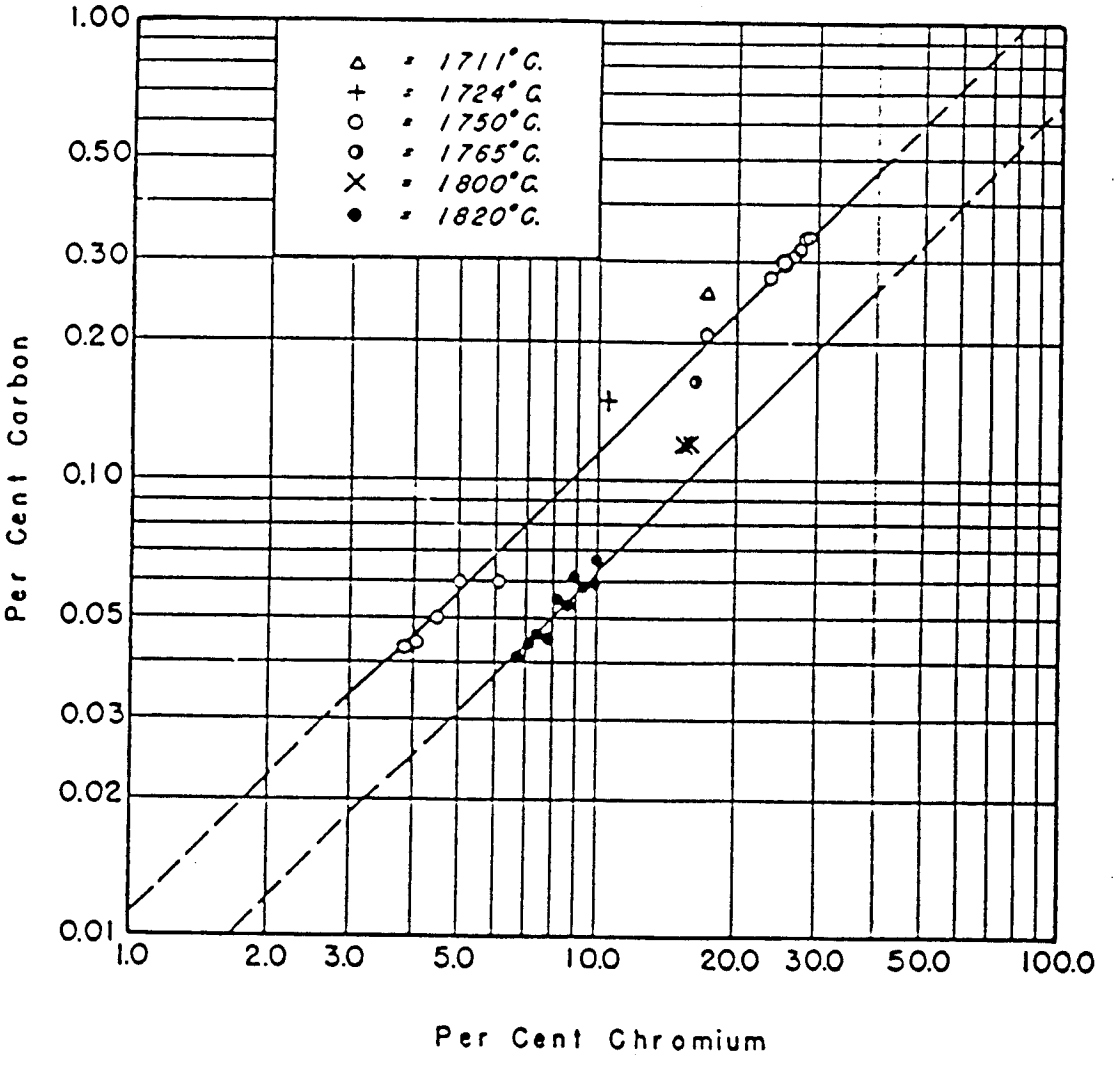


Fig. 1.15 Relation of chromium to carbon in molten chromium steel at constant temperature (22).

for which

$$K_2 = \frac{(a_{[Cr]})^2}{(a_{[C]})^3} = \frac{(\gamma_{[Cr]}\ [\%Cr])^2}{(\gamma_{[C]}\ [\%C])^3} \qquad (1.25)$$

where a's and $\gamma$'s are the activities and activity coefficients. The carbon-chromium relation for this equilibrium is shown in Fig. 1.16 for 1 atm. CO. They explained Hilty's observation by saying that the activity coefficient of carbon is lowered by the chromium in such a way that [%Cr] / [%C] remains almost constant. From Fig. 1.16, it is evident that for a given concentration, the higher the temperature the lower the equilibrium carbon content of the metal. For this reason, the chromium losses to the slag are minimised by decarburising the melt with oxygen blowing at elevated temperatures. Another important feature of reaction 1.25 is that, for a given chromium concentration, the lower the partial pressure of CO in the gas the lower the equilibrium concentration of carbon. These two effects on the oxidation of chromium are shown in Fig. 1.17 for melts saturated with chromic oxide[24]. In most current steel making practices, the chromium steels are decarburised by bottom blowing of argon-oxygen mixtures to cut down on the oxidation of chromium without excessive increase of temperature.

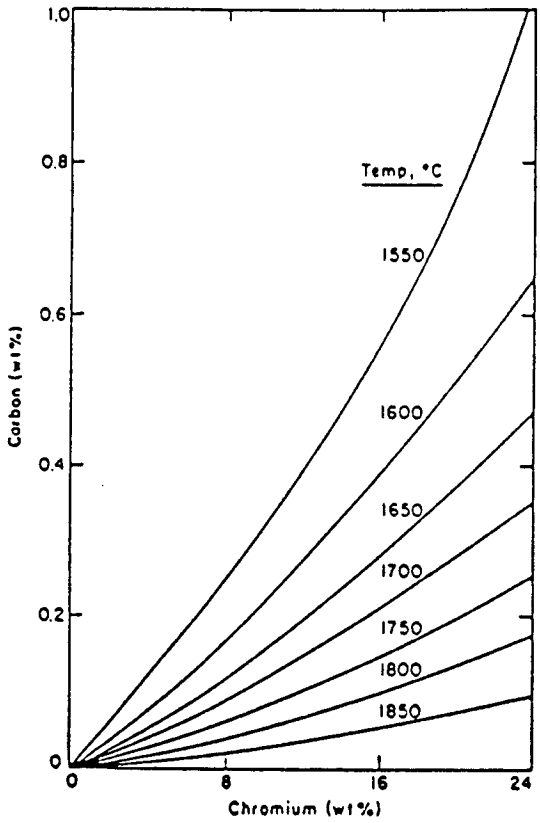


Fig. 1.16 Equilibrium concentrations of carbon and chromium in Fe-Cr-C melts in equilibrium with solid $Cr_2O_3$ at 1 atm CO and indicated temperatures (23).

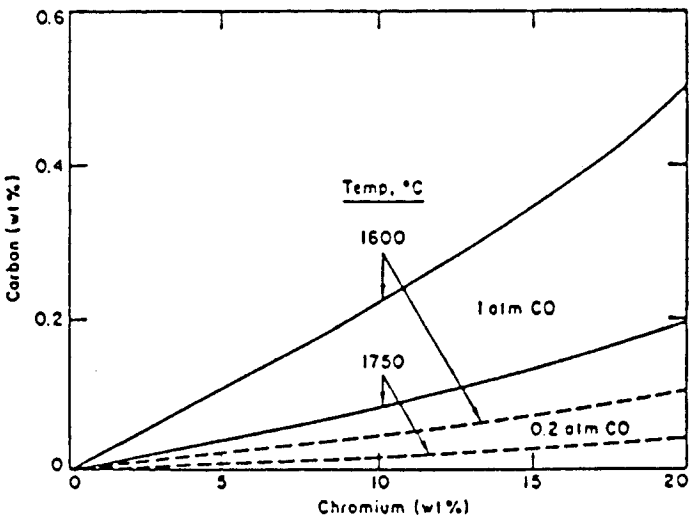


Fig. 1.17 Carbon-Chromium relation in liquid steel in equilibrium with solid $Cr_2O_3$ at indicated temperatures and CO pressures (24).

## 1.5 Reaction Kinetics.

### 1.5.1 Kinetics of Metallurgical Reactions

A study of thermodynamics provides information regarding the chemical equilibrium of a metallurgical reaction and indicates the direction in which a reaction will proceed under the stated conditions. However, it does not provide any information on the rate of a reaction. A knowledge of equilibrium constant is not enough and it is scarcely of any use having a favourable equilibrium constant if it takes a long time for the establishment of equilibrium. The velocity of a reaction is thus of great significance for the economic production of any substance. Therefore, consideration of both thermodynamics and reaction kinetics is required to provide a full understanding of any metallurgical process.

Homogeneous reactions are those which take place within one single phase such as a gas or a liquid, whilst heterogeneous reactions are those which take place between different phases, such as a gas/solid or a slag/metal reaction. Most metallurgical reactions are heterogeneous. The main types of reactions that take place in iron and steel production are:

(1) gas-solid, e.g. reduction of iron ore with CO in the blast furnace

(2) gas-liquid, e.g. oxygen lancing in steelmaking

(3) liquid-liquid, e.g. metal-slag refining reactions.

The overall rates of these reactions will be dependent on three main process steps which are present in all reactions

(1) rate of transport of reactants to the reaction site

(2) chemical reaction rate at the reaction site

(3) rate of transport of products away from the reaction site.

In some cases reaction rates may be limited by nucleation rates of a product. Reaction kinetics of metallurgical reactions is thus a study of the rate of reactions by consideration of these individual reaction steps, the mechanism by which they proceed and the effect of process variables on the reaction rate.

### 1.5.1.1 Diffusion control and the mass transfer coefficient.

Some reactions have the diffusion of reactant molecules through a solvent as the rate determining step. In extraction metallurgy where temperatures in excess of the

melting points of metals are normally used, the chemical reaction rate is not normally the rate determining step. The transport of reactants to and/or products away from the reaction site tends to be the rate controlling step. Therefore, increasing turbulence, providing large slag-metal interfacial areas in liquid metal refining processes, and the use of gaseous reductants, with their improved diffusivity, are used to improve the reaction kinetics in process metallurgy.

The study of mass transfer theory is useful when the rate controlling step is the transport of a substance to or away from the reaction interface. Mass transfer in the bulk of liquids and gases is mainly by convection or turbulence (forced convection), but within a small distance $\delta$, of the interface (the effective boundary layer) molecular diffusion is the main mode of transport. The rate of molecular diffusion can be represented by Fick's first law which states that

$$J = - D \frac{dc}{dx} \qquad (1.26)$$

where J (the flux) is the mass (m) of substance transported in unit time (t) through unit area (A) of a plane at right angles to the direction of diffusion and can be represented as $(dm/dt)\ A^{-1}$. The term D is the diffusion coefficient and dc/dx the concentration (c)

gradient within a distance x from the interface (Fig. 1.18). Hence within the effective boundary layer, $\delta$, the flux can be defined as

$$J = \frac{1}{A} \frac{dm}{dt} \tag{1.27}$$

or

$$J = \frac{D}{\delta} \frac{dc}{dx} \tag{1.28}$$

Therefore

$$\frac{1}{A} \frac{dm}{dt} = \frac{D}{\delta} \frac{dc}{dx} \tag{1.29}$$

If the limits of concentration of the diffusing substance at the interface and at the extent of the effective boundary layer (bulk concentration) are $C_i$ and $C_b$ respectively, equation (1.29) can be written as

$$\frac{dm}{dt} = \frac{D\ A}{\delta} (C_i - C_b) \tag{1.30}$$

From equation (1.30) it can be seen that the rate of mass transfer, dm/dt, within the effective boundary layer is dependent on D,A and $\delta$. Therefore, decreasing $\delta$ by increasing turbulence, e.g. inert gas or oxygen blowing, and increasing the interfacial area will improve the rate of mass transfer and hence the reaction kinetics of the

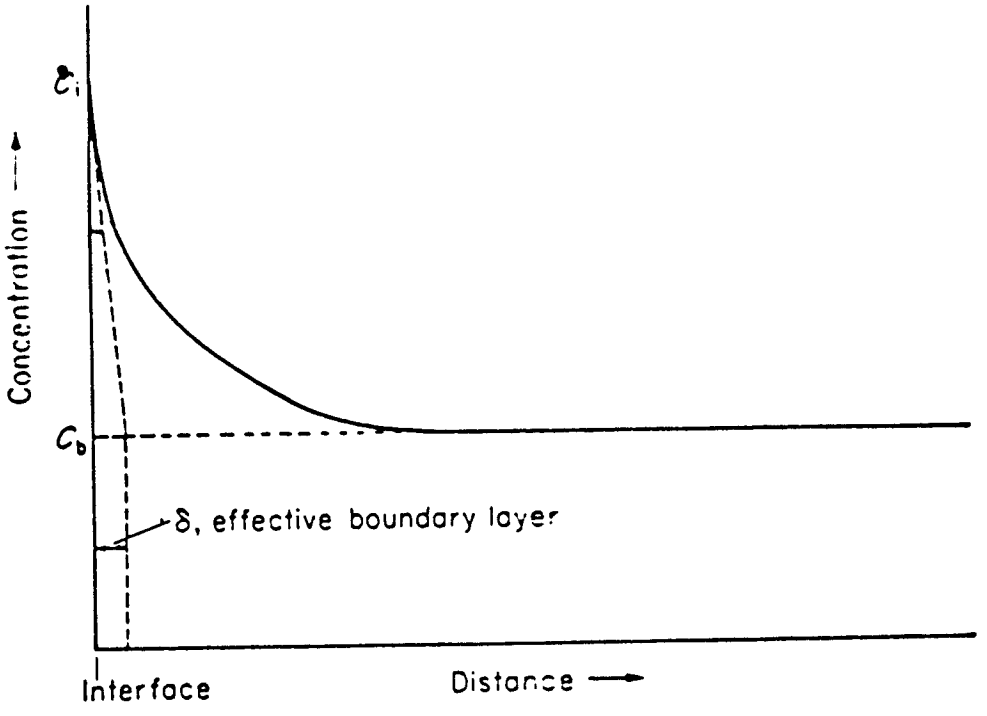


Fig. 1.18 Concentration gradient of a solute adjacent to an interface and graphical construction of the associated effective boundary layer, (25).

process. $D A/\delta$ is called the mass transfer coefficient i.e.

$$\frac{dm}{dt} = k_m (C_i - C_b) \qquad (1.31)$$

This is the basic equation for the transfer of materials to or away from a phase boundary layer.

### 1.5.1.2 Chemical reactions as the slow step.

The majority of reactions of importance in extraction metallurgy have been shown to follow first-order reaction kinetics. A general reaction form can be represented as[26]:

$$X + Y + .... \underset{k_2}{\overset{k_1}{\rightleftharpoons}} G + H + .... \qquad (1.32)$$

where the rate of the forward reaction is

$$\text{Rate} = k_1 C_x^{\alpha}, C_y^{\beta} \qquad (1.33)$$

and the order of the reaction is given by $\alpha + \beta + .....$ Thus for a first-order heterogeneous reaction:

$$\text{Rate} = k_1 C_x \quad \text{mol cm}^{-2} \text{ s}^{-1} \tag{1.34}$$

and for a second order reaction either

$$\text{Rate} = k_1 C_x C_y \quad \text{mol cm}^{-2} \text{ s}^{-1} \tag{1.35}$$

or

$$\text{Rate} = k_1 C_x^2 \quad \text{mol cm}^{-2} \text{ s}^{-1} \tag{1.36}$$

The constant $k_1$ is known as the forward rate constant and can be seen to have dimensions of $\text{cm} \cdot \text{s}^{-1}$ for a first-order reaction. The rate constant provides a useful measure of the rate of a chemical reaction at a specific temperature. It is important to realise that its units depend on the order of the reaction. If the reaction rate at the reaction site is slower than transport of reactants or products, then the chemical reaction becomes rate controlling. Determination of the rate constants for the reaction steps provides more information as to which reaction step is the slowest and thus the rate determining step. The overall rate is thus controlled by the rate of the slowest step.

The activation energy is a useful parameter in determining reaction mechanisms and in predicting reaction rates at given temperatures. Of importance in determining the activation energy is the Arrhenius

equation given by

$$\text{Ln } k = \text{Ln } A - \frac{E}{R\,T} \qquad (1.37)$$

or in exponential form as

$$k = A \times e^{-E/RT} \qquad (1.38)$$

where k is the rate constant of the reaction

E , the activation energy

A, the frequency factor.

To obtain the activation energy, the values of k, the rate constant, at two different temperatures at least are required. Preferably more data should be available so that calculation can be done graphically.

According to King[27] the activation energies for reactions which are transport-controlled by diffusion in liquid metals are between 5 and 30 kcal/mol and presumably between 30 and 70 kcal/mol if diffusion in slags is the rate controlling process. Generally, the activation energies for diffusion in slags is about ten times those for metals. Activation energies for chemical reaction-controlled reactions are generally higher than mass transport-controlled reactions. Grimeley et al[28] have found the energy required to

break Cr-O bonds to be approximately 102 kcal/mol. The activation energy of CrO reduction by silicon, a chemical reaction-controlled process, obtained by Robison et al[31] was 130 kcal/mol.

## 1.6 Previous work on the reduction of chromium oxide.

The reduction of chromium oxide has been studied for a long time because of its importance in the production of steel and chromium ore smelting. Most studies have been carried out in slag-metal systems under oxidising conditions. Although there is little information on the reduction of chromium oxide, there seems to be conflicting opinions as to what the rate determining step governing the reduction reactions is.

McCoy and Philbrook[20] studied the reduction of chromium oxide from lime-silica-alumina slags by carbon-saturated iron in rotating graphite crucibles. They observed chromium oxide to be present in slag as CrO, under the conditions studied, and its reduction was controlled by a chemical reaction which follows a first-order process with respect to chromium and having a rate of 0.001 g Cr $min^{-1}$ $cm^{-2}$ $(\%Cr)^{-1}$. They found the rate to be substantially independent of temperature in the range from 1500 to 1650°C and of slag basicity in the range from 0.6 to

2.5 lime-silica ratio. A constant slag-metal distribution ratio for chromium was not found because of simultaneous reduction of silica from the slag, which was about 20 to 60 times slower than chromium reduction under the conditions studied.

Strater and Mantell[29] studied the reduction of pure solid chromium oxide by hydrogen in the temperature range from 1130 to 1490°C, by comparing the measured water-vapour concentration to the equilibrium water-vapour concentration for the equilibrium between $Cr_2O_3$ and chromium. They observed that $Cr_2O_3$ was reduced directly to chromium without forming the intermediate, CrO, and assumed chemical reaction at the oxide-metal interface to be rate controlling. They found the activation energy for $Cr_2O_3$ to be 29.6 kcal.

A parallel reduction of silica was also observed by Boronenkov et al[30] in their study of the kinetics of reduction of chromium oxide from a synthetic slag containing 35%$SiO_2$, 30%MgO, 30%$Al_2O_3$ and 5%CaO and additions of $Cr_2O_3$ from 16-20% at 1600°C by continous automatic weighing of graphite crucibles containing the charge. They explained their results by the electrochemical mechanism of the reduction reaction which is a sum of two stages:

$$Cr^{3+} + 3e^- = Cr \qquad (1.39)$$

$$C + O^{2-} - 2e^- = CO_{ads.} = CO(g) \qquad (1.40)$$

With concentrations of $Cr_2O_3 \geq 6\%$ the process was controlled by carbon oxidation (reaction 1.40) while with sufficiently low (less than 2%) concentrations of $Cr_2O_3$ diffusion of chromic ions in the slag (reaction 1.39) was controlling the process.

Robison and Pehlke[31] studied the reduction of chromium oxide from a basic steelmaking slag (45%CaO, 35%$SiO_2$, 10%MgO and 10%$Al_2O_3$), at steelmaking temperatures by silicon dissolved in liquid iron, with the slag and metal phases held in zirconia crucibles. They suggested that the reduction reactions take place in two distinct stages:

$$(Cr_2O_3) + [Si] = (SiO_2) + (CrO) + [Cr] \qquad (1.41)$$

$$(CrO) + \frac{1}{2}[Si] = \frac{1}{2}(SiO_2) + [Cr] \qquad (1.42)$$

and that both reactions were rapid with equilibrium being attained within two hours at 1575°C. From the effects of changes in composition, stirring rate and temperature they found the rate-determining step for reduction of trivalent chromium to be the transport of trivalent chromium from the bulk slag to the slag/metal interface.

The reduction of divalent chromium was found not to be sensitive to variations in stirring rate or silicon content of the metal but the effect of temperature was large. The rate determining-step for the reduction of divalent chromium was found to be an interfacial chemical reaction which was first-order with respect to divalent chromium in the slag.

Sevinc and Elliot[32] studied the kinetics of reduction of solid $Cr_2O_3$ by carbon dissolved in liquid Fe-Cr alloys in the temperature range from 1540 to 1705°C. The experiments were done by rotating cylinders of the oxide in the liquid alloy and following the progress of the reaction by measuring the volume of CO gas evolved as a function of time. They considered the overall rate to consist of a series of steps involving chemical reaction and transport processes. Based on theoretical and experimental considerations, they concluded that the reaction rate was determined by transport of oxygen in the liquid metal at either or both of the oxide/metal and gas/metal interfaces as shown in Fig. 1.19.

An investigation into the rate of reduction of $Cr_2O_3$ by carbon dissolved in liquid iron alloys, and the decarburisation of Fe-Cr-C alloys studied by Fruehan[33], in the temperature range from 1300 to 1600°C, showed that the initial rate of reduction of $Cr_2O_3$ by solid carbon

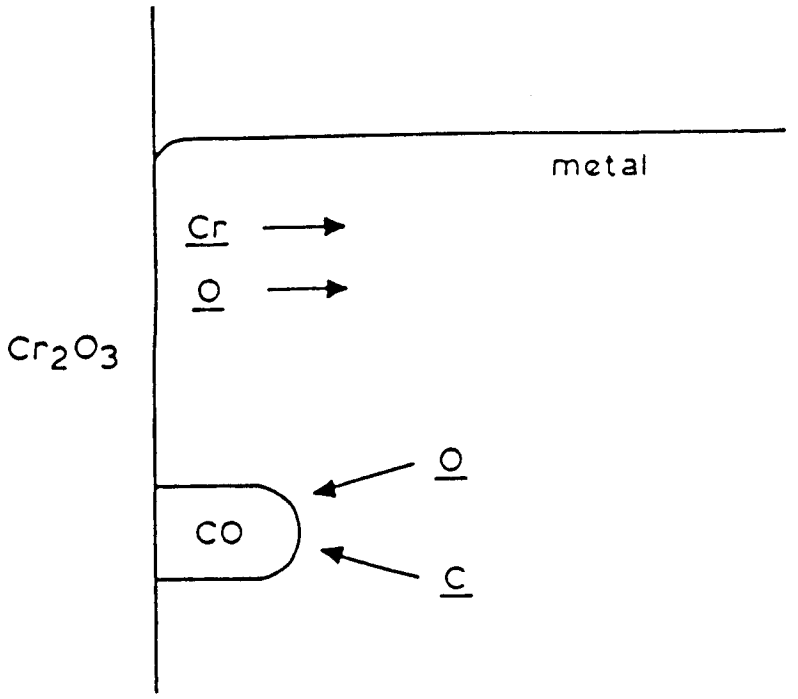


Fig. 1.19 Schematic diagram of reacting system (32).

was controlled by gas-phase mass transport of CO away from the reactants. He also concluded that the decarburisation of Fe-Cr-C alloys by $Cr_2O_3$ was controlled by diffusion of carbon to the liquid $Cr_2O_3$ surface. The chemical diffusion coefficient of carbon in liquid derived from his experimental results is 8.5 x $10^{-5}$ $cm^2$ $s^{-1}$.

Suzuki and Mori[34] studied the rate of reduction of $Cr_2O_3$ by carbon dissolved in Fe-Cr melts at 1580°C in an Ar atmosphere. A cylinder of oxide was rotated in the melt and the rate of reaction was determined from the rate of decrease in the diameter of the cylinder. They found the rate of reduction of $Cr_2O_3$ by carbon in the melt to be influenced by the rotational speed of the cylinder and the extent of CO evolution at the oxide/melt interface. The rate of reduction was found to be controlled by the rate of mass transfer of oxygen across the boundary layer in the melt at the solid/melt interface.

From his study on the reduction of $Cr_2O_3$ from slag at temperatures in the range from 1400 to 1470°C, Hacioglu[35] proposed that the reduction of chromium oxide takes place in two steps. In the initial period $Cr_2O_3$ is reduced to CrO in slag at a very fast rate and in the following period CrO is reduced to Cr in metal at

a slower rate. This is in accord with the observation of Robison and Pehlke[31]. He observed that FeO is formed by an exchange reaction between iron and chromium oxide. From the effects of different variables he found the rate limiting step for $Cr_2O_3$ reduction to be an interfacial chemical reaction, taking place at the slag/gas interface.

Maeda and Sano[16] used a graphite lined rocking furnace in their study of the rate of chromium reduction from slag (35% CaO, 19.3% MgO, 13.2% $Al_2O_3$, 31.5% $SiO_2$ and 2.2 %Cr) by carbon dissolved in iron. About two kilogrammes of slag and four kilogrammes of metal were used in the runs. A first-order reaction in terms of chromium concentration in slag was observed. They found a close relationship between the behaviour of silica and chromium oxide in the slag i.e. the chromium in the slag was reduced as the reduction of silica proceeded. Using a slag of the composition 7.2% CaO, 25.4% MgO, 21.3% $Al_2O_3$, 29.6% $SiO_2$ and 8.8 %Cr, they found that a small addition of silica markedly improved the rate of reduction of chromium from slag. Microscopic analysis clarified this point and they showed that the original slag contained undissolved chromite which disappeared by silica addition.

Shimoo et al[36] studied the rate of reduction of

chromium oxide from aluminate slags by solid carbon (graphite crucible) by means of thermogravimetry under an Ar atmosphere. They observed that the reduction of CrO occurs at an interface between the slag and the carbon containing chromium melt, which is formed on the crucible wall after contact of the molten slag with the graphite. The rate of CrO reduction was represented by the first-order type rate equation and the rate constant ranges from $10^{-4}$ to $10^{-3}$ kg $m^{-2}s$ at 1620°C. The rate constant was found to increase with increasing $CaO/Al_2O_3$ ratio. They concluded that at low concentrations of CrO the reduction is controlled by chemical processes.

Anyakwo[37] studied the rate of reduction of $Cr_2O_3$ from $CaO-SiO_2-Al_2O_3$ and $CaO-SiO_2-MgO$ slags by carbon dissolved in molten iron at temperatures in the range from 1400 to 1550°C. In accord with the observation of Robison and Pehlke[31] and later Hacioglu[35], he observed the presence of two reaction regimes in the reduction reactions, an initial fast reduction of $(Cr^{3+})$ to $(Cr^{2+})$ followed by a slower reduction of $(Cr^{2+})$ to [Cr] which takes place concurrently with silica reduction. He concluded that $(Cr^{3+})$ reduction is limited by its transport from the slag to the reaction interface and $(Cr^{2+})$ reduction by interfacial chemical reaction. By introducing surface active elements (sulphur and antimony) into the system, the rate of reduction of all

the chromium species was markedly increased with an attendant increase in FeO concentration in the slag. Enhanced metal emulsification which increases the surface area for the reduction reactions to take place, was thought to be responsible for the increase in the rate of chromium oxide reduction.

A kinetic study on the smelting reduction of bottom-injected chromite ore powder by dissolved carbon in liquid iron melt was conducted by Kawakami et al[39] at steelmaking temperatures. They injected pulverised chromite ore from the bottom of the crucible into 20 kg of a liquid iron-carbon alloy so that the ore was reduced by the dissolved carbon. A linear increase in the chromium yield with temperature was observed. From the study of the effects of [Cr] and [C] on the reduction rate, they concluded that the rate determining-step was the transport of oxygen, either from the ore/melt interface to the bulk, or from the bulk to the bubble/melt interface where CO would be evolved. Their conclusion is in accord with that of Sevinc and Elliot[32] and Suzuki and Mori[34]. The injection rate was found to have no effect on the rate of reduction of the chromium ore.

Fukagawa and Shimoda[40] investigated the smelting reduction mechanism of chromium ore sinter by solid

carbon at 1650°C. By microscopic analysis of slag samples (taken at different times) they observed that chromium ore particles are dispersed in molten slag and gradually dissolve in the slag as the reduction progresses. The reduction rate was found to be controlled by the reduction of chromium oxide in the slag at the slag/graphite interface.

Shimoo et al[41] investigated the rates and mechanism of the reduction of chromium oxide in $CaO-SiO_2$ slags by solid carbon in the temperature range from 1500 to 1700°C and concentrations of $Cr_2O_3$ ranging from 10 to 50 wt% with the slag basicity $CaO/SiO_2$ taking values from 0.5 to 1.4. The rate of reduction was determined from the weight loss, measured by means of thermogravimetry under an Ar atmosphere. They observed that the rate of reduction increased up to a basicity of about 0.9, and decreased as the basicity increased up to 1.4. An acceleration of the reduction of $Cr_2O_3$ at an early stage was caused by an increase in contact area of the slag and graphite.

The smelting reduction rate of chromium ore in top-and-bottom blowing converter was quantitatively estimated by Kitamura et al[42] using a 600 kg scale experiment and a 100 t scale industrial furnace (LD-OB). They found the rate of reduction of chromium oxide in the

slag to show zero-order reaction kinetics. The rate was proportional to the stirring energy and the diameter of the furnace. According to their results, they postulated that the transfer of chromium oxide in molten slag phase to the carbon/slag and the metal/slag interfaces was the rate controlling step.

# CHAPTER 2

# APPARATUS & EXPERIMENTAL TECHNIQUES

# Chapter 2

# APPARATUS AND EXPERIMENTAL TECHNIQUES.

## 2.1 Furnace and Reaction tube.

The experiments were carried out in a vertical carbolite silicon carbide resistance furnace containing an impevious mullite reaction tube of 50 mm internal diameter and 900 mm long. The furnace was heated by six silicon carbide rods connected in series.

The mullite reaction tube was sealed at both ends by water cooled brass furnace ends. The top brass end had a central hole for viewing and sampling plus a gas inlet hole. The bottom brass end had a gas outlet hole and a hole through which the thermocouple for taking the actual temperature was inserted. Fig. 2.1 shows a schematic representation of the silicon carbide resistance furnace used.

Control of temperature was done using a Eurotherm type PID/SCR Thyristor controller with an accuracy of $\pm$ 10$^{o}$C and a maximum temperature of 1600$^{o}$C. It was operated by a Pt/13% Pt-Rh thermocouple located in the middle of the furnace. The actual experimental temperature was

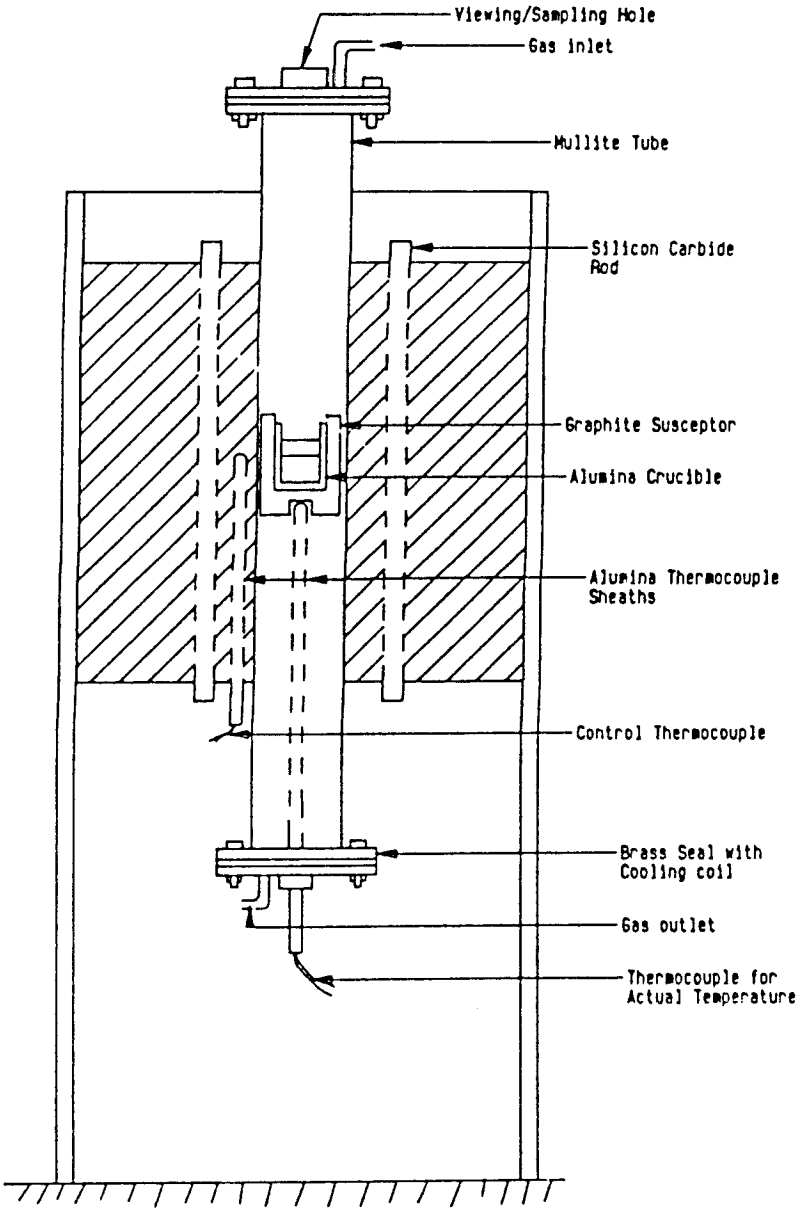


Fig. 2.1 Schematic representation of Silicon Carbide Resistance Furnace.

measured by a Cambridge Potentiometer connected to a Pt/13% Pt-Rh thermocouple in a mullite sheath which supported the graphite susceptor in which the alumina reaction crucible was placed.

The hot-zone of the furnace was located by carrying out a temperature profile along the reaction tube from the bottom. This was done each time the reaction tube was changed. The hot-zone was found to be between 4-5 cm high and this is were the crucible assembly was placed during the experimental runs. Fig. 2.2 shows an example of the determination of the hot-zone and Fig. 2.3 a plot of the temperature profile along the reaction tube.

## 2.2 Materials and Preparation

### 2.2.1 Materials

(a) Iron

Japanese electrolytic iron, >99.9% purity was used to produce iron-carbon alloys.

(b) $Al_2O_3$, $CaCO_3$, $CaF_2$

The 'Analar' grade of the chemicals supplied by BDH were used.

Furnace control temperature at 1540°C

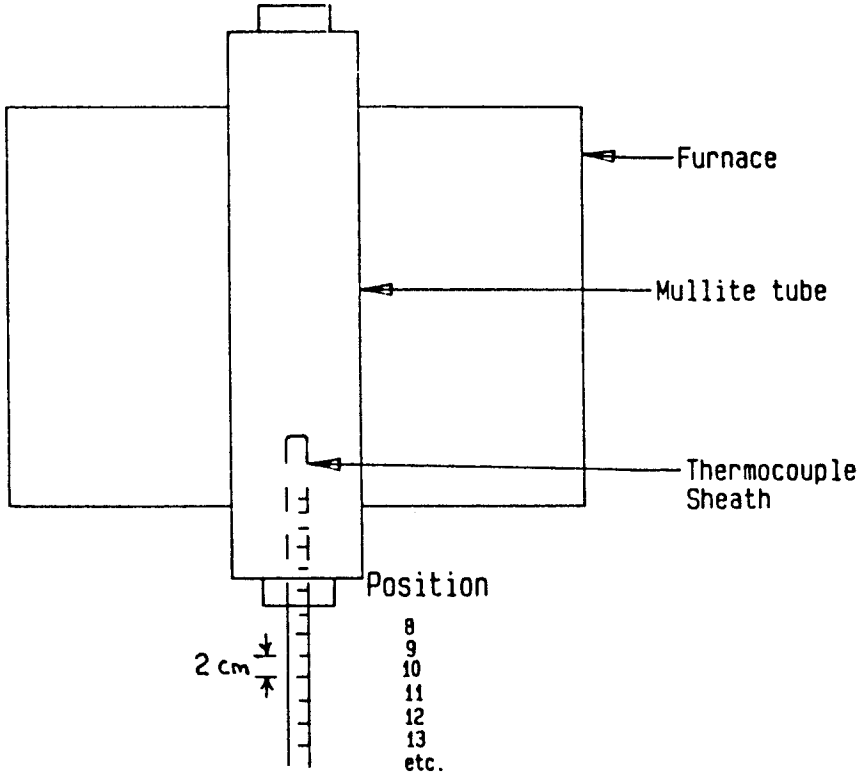


| Position | Temperature °C |
|---|---|
| 8 | 1085 |
| 9 | 1147 |
| 10 | 1244 |
| 11 | 1300 |
| 12 | 1374 |
| 13 | 1425 |
| 14 | 1473 |
| 15 | 1505 |
| 16 | 1519 |
| 17 | 1520 |
| 18 | 1510 |
| 19 | 1490 |
| 20 | 1470 |
| 21 | 1450 |
| 22 | 1420 |

Fig. 2.2 Determination of Hot-zone in Furnace tube.

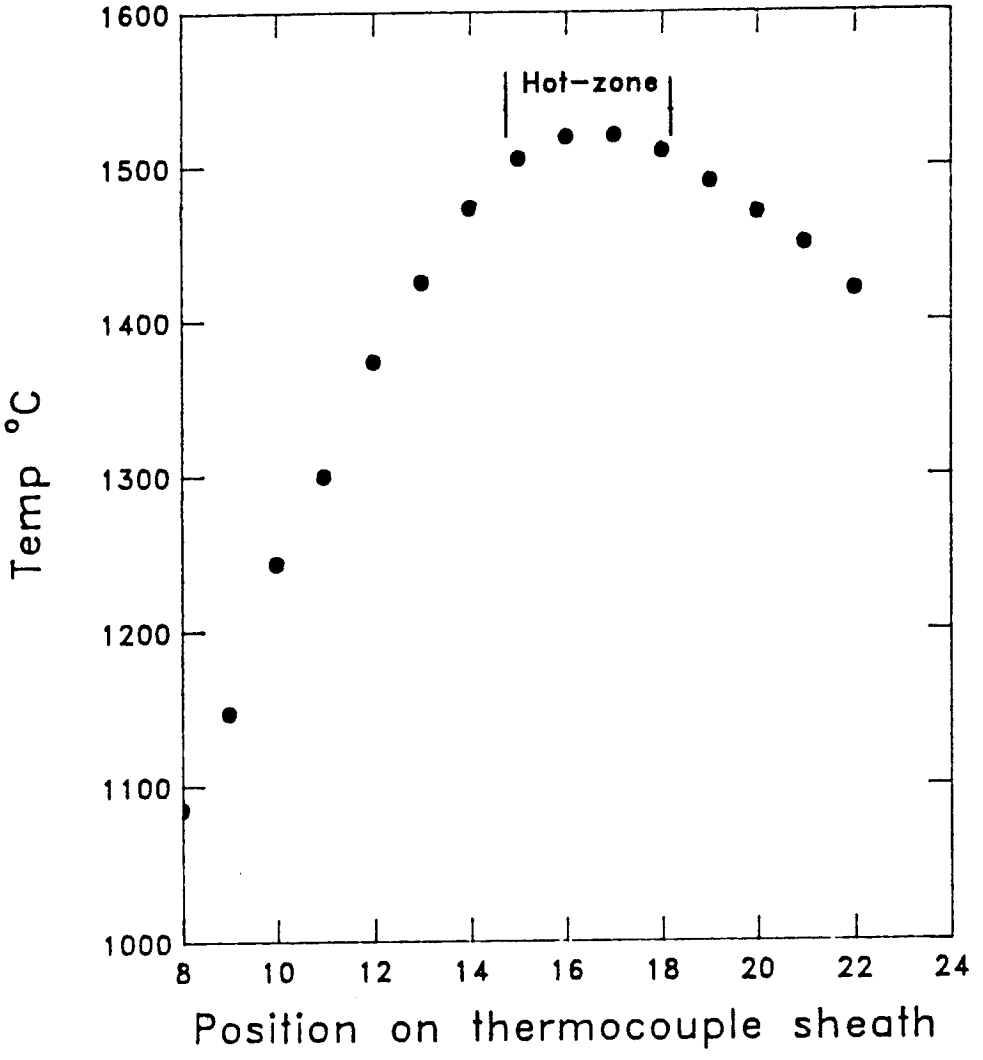


Fig. 2.3 Plot of temperature against position on thermocouple sheath.

(c) Silica

Silica was prepared by alternately washing silica sand repeatedly with hot concentrated hydrochloric acid and deionised water until no colour change was observed on further addition of the acid, an indication that the iron oxides had been removed. It was then dried and fired in an electric muffle furnace at 1000°C for 24 hours.

(d) $Cr_2O_3$

A general purpose reagent chromic oxide, supplied by BDH was used.

(e) FeS

Technical grade ferrous sulphide sticks supplied by Gallenkamp and Co. ltd was used.

(f) FeO

Iron oxide was made from ferrous oxalate in an iron tube by heating slowly through the 400-600°C region untill most of the gas evolution had completed and then increasing the temperature to 950°C more rapidly. The progress of gas evolution was followed by bubbling through water and when it had completely finished, the iron tube containing the FeO was quenched in water. The FeO produced was finely ground, demagnitised and analysed for its iron content. The phase identified using X-ray diffraction was mainly FeO.

(g) CaS

A general purpose grade calcium sulphide supplied by BDH was used.

(h) Se

'Analar' grade selenium supplied by BDH was used.

(i) Argon

High purity ( >99.998% ) argon gas was used as supplied by BOC ltd. The gas had the following impurities:

Oxygen < 3 vpm

Moisture < 3 vpm

Nitrogen < 8 vpm

Hydrocarbon < 1 vpm.

(j) Carbon monoxide

Carbon monoxide gas as supplied by BOC ltd. was used.

## 2.2.2 Metal preparation

Iron-carbon alloys of high carbon content (about 4.5 %) were prepared by melting Japanese electrolytic iron in a graphite crucible by high frequency induction heating. After the metal had melted, it was homogenised by stirring using a graphite rod and was then cast into graphite moulds, 28 mm in diameter, to form iron-carbon

alloy rods of 100-120 g. The rods were cut by a corrundum wheel into pellets weighing 50-60 g. Before using them, the pellets were buffed to remove any oxide adhering to the surface.

Carbon-saturated iron-sulphur and iron-selenium alloys were prepared by putting an appropriate weight of iron sulphide or selenium at the bottom of the alumina crucible under the carbon-saturated iron before an experiment.

### 2.2.3 Slag preparation

The master slag chosen for this study was a 42% $SiO_2$, 38% CaO, and 20% $Al_2O_3$ having a melting point of about 1265°C.

In making the slag, appropriate weights of the slag constituents were weighed out and mixed thoroughly in a container. An allowance in weighing $CaCO_3$ was made to take account of the $CO_2$ gas evolved on heating. The mixture was then put in a graphite crucible, compressed using a graphite rod and holes pierced in it for $CO_2$ to escape through on heating. The crucible was covered with a graphite lid to minimise material loss during calcination of calcium carbonate. The lid had a hole in the centre which served as a vent for liberated gas. The

crucible containing the mixture was then heated slowly in an induction furnace until gas evolution subsided, before increasing the temperature for the slag to melt. Once molten, the slag was homogenised by stirring several times with a graphite rod. The slag was then cast in an iron mould, ground to a fine powder and heated for 24 hours in an electric muffle furnace at 800$^{o}$C to decarburise it. After decarburisation, the master slag was kept in a dessicator to be used in the experimental runs.

For use in the runs, weighed quantities of the master slag were mixed with measured quantities of $Cr_2O_3$ and other slag additives, depending on the experimental conditions, to make a 20 g slag. The mixture was then pelletised in an electric press under a load of 15 tons before use.

### 2.2.4 Crucible assembly

Recrystallised alumina crucibles supplied by Morgan Co. Ltd. were used in all the experimental runs. They had the following dimensions:

| | |
|---|---|
| OD | 35 mm |
| ID | 32 mm |
| Height | 65 mm |
| Depth | 63 mm |

The alumina crucible containing metal and slag was held in a graphite susceptor of dimentions 45 mm OD, 35 mm ID and 110 mm in length with a central hole at the bottom of 10 mm diameter and 20 mm depth into which the thermocouple sheath fits (Fig. 2.4). The thermocouple acts as support for the crucible assembly in the reaction tube.

## 2.3 Experimental procedure

The master slag (with required amount of $Cr_2O_3$ and other additives) and metal pellets were placed in an alumina crucible and held in a graphite susceptor as shown in Fig. 2.4. The central hole at the bottom of the graphite susceptor was then fitted onto the thermocouple sheath containing the thermocouple to take actual experimental temperatures. The thermocouple sheath acted as a support for the crucible assembly in the furnace. The crucible assembly was raised in the reaction tube to a predetermined position where it was held at a temperature of about 1000$^{o}$C until it attained a uniform temperature. This took about 10 minutes. Once this was achieved, the assembly was raised quickly into the hot-zone of the reaction tube, this time being taken as the zero time of an experimental run. Argon or carbon monoxide was passed through the reaction tube at one atmosphere pressure to maintain a neutral atmosphere.

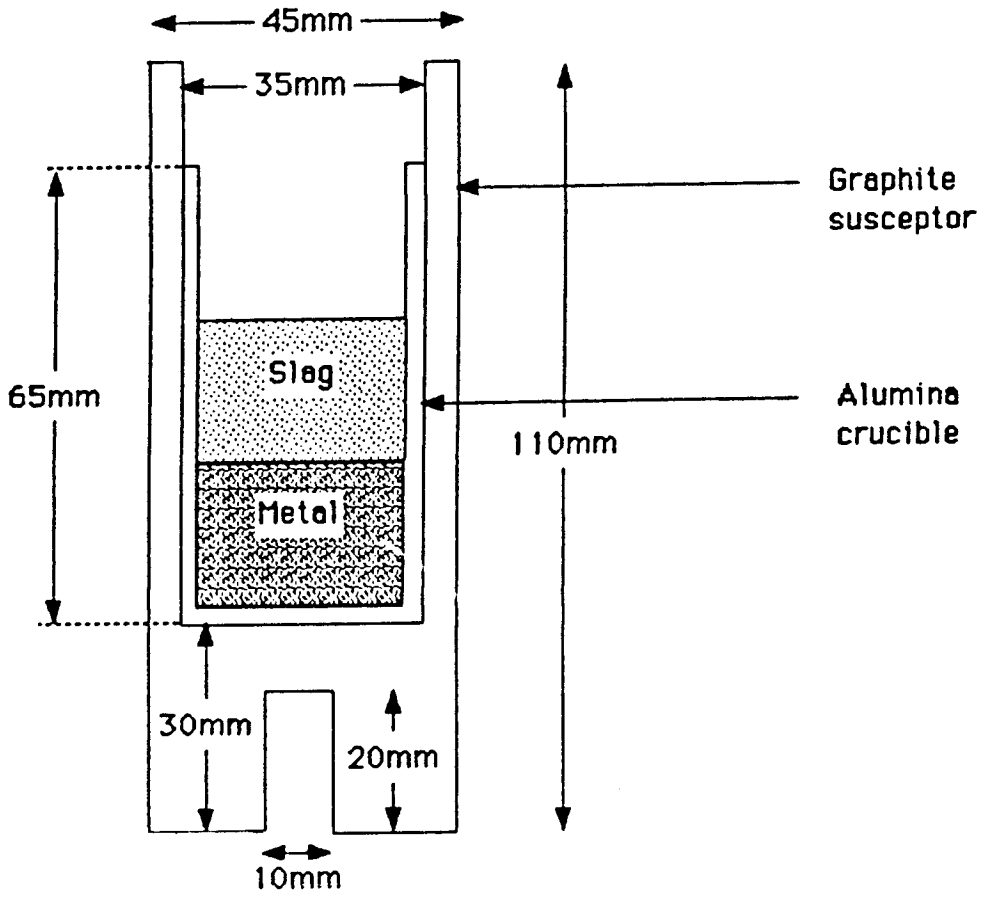


Fig. 2.4 Schematic representation of crucible assembly.

The slag was sampled at predetermined time intervals by chilling it at the copper tip of a steel sampling rod. A metal sample was taken, at the end of each run, by suction into a 5 mm ID silica tube. The crucible assembly was then quickly removed from the furnace. The slag samples were ground in an agate mortar and treated with a bar magnet to remove any iron particles before analysis, as this could interfere with the iron analysis.

The slags were analysed for total iron, total chromium and divalent chromium. Trivalent chromium was obtained by difference between the total and divalent chromium values. In the runs where sulphur was added to the metal or slag, the slag and final metal were analysed for their sulphur contents. The metal was analysed for the chromium and carbon content at the end of each run.

## 2.4 Analysis methods

### 2.4.1 Analysis of total Iron in slag

The total iron concentration of the slag was determined using a Perkin-Elmer model 103 atomic absorption spectrophotometer.

The iron stock standard solution (1000 $\mu g\ ml^{-1}$) was

prepared by dissolving 1 g of iron wire in 50 ml of (1+1) nitric acid and diluting to 1000 ml with deionised water. Standard solutions were made from the stock solution to fall within the linear working range for Fe (up to approximately 5 $\mu g\ ml^{-1}$ in aqueous solution) for the conditions described in the Perkin Elmer, model 102 and 103 instruction manual[43].

Slag sample stock solutions (1000 $\mu g\ ml^{-1}$) were prepared by fusing 0.1 g of slag samples with 0.7 g sodium carbonate and 0.3 g sodium tetraborate in a platinum crucible over a meker burner. Once fusion was attained, the mixture was dissolved in 20 ml (1+1) nitric acid, transfered to a 100 ml volumetric flask and made up to the mark with deionised water. Appropriate aliquots were pipetted from the slag sample stock solutions and made up to 100 ml to bring them within the linear working range for iron analysis. The standard and slag sample solutions were then aspirated to determined the total iron content using an air-acetelyne flame and the conditions specified in the instruction manual[43]. The iron content of the slag samples was then determined by comparison with the calibration curves obtained from the standard solutions.

To ascertain the precision of this technique, multiple analyses were performed on a B.C.S. slag containing a

suitable range of iron. Using the 95% confidence interval the uncertainty in the slag iron content was found to be ± 0.02 wt% Fe.

Iron in the slag was assumed to be present as FeO, and as such the Fe analysis obtained was considered to be the $Fe^{2+}$ ion content of the slag. In order to substantiate this assumption, slag samples for a particular run were analysed for total iron and $Fe^{2+}$ to see whether similar values could be obtained. The method used for $Fe^{2+}$ analysis is described in the next section.

### 2.4.2 Analysis of $Fe^{2+}$ ion

0.4 g of sample was dissolved in 25 ml boiling 1:1 hydrochloric acid. A few drops of hydrofluoric acid were added to the solution to dissolve insoluble silica. The solution was then cooled slowly to room temperature under tap water. This was followed by addition of 10 ml of 15% orthophosphoric, 15% sulphuric acid mixture and 8-10 drops of 0.2% sodium diphenylamine sulphonate solution as an internal indicator. This solution was finally titrated against N/100 standard potassium dichromate solution to an intense purple end point. All the steps above were carried out under a stream of argon which provided an inert atmosphere to prevent oxidation of ferrous to ferric ion.

Multiple similar analyses on a B.C.S. slag containing suitable range of FeO gave an uncertainty of approximately ± 0.02 wt% $Fe^{2+}$.

Comparison of the values from $Fe^{2+}$ analysis with those from the total iron analysis showed that they were similar within experimental error. This result was in accord with the assumption that Fe was present in the slag as FeO.

### 2.4.3 Analysis of total chromium in slag

An atomic absorption method was used for total chromium analysis. A chromium stock standard solution (1000 μg $ml^{-1}$) was prepared by dissolving 3.735 g of potassium dichromate, $K_2CrO_4$, in 1000 ml of deionised water. Standards were made by pipetting appropriate aliquots from the standard stock solution and made up to 100 ml to fall within the linear working range for chromium analysis (up to concentrations of approximately 5 μg $ml^{-1}$ in aqueous solution) to determine the calibration curve. Appropriate aliquots were pipetted from the slag sample stock solutions prepared in the total iron analysis and made up to 100 ml to fall in the linear working range for chromium analysis for the conditions specified in the instruction manual. The chromium content of the slag was

then determined by comparison with calibration curve obtained from the standard solutions.

This method was checked by carrying out multiple analyses of a B.C.S. slag containing a suitable range for chromium. An uncertainty of about ± 0.03 wt% $Cr_t$ was found using the 95% confidence interval.

### 2.4.4 Analysis of Divalent chromium in slag

In the analysis of divalent chromium in the slag the method of Robison and Pehlke[44] was applied. Basically, the chromous and ferrous ions of the slag are oxidised by vanadate ions, $VO_3^-$, of known concentration. The excess vanadate ions are then estimated by titration with ferrous sulphate solution of known concentration. Knowing the $Fe^{2+}$ concentration of the slag (from atomic absorption analysis) the $Cr^{2+}$ concentration can then be evaluated.

About 0.1-0.4 g of slag sample was placed in a 250 ml beaker into which 20 ml of 0.02 N sodium metavanadate solution followed by 150 ml of 0.6 M sulphuric acid were added. The beaker was then placed on a hot plate and the solution digested for about 30 minutes. After complete digestion, the beaker was placed in an ice bath and the

solution acidified to 6 M with concentrated sulphuric acid. The digestion was done in air, as pointed out by Robison and Pehlke[44] who found no difference in the results when digestion was accomplished under air or argon so long as an excess of oxidising agent, in this case $VO_3^-$, is present.

The digested solution was then potentiometrically titrated with 0.02 N ferrous sulphate solution. The titre established the total number of moles of $Cr^{2+}$ and $Fe^{2+}$ in the original sample. Blank titrations using solutions similarly prepared but bearing no slag samples were carried out and their titres used in the calculation of the $Cr^{2+}$ content of the slag.

The titration apparatus was developed from a similar set-up described by Lingane and Pecsock[45]. The titration vessel was a 250 ml beaker and agitation of the solution was electromagnetically perfomed using a GallenKamp Magnetic Stirrer/Hot plate. The platinum wire which serves as indicator electrode was wound as a spiral on the bottom of a glass rod and dipped into the solution. The other end of the platinum wire was connected to a potentiometer model 7020 supplied by EIL. The two beakers containing the saturated potassium chloride solution and the digested slag solution were elctrically connected by a salt bridge (containing about

1-2 N sulphuric acid) with ends closed by internal ground-glass plugs. A saturated Calomel reference electrode dipping into a beaker containing saturated potassium chloride solution was also connected to the potentiometer. A set-up of the titration apparatus for chromous solutions used is shown in Fig. 2.5.

The $Cr^{2+}$ content of the slag was calculated from the titre as follows: Suppose 0.2 g of the slag sample containing 0.25% Fe is titrated with 0.02 N ferrous sulphate solution giving a titre of 18.7 ml $FeSO_4.7H_2O$. Assume a blank titration of 19.6 ml. The titre establishes the number of moles of $Cr^{2+}$ and $Fe^{2+}$ in the slag sample from the following reactions

$$Cr^{2+} + V^{5+} = Cr^{3+} + V^{4+} \qquad (2.1)$$

$$Fe^{2+} + V^{5+} = Fe^{3+} + V^{4+} \qquad (2.2)$$

Now, 0.02 N $FeSO_4.7H_2O$ contains 5.5602/1000 g of $FeSO_4.7H_2O$ $ml^{-1}$. Therefore

0.9 ml of $FeSO_4.7H_2O$ contains (5.5602/1000) * 0.9 g of $FeSO_4.7H_2O$

In terms of moles, this is equivalent to

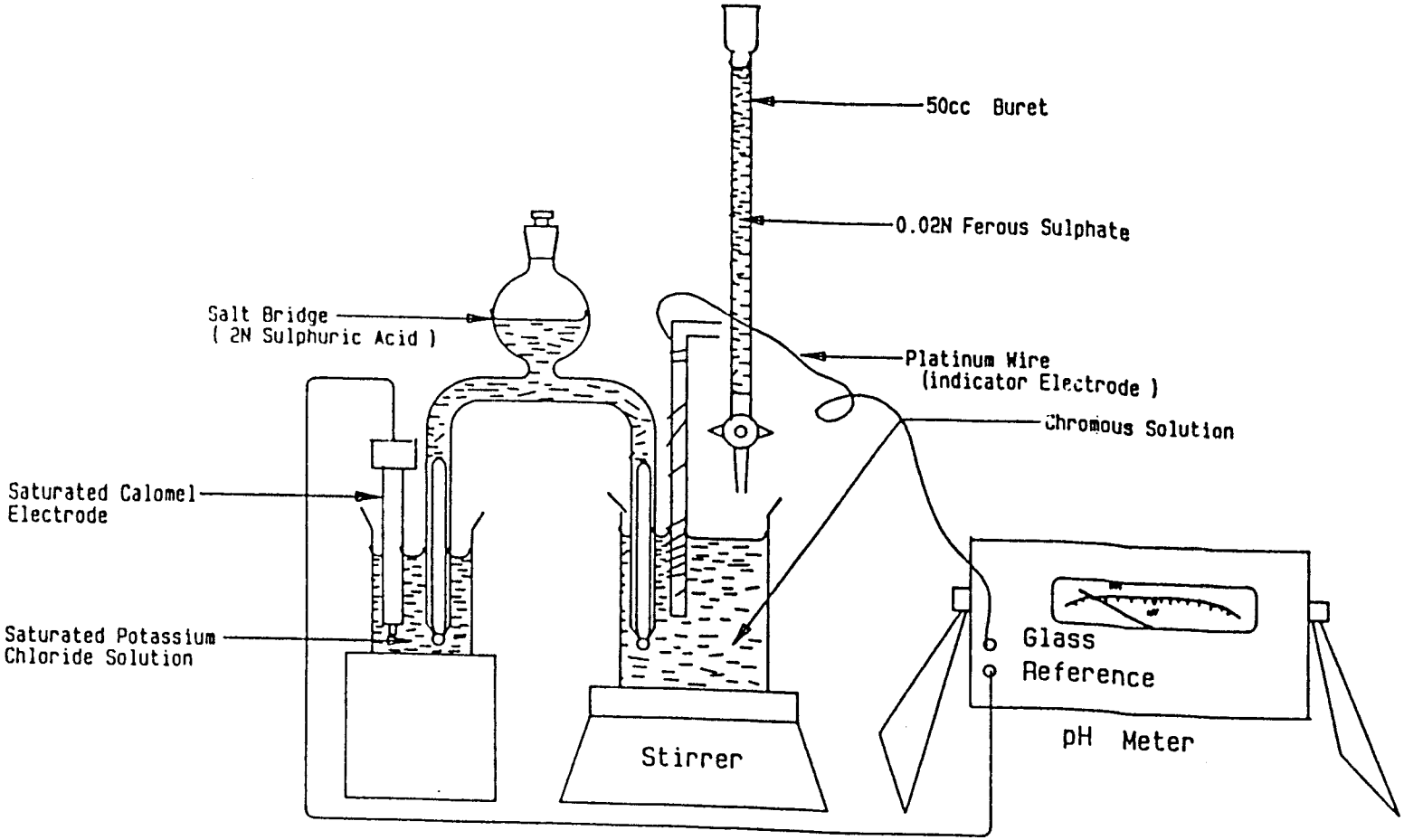


Fig. 2.5 Titration apparatus for titration with chromous solutions.

$$M = \frac{5.5602 \times 0.9}{1000 \times 278.01} \quad \text{moles } FeSO_4.7H_2O$$

This is also equal to the number of moles of $Cr^{2+}$ and $Fe^{2+}$ in the slag sample titrated. The number of moles of $Fe^{2+}$, W, in 0.2 g slag sample is calculated and subtracted from M.

Therefore,

moles of $Fe^{2+}$ in slag

$$W = \frac{0.25 \times 0.2}{100 \times 56} \quad \text{moles}$$

and moles of $Cr^{2+}$ in slag = M - W. Thus

$$\text{wt\% } Cr^{2+} = \frac{(M - W) \times 51.996 \times 100}{0.2}$$

The precision of this technique was checked by carrying out multiple $Cr^{2+}$ analyses on a crushed slag sample. The uncertainty using the 95% confidence interval was found to be $\pm$ 0.02 wt% $Cr^{2+}$.

### 2.4.5 Analysis of chromium in metal

The concentration of chromium in the metal was determined using atomic absorption spectrophotometric method.

Chromium stock standard solutions were prepared as in the analysis of total chromium in slag. The calibration curve was obtained by analysing standard solutions prepared by pipetting appropriate aliquots from the stock solution and making them up to 100 ml to make them fall within the linear working range for chromium analysis (up to concentrations of 5 $\mu g\ ml^{-1}$ in aqueous solutions).

Metal sample stock solutions were prepared by digesting 0.5 g of metal in 10 ml (1+1) hydrochloric acid on a hot plate until all soluble material was dissolved. The solution was oxidised by adding 3-4 drops of concentrated nitric acid and boiled to remove nitrous oxide fumes. It was then transfered to a 100 ml volumetric flask and made up to the mark. Appropriate aliquots were then pipetted from the sample stock solutions and made up to 100 ml to bring them in the linear working range for chromium analysis. The solutions were then aspirated and the chromium content of the metal was determined by comparison with the calibration curve. A nitrous oxide/acetylene flame was used plus other conditions as specified in the Pelkin Elmer instruction manual.

This method was checked by multiple analyses of a B.C.S. metal sample containing a suitable range of chromium. Using the 95% confidence limit, the uncertainty in the analysis was found to be approximately ± 0.02 wt% Cr.

### 2.4.6 Analysis of carbon in metal

The carbon content of the metal was determined using a Non-aqueous titration method[46]. Basically, carbon is oxidised to carbon dioxide by high temperature combustion of the sample in oxygen. The exit gases are passed through manganese dioxide to remove sulphur gases before absorbing the carbon dioxide in a mixture of formdimethylamide-ethanolamine. The carbon content of the sample is determined by titration with tetra-n-butylammonium hydroxide to the change point of thymolphthalein. The apparatus used is illustrated diagrammatically in Fig. 2.6.

The absorption solution (Formdimethylamide) was prepared by mixing 1800 ml of dimethylformamide with 60 ml mono-ethanolamine and 24 ml thymophthalein indicator (0.1 % w/v solution of thymophthalein in anhydrous methanol). With the furnace at 1250$^{o}$C, 20 ml of the absorption solution was introduced in the absorption/titration cell. The flow of oxygen from the supply line was regulated at

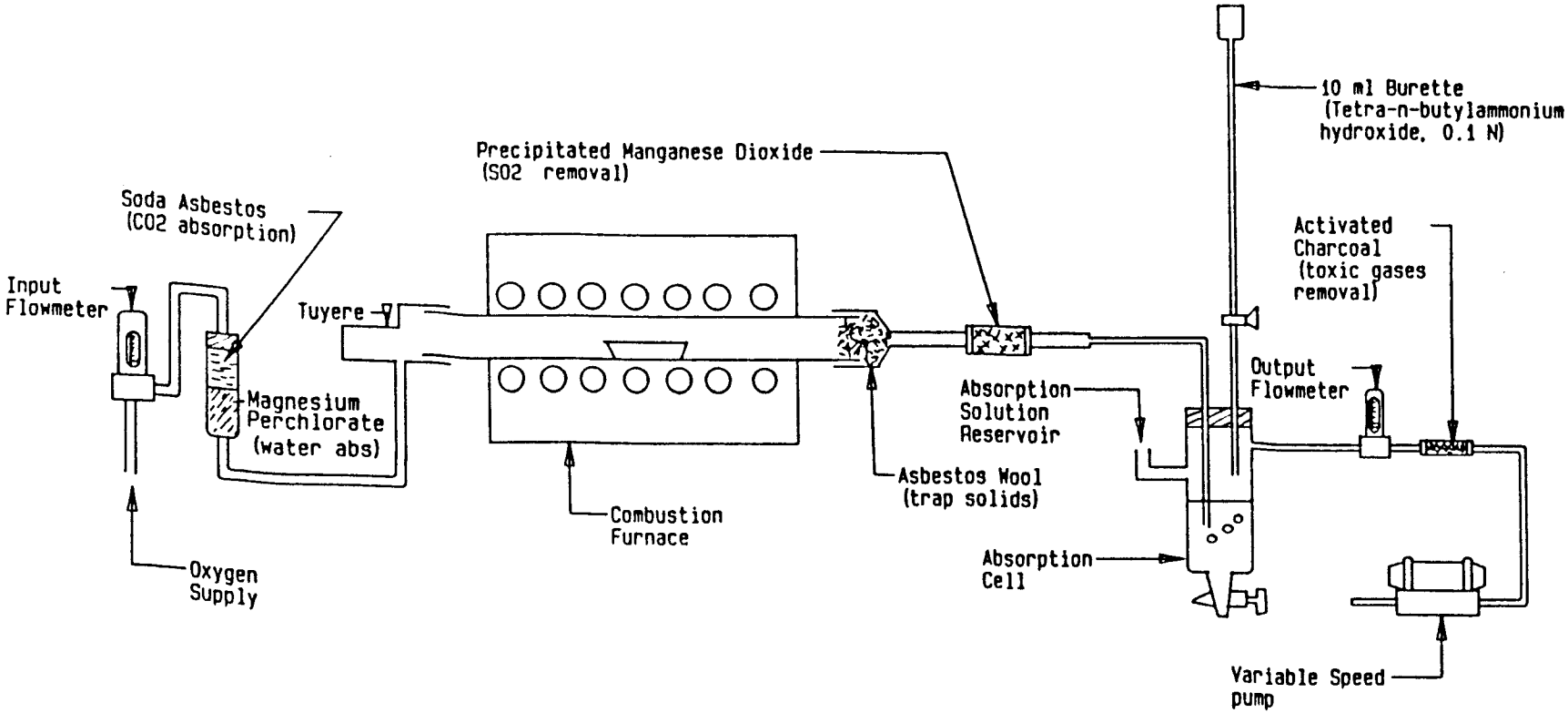


Fig. 2.6 Apparatus for the determination of carbon: Non-aqueous titration.

2 litres per minute on the input flowmeter, then by means of a variable speed pump oxygen was drawn through the system at 500 ml per minute as registered on the output flowmeter.

An empty boat was then transfered to the combustion furnace and oxygen passed at a regulated rate for 2-3 minutes to ensure complete oxidation of carbonaceous matter. The boat was removed from the furnace and left to cool. Before introducing a sample in the furnace, the absorption solution was titrated with tetra-n-butylammonium hydroxide solution (0.1 N) to a blue end point.

About 0.2 g of fine millings of the sample was transfered to a previously ignited combustion boat and covered with lead foil (flux), the boat was then pushed in the hot zone of the furnace.

As the absorption solution became decolorised during the combustion period, the titration with tetra-n-butylammonium hydroxide solution was continued as required until a *stable blue colour marked the end point.* The blank value of the apparatus, boat and flux using the same conditions *as in the test runs was determined to make the appropriate* correction in the carbon content calculation. The carbon content was determined using the following expression:

$$\%C = \frac{(A - B) \times 1.2 \times N}{W}$$

where A = titre in ml

B = blank titre in ml

N = Normality of titrant

W = Weight of sample in gm

Multiple analyses were carried out on B.C.S. metal sample to check the accuracy of the method. Using the 95% confidence limit, the uncertainty of the analysis was found to be ± 0.05 wt%C.

### 2.4.7 Analysis of sulphur in slag

A stoichiometric combustion method for the determination of sulphur in slags developed by Fincham and Richardson[47] was used. The apparatus used consisted of a horizontal electric furnace with a 3 mm diameter mullite combustion tube connected to the absorption vessels. Fig. 2.7 shows a schematic diagram of the apparatus used. Two vessels containing the absorption solution were used with the second vessel serving as a trap for the $SO_2$ gas not absorbed in the first one. The ingoing combustion gas ($CO_2$) was measured by a flowmeter. The outgoing gases were passed through a glass-wool trap

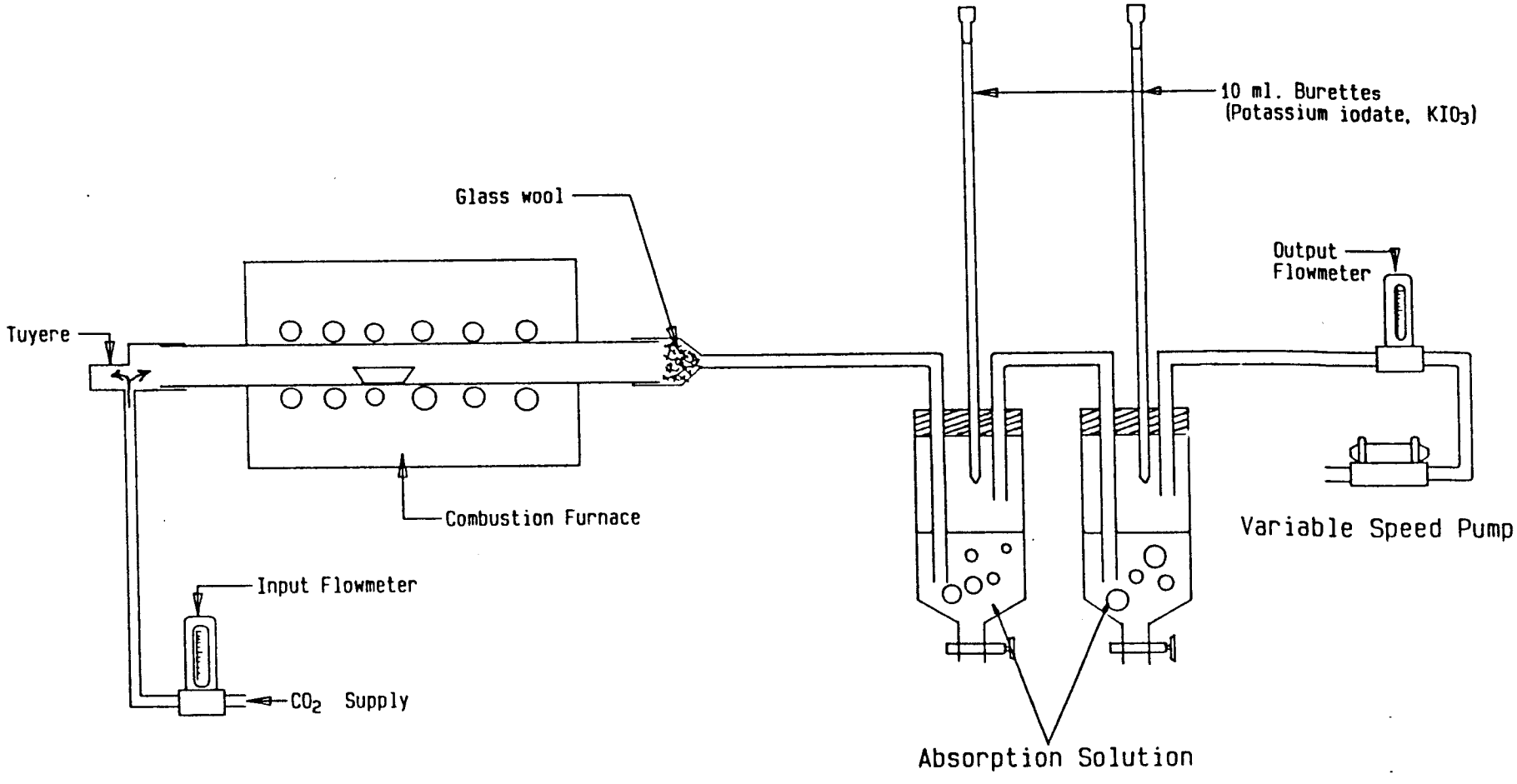


Fig. 2.7 Apparatus for the determination of sulphur in slag.

(to catch dust), and then bubbled through the absorbant contained in the vessels.

The absorbing solution consisted of 100 ml of deionised water, 5 ml of 1:4 dilute hydrochloric acid and 1 ml of freshly prepared indicator solution containing 1.5 g potassium iodate and 0.9 g starch in 100 ml deionised water. Pre-ignited fire clay combustion boats were used to hold the slag.

About 0.1 g of the slag sample was placed in a pre-ignited fire clay combustion boat and pushed quickly into the furnace so as to keep the influx of air at a minimum. The combustion temperature was 1450$^{o}$C and $CO_2$ flowrate was 250 cc $min^{-1}$. The sulphur given off as $SO_2$ was titrated, as it was being absorbed, with standard potassium iodate solution (containing 0.2225 g $KIO_3$/litre so that 1 ml of the solution was equivalent to 0.0001 g of sulphur) until continued gas bubbling produced no further colour change. The combustion took about 30 minutes. The fresh absorbing solution was always titrated before use to determine the blank titre.

The method was checked, periodically, by analysing B.C.S. slag standards and the accuracy of the analysis method was considered to be ± 2% of the total sulphur.

## 2.4.8 Analysis of sulphur in metal

The method for the determination of sulphur in iron and steel by Jones et al[48] was used. Basically, the material to be analysed is burnt in a stream of air at a temperature of 1400°C. The sulphur gases are absorbed in neutralised hydrogen peroxide and the sulphuric acid formed is titrated with standard sodium borate solution. Screened methyl red is used as an indicator. The reactions proceed as follows:

$$SO_2 + H_2O_2 = SO_3 + H_2O \qquad (2.3)$$

$$SO_3 + H_2O = H_2SO_4 \qquad (2.4)$$

$$H_2SO_4 + Na_2B_4O_7 = Na_2SO_4 + H_2B_4O_7 \qquad (2.5)$$

The apparatus used was similar to the one used in the analysis of sulphur in slag except that in this case combustion was carried out in a stream of air to suppress formation of ferric oxide dust associated with the more vigorous oxidation in pure oxygen. Compressed air was purified by passing it through silica gel and manganese perchlorate (to remove water vapour) and soda asbestos (to remove oxides of carbon and sulphur) before entering the combustion furnace.

About 0.5 g of the metal sample was weighed and diluted with electrolytic iron to maintain the carbon concentration at less than 1 wt% so that formation of ferric oxide fumes would be minimised. The metal sample was then placed in the furnace maintained at 1400°C. It was burnt in a stream of air regulated to flow through the apparatus at 1 litre per minute. The input flow rate was 2 litres per minute. The evolved sulphur gases were absorbed in 40 ml of hydrogen peroxide solution. After 5 minutes the sulphuric acid formed was titrated with N/160 sodium borate solution. The absorption solution was prepared with 7.5 ml of hydrogen peroxide (20 vols.) made up to 250 ml with deionised water. 0.5 ml of screened methyl red was added as an indicator.

The sulphur content was calculated as follows:

$$\%S = \frac{(A - B) \times N \times 1.603}{W}$$

where A = test titre (ml)

B = 'blank' titre (ml)

N = strength of sodium borate (normality)

W = weight of sample (g)

The method was checked by analysing B.S.C. steel samples and the accuracy was found to be ± 2% of the total sulphur.

## 2.4.9 Analyais of Lime, Silica and Alumina in master slags.

Atomic absorption spectrophotometric method was used for analysis of these components.

Since standard slags containing the same components as those used in this study were not available, standard solutions containing slag components in the concentration range used were made to provide a similar analytical environment. The standard solutions were made by mixing standard solutions of the individual slag components to give a required concentration range.

Sample stock solutions (100 $\mu g\ ml^{-1}$) were made by fusing 0.1 g of slag with 0.7 g of sodium carbonate and 0.3 g of sodium tetraborate. After cooling, the mixture was dissolved in 20 ml (1+1) nitric acid and made up to 1000 ml.

The stock standard solutions for calcium oxide (100 $\mu g\ ml^{-1}$) were prepared by fusing 0.1785 g 'analar' grade calcium carbonate, $CaCO_3$, with 0.7 g sodium carbonate and 0.3 g sodium tetraborate and dissolving in 20 ml (1+1) nitric acid. The solution was then diluted to 1 litre with deionized water.

Silica stock standard solutions (100 μg $ml^{-1}$) were prepared by fusing 0.1 g of acid-washed silica sand with 0.7 g sodium carbonate and 0.3 g sodium tetraborate and dissolving in 20 ml (1+1) nitric acid. A few drops of hydrogen peroxide were added and the solution made up to 1000 ml with deionized water.

Alumina stock standard solutions were prepared as the silica stock standard solutions by fusing 0.1 g of 'analar' garde alumina.

The standard solutions for slag analysis were then prepared by mixing standard solutions of the individual slag components. For example, to make a solution containing 42% $SiO_2$, 38% CaO and 20% $Al_2O_3$, 42 ml of silica, 38 ml of CaO and 20 ml of $Al_2O_3$ appropriately diluted solutions were mixed. Depending on the component being analysed, its concentration in the standard solutions was varied.

For analysis of CaO, the standard and sample solutions were diluted so that they were within the linear working range for Ca (up to concentrations of approximately 7 μg $ml^{-1}$ in aqueous solution). About 1% lanthanum oxide was added to the solutions to eliminate chemical and ionisation interference. The concentration was then obtained by comparison with the calibration curve. An

air/acetylene flame was used and other conditions are as specified in the Instruction manual[43].

Silica standard solutions were made to fall within the linear working range for silicon, up to 150 $\mu g\ ml^{-1}$. Nitrous oxide/acetylene flame was used. The concentration was determined by comparison with the calibration curve.

Appropriate aliquots for alumina analysis were pipetted from the stock standard and sample solutions and diluted to bring them within the linear working range for aluminium, up to 50 $\mu g\ ml^{-1}$. 20 ml of potassium chloride (100000 $\mu g\ ml^{-1}$) was added to the solutions to suppress the ionization of aluminium. The concentrations were determined by comparison with the calibration curve. An air/acetelyne flame was used.

Multiple analyses of the master slag for CaO, $SiO_2$ and $Al_2O_3$ and using the 95% confidence limit, the uncertainty in the analysis of these elements was found to be ± 1 wt%.

# CHAPTER 3

# RESULTS & OBSERVATIONS

# Chapter 3

# RESULTS AND OBSERVATIONS

## 3.1 Results

This chapter presents the results obtained and the experimental observations encountered during the course of this study. A brief description of the object of each series of experiments is also presented. The results are tabulated in Table 3.1 together with the experimental conditions used for each run. Table 3.2 shows a summary of the experimental conditions. The results are discussed in the next chapter.

As outlined in chapter 2, the progress of the experiments were followed by sampling slag at predetermined time intervals and analysing them for total chromium, total iron and divalent chromium. Trivalent chromium was obtained by difference between total and divalent chromium. Initial and final metal samples were also taken in each run and analysed for carbon and chromium (final metal sample) contents.

### 3.1.1 Reproducibility of Results

In order to determine the consistency of experimental results, repeat runs were carried out using same conditions, and the results compared. Two sets of runs were conducted, runs AS1 and AS6, and runs AS22 and AS22R. In runs AS22 and AS22R, 2 wt% $CaF_2$ was added to the slag. The results are shown in Table 3.1 and plotted in the concentration-time curves shown in Figs 3.1 and 3.2. The figures show that the results are identical in both cases, within experimental error, an indication that the experimental procedure gives reproducible results.

### 3.1.2 Reaction site

There is the possibility of gaseous reduction of $Cr_2O_3$ taking place at the slag/gas interface, gas in this case being the furnace atmosphere, especially in a CO atmosphere. To investigate this possibility, runs AS9 and AS10 were carried out in an argon and a carbon monoxide atmosphere, respectively, without any metal present. The results are shown in Table 3.1. The results showed that there was a small difference in the concentrations of $(Cr^{3+})$ and $(Cr^{2+})$ obtained from the different atmospheres used. An initial, slight reduction of $(Cr^{3+})$ to $(Cr^{2+})$ occurred after which the concentrations remained constant.

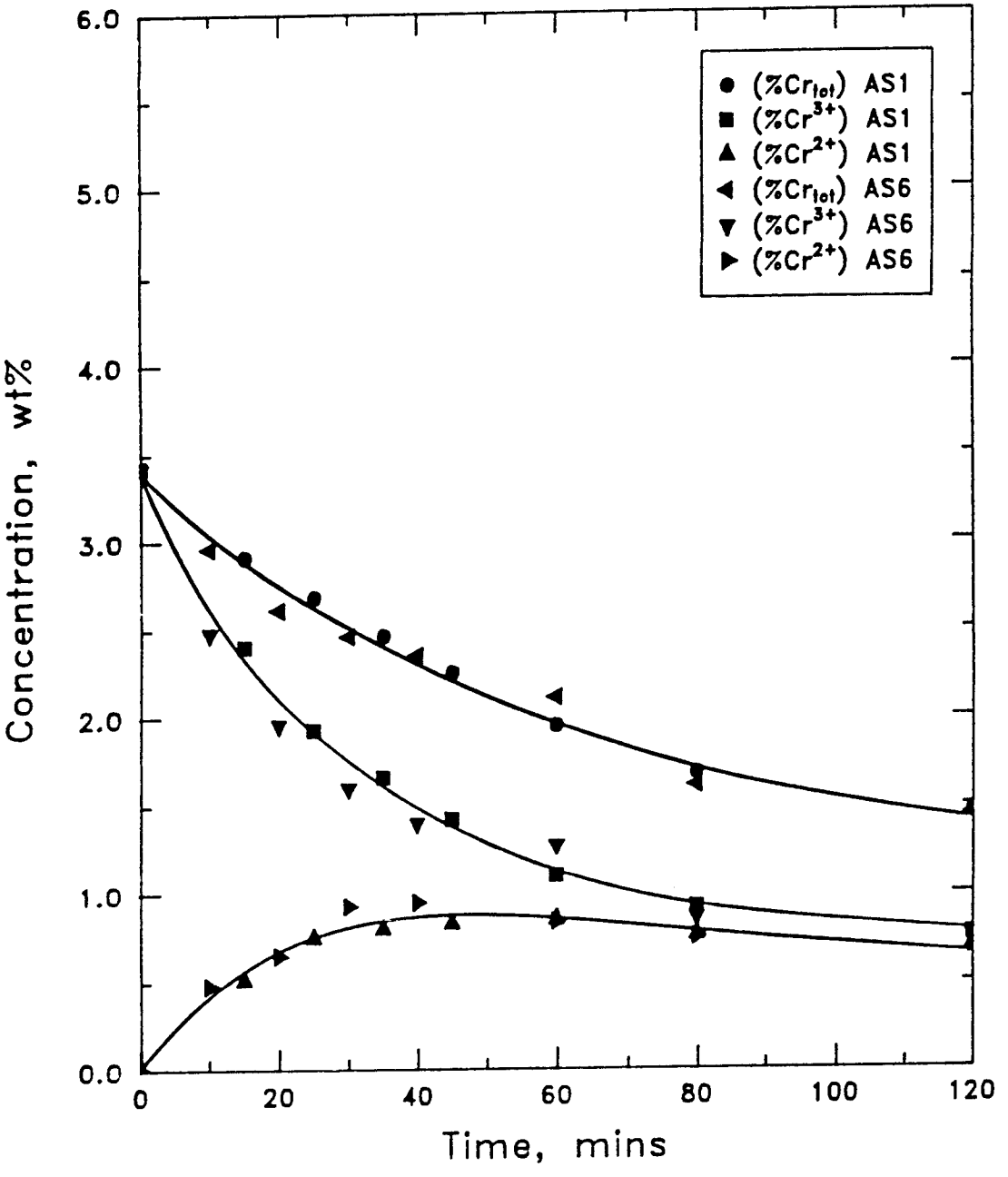


Fig. 3.1 Concentration-time curves showing reproducibility of experimental results for runs AS1 and AS6.

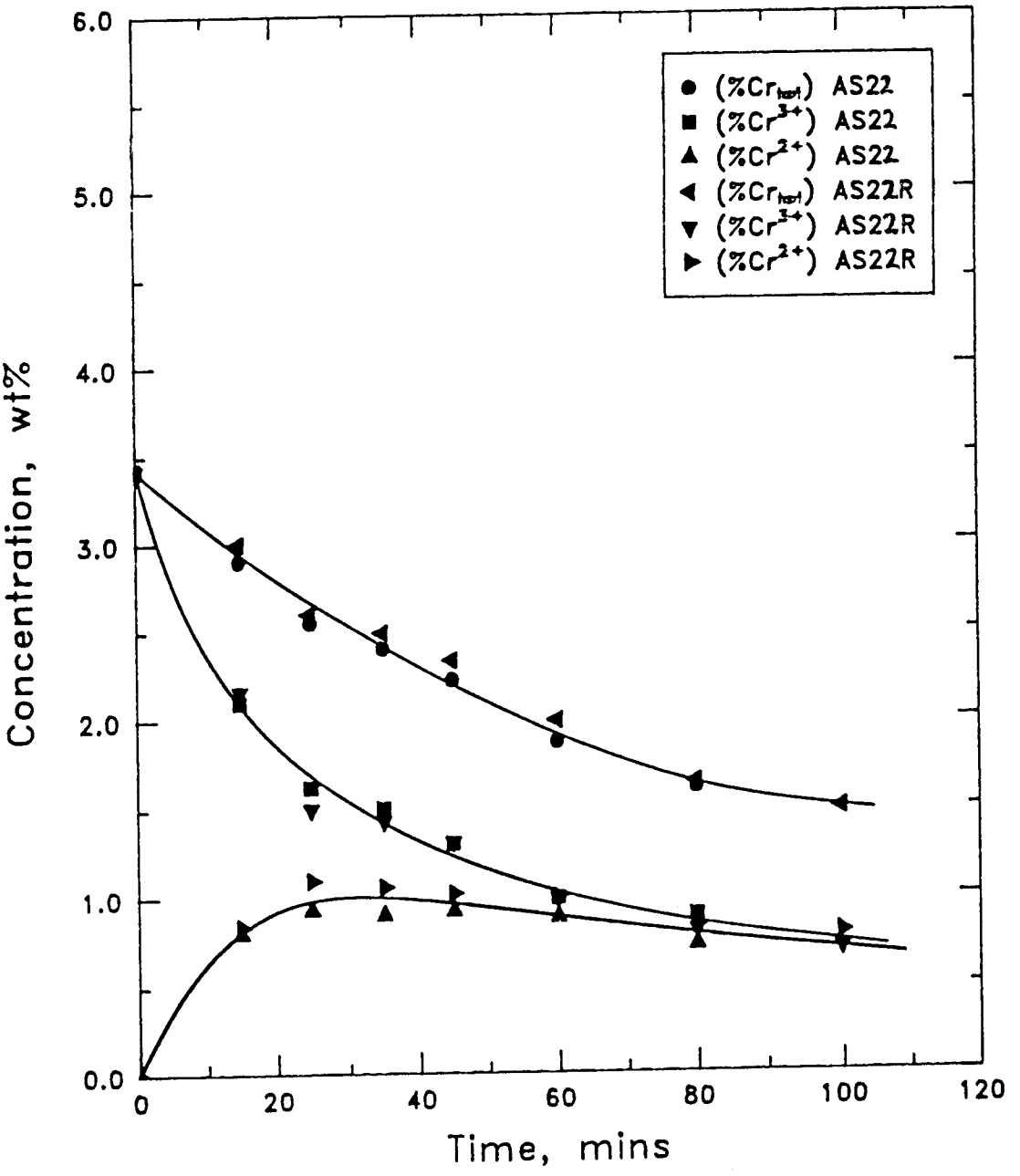


Fig. 3.2 Concentration-time curves showing reproducibility of experimental results for runs AS22 and AS22R.

### 3.1.3 Effect of furnace atmosphere

By conducting $Cr_2O_3$ reduction experiments under an argon and a carbon monoxide atmosphere, one would expect no difference in reduction rates because the bubble pCO for both systems is not expected to differ. To examine this, runs AS1 and AS5 were conducted under an argon and a carbon monoxide atmosphere, respectively. The results are shown in Table 3.1.

### 3.1.4 Effect of oxide concentration

Changes in concentration alter the rate of reaction by changing the driving force for the reaction. Runs AS1, AS2, AS3 and AS4 in which the initial $Cr_2O_3$ concentration were 5, 8, 10 and 3 wt% respectively, were carried out to study the effect on the reduction rate of the oxide. The results are shown in Table 3.1.

### 3.1.5 Effect of metal chromium content

Increasing the metal chromium content will reduce its concentration gradient between the bulk metal and interface. It will also have an effect on the concentration gradient of the chromium species in the

slag phase and so will help to determine if transport of chromium in the metal phase is rate limiting for $Cr_2O_3$ reduction. Two runs, AS7 and AS8, were carried out in which the metal chromium content was 15 and 4 wt% Cr, respectively. The results are shown in Table 3.1.

### 3.1.6 Effect of surface-active elements, sulphur and selenium

Surface-active elements are known to segregate to the reaction interface and hence can slow down the rate of interfacial reactions by reducing the area available for reaction. To investigate this phenomenon, two surface-active elements, sulphur and selenium, were added to the metal and the rate of $Cr_2O_3$ reduction studied. The effect of sulphur additions to the slag were also investigated.

Runs AS11 and AS12 were carried out in which 0.05 and 0.1 wt%S respectively, were added to the metal. Further runs, AS13 and AS14, in which more sulphur additions to the metal were made i.e. 0.3 and 0.5 wt%S respectively, were conducted to see whether an increase in the sulphur content would affect the reduction rate of $Cr_2O_3$.

The effect of sulphur additions to the slag was studied

in runs AS15 and AS16 in which 0.2 wt%S was added to the slag in form of CaS and FeS respectively. Selenium additions to the metal of 0.005 and 0.02 wt%Se were made in runs AS20 and AS21, respectively, to study its effect on the reduction rate of $Cr_2O_3$. The results are shown in Table 3.1.

### 3.1.7 Effect of FeO addition to slag

To investigate the effect of FeO on the reduction rate of $Cr_2O_3$, run AS26 was carried out in which the same stoichiometric amount of Fe as in run AS16 was added to slag in form of FeO. The results are shown in Table 3.1.

### 3.1.8 Effect of Calcium Fluoride addition to slag

Calcium fluoride additions to slag lowers the melting point to necessitate use of higher basicity slags and decrease the slag viscosity. A decrease in viscosity will increase the rate of transfer of the species in the slag phase and this will ultimately affect the reactions taking place at the slag/metal interface. In view of this, three runs AS22, AS23 and AS24 were carried out in which 2, 3.5 and 5 wt% $CaF_2$ were added to the slag, respectively. Run AS25, in which a slag containing 10

wt% $Cr_2O_3$ and 5 wt% $CaF_2$ was conducted to further study the effect of calcium fluoride additions on $Cr_2O_3$ reduction rate. The results are shown in Table 3.1.

## 3.2 Practical Observations

A notable observation made during the experiments was the rapid change in colour of the slag from bright green to deep blue during the initial stages of the reduction process. It is thought that the colour change is due to the reduction of chromic ($Cr^{3+}$) ions to chromous ($Cr^{2+}$) ions[31,37]. This is evidenced by rate plots shown in Figs. 3.1 and 3.2, which show a rapid reduction rate of ($Cr^{3+}$) during the initial stages of reduction accompanied by a rapid production rate of ($Cr^{2+}$).

Immediately after melt down of the charge, there was a period of rapid gas evolution causing slag foaming. Chilled slag samples taken during the initial period of the experiments revealed fine pores embeded in the slag indicating gas entrapment in it. Slag samples taken at later times showed little or no pores in them. The reason for the initial rapid gas evolution is due to the high oxygen potential in the system resulting in high production of CO gas. As the reduction process proceeds the oxygen potential of the system and, hence, gas produ-

*ction decrease, leading to a quieter bath at longer* times.

Runs aborted during the early stages of the experiments showed evidence of the presence of gas bubbles at the slag/metal interface. Plate 3.1 shows the buoyant effect of the gas bubbles. It is a photograph of a chilled specimen showing a metal bath and a vertical crosssection through the slag bath of a run aborted after 25 minutes of the reduction process. Distinct cavities can be seen in the slag body immediately above the metal surface and in the slag bath. This shows that a gas/metal and gas/slag area is created at the expense of slag/metal area by a gas film which is essentially a mixture of CO and $CO_2$ at the commencement of the reactions. It is thought that this gas film acts as a ferrying medium for oxygen from slag to metal surface via CO and $CO_2$. Plate 3.2 shows the surface of the metal from the same run at the slag/metal interface. Scattered about the surface of the metal can be seen numerous circular cavities of various sizes produced by gas bubbles. Plates 3.1 and 3.2, therefore, give evidence of the presence of gas bubbles at the slag/metal interface in the present study.

Although metal droplets were found in most slag samples, they were more numerous in slags obtained from runs carried out in the presence of a surface-active element

Plate 3.1 Chilled specimen of a run aborted after 25 minutes.

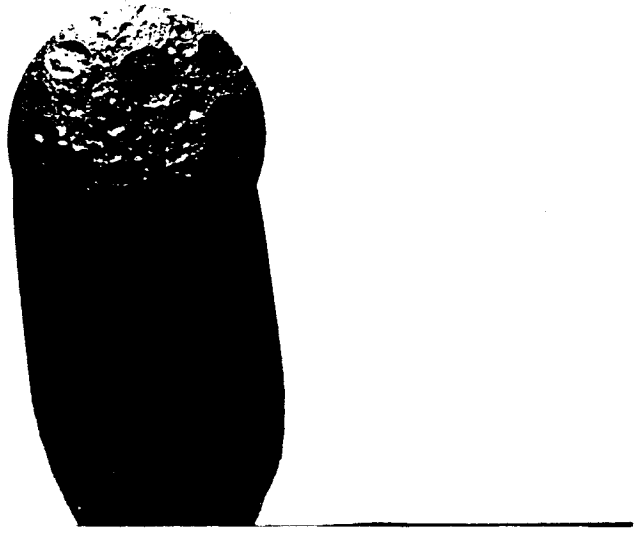

Plate 3.2 Metal specimen showing the presence of gas bubbles, aborted after 25 minutes.

in the system. The reasons for the presence of numerous metal droplets in the slag from such cases is highlighted in chapter 5. The above was substantiated by carrying out runs AS18 and AS19 in which no sulphur and 0.1 [wt%S] were added to the metal respectively. The runs were aborted after 25 minutes and the slags crushed and analysed for the relevant species. Metal droplets found in the slag from both runs were collected and weighed. The results are shown in Table 3.1. Run AS19 contained about 0.36 g of metal droplets while run AS18 had only 0.03 g. Plate 3.3 shows metal droplets of various sizes removed from crushed slag of run AS19.

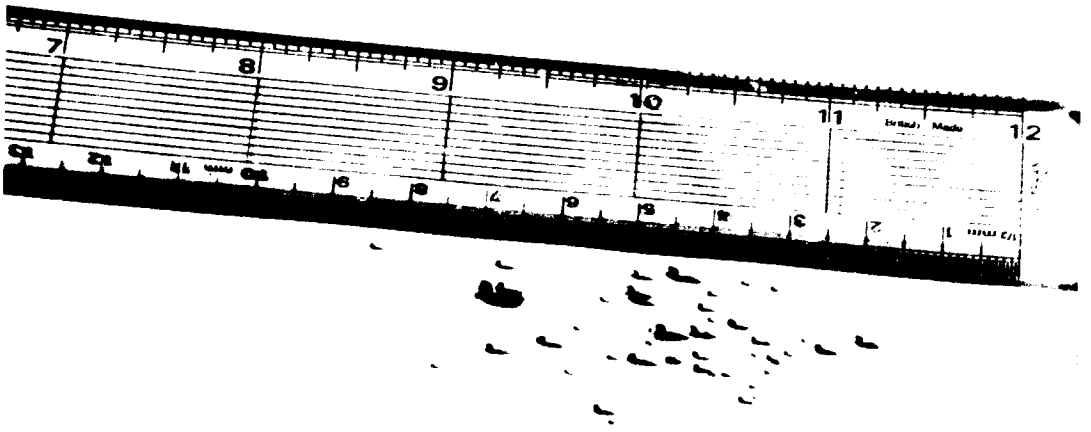

Plate 3.3 Metal droplets removed from crushed slag from run AS19.

**Table 3.1**

| | |
|---|---|
| Experiment No. | AS 1 |
| Fe-C alloy wt. | 60 g |
| Initial wt.[%C] | 4.25 |
| Final wt.[%C] | 3.84 |
| Initial wt.(%$Cr_2O_3$) | 5 |
| Initial wt.[%Cr] | 0 |
| Final wt.[%Cr] | 0.54 |
| Slag wt. | 20 g |
| Slag type | 42%$SiO_2$, 38%CaO, 20%$Al_2O_3$ |
| Crucible type | 32 mm dia alumina |
| Temperature | 1470$^{o}$C |
| Furnace atmosphere | Ar ( 1 atm pressure ) |

| Time (mins) | Sample-wt (g) | Slag-left (g) | (%$Cr_{tot}$) | (%$Cr^{3+}$) | (%$Cr^{2+}$) | (%$Fe^{2+}$) | [%Cr] |
|---|---|---|---|---|---|---|---|
| 0 | 0.00 | 20.00 | 3.42 | 3.42 | 0.00 | 0.00 | 0.00 |
| 15 | 0.51 | 20.00 | 2.91 | 2.40 | 0.51 | 0.07 | 0.17 |
| 25 | 0.87 | 19.49 | 2.68 | 1.93 | 0.75 | 0.09 | 0.24 |
| 35 | 0.66 | 18.62 | 2.46 | 1.66 | 0.80 | 0.12 | 0.36 |
| 45 | 0.48 | 17.96 | 2.25 | 1.42 | 0.83 | 0.11 | 0.38 |
| 60 | 0.46 | 17.48 | 1.95 | 1.10 | 0.85 | 0.13 | 0.46 |
| 80 | 0.96 | 17.02 | 1.68 | 0.92 | 0.76 | 0.14 | 0.54 |
| 120 | 1.78 | 16.06 | 1.46 | 0.76 | 0.70 | 0.15 | 0.60 |

**Table 3.1 continued**

| | |
|---|---|
| Experiment No. | AS 2 |
| Fe-C alloy wt. | 60 g |
| Initial wt.[%C] | 4.25 |
| Final wt.[%C] | 3.80 |
| Initial wt.(%$Cr_2O_3$) | 8 |
| Initial wt.[%Cr] | 0 |
| Final wt.[%Cr] | 0.63 |
| Slag wt. | 20 g |
| Slag type | 42%$SiO_2$, 38%CaO, 20%$Al_2O_3$ |
| Crucible type | 32 mm dia alumina |
| Temperature | 1470$^{o}$C |
| Furnace atmosphere | Ar ( 1 atm pressure ) |

| Time (mins) | Sample-wt (g) | Slag-left (g) | (%$Cr_{tot}$) | (%$Cr^{3+}$) | (%$Cr^{2+}$) | (%$Fe^{2+}$) | [%Cr] |
|---|---|---|---|---|---|---|---|
| 0 | 0.00 | 20.00 | 5.47 | 5.47 | 0.00 | 0.00 | 0.00 |
| 15 | 3.35 | 20.00 | 4.96 | 4.08 | 0.88 | 0.08 | 0.17 |
| 25 | 1.68 | 16.65 | 4.45 | 3.64 | 0.81 | 0.10 | 0.31 |
| 35 | 0.94 | 14.97 | 3.98 | 2.93 | 1.05 | 0.15 | 0.43 |
| 45 | 1.16 | 14.03 | 3.38 | 2.25 | 1.13 | 0.15 | 0.56 |
| 60 | 1.43 | 12.87 | 2.87 | 1.77 | 1.10 | 0.16 | 0.67 |
| 80 | 0.91 | 11.44 | 2.44 | 1.31 | 1.13 | 0.17 | 0.75 |
| 110 | 1.78 | 10.53 | 1.97 | 0.96 | 1.01 | 0.18 | 0.84 |

**Table 3.1 continued**

| | |
|---|---|
| Experiment No. | AS 3 |
| Fe-C alloy wt. | 60 g |
| Initial wt.[%C] | 4.17 |
| Final wt.[%C] | 3.63 |
| Initial wt.($\%Cr_2O_3$) | 10 |
| Initial wt.[%Cr] | 0 |
| Final wt.[%Cr] | 0.84 |
| Slag wt. | 20 g |
| Slag-type | 42%$SiO_2$, 38%CaO, 20%$Al_2O_3$ |
| Crucible type | 32 mm dia alumina |
| Temperature | 1470$^{o}$C |
| Furnace atmosphere | Ar ( 1 atm pressure ) |

| Time (mins) | Sample-wt (g) | Slag-left (g) | ($\%Cr_{tot}$) | ($\%Cr^{3+}$) | ($\%Cr^{2+}$) | ($\%Fe^{2+}$) | [%Cr] |
|---|---|---|---|---|---|---|---|
| 0 | 0.00 | 20.00 | 6.84 | 6.84 | 0.00 | 0.00 | 0.00 |
| 15 | 1.77 | 20.00 | 6.11 | 5.26 | 0.85 | 0.08 | 0.24 |
| 25 | 1.54 | 18.23 | 5.09 | 4.18 | 0.91 | 0.10 | 0.55 |
| 35 | 0.70 | 16.69 | 4.85 | 3.64 | 1.21 | 0.12 | 0.62 |
| 45 | 0.74 | 15.99 | 4.80 | 3.40 | 1.40 | 0.13 | 0.63 |
| 60 | 0.66 | 15.25 | 4.12 | 2.70 | 1.42 | 0.16 | 0.80 |
| 80 | 0.73 | 14.59 | 3.63 | 2.20 | 1.43 | 0.19 | 0.92 |
| 120 | 1.34 | 13.86 | 2.57 | 1.34 | 1.23 | 0.20 | 1.16 |

**Table 3.1 continued**

| | |
|---|---|
| Experiment No. | AS4 |
| Fe-C alloy wt. | 60 g |
| Initial wt.[%C] | 4.17 |
| Final wt.[%C] | 3.84 |
| Initial wt.(%$Cr_2O_3$) | 3 |
| Initial wt.[%Cr] | 0 |
| Slag wt. | 20 g |
| Slag type | 42%$SiO_2$, 38%CaO, 20%$Al_2O_3$ |
| Crucible type | 32 mm dia alumina |
| Temperature | 1470°C |
| Furnace atmosphere | Ar ( 1 atm pressure) |

| Time (mins) | Sample-wt (g) | Slag-left (g) | (%$Cr_{tot}$) | (%$Cr^{3+}$) | (%$Cr^{2+}$) | (%$Fe^{2+}$) | [%Cr] |
|---|---|---|---|---|---|---|---|
| 0 | 0.00 | 20.00 | 2.05 | 2.05 | 0.00 | 0.00 | 0.00 |
| 15 | 0.70 | 20.00 | 2.00 | 1.90 | 0.10 | 0.06 | 0.02 |
| 25 | 2.97 | 19.30 | 1.85 | 1.44 | 0.41 | 0.09 | 0.06 |
| 35 | 0.50 | 16.33 | 1.78 | 1.12 | 0.66 | 0.10 | 0.08 |
| 45 | 0.98 | 15.83 | 1.70 | 1.00 | 0.70 | 0.09 | 0.09 |
| 60 | 0.65 | 14.85 | 1.60 | 0.89 | 0.71 | 0.11 | 0.13 |
| 80 | 1.95 | 14.20 | 1.14 | 0.58 | 0.56 | 0.12 | 0.24 |
| 120 | 3.24 | 12.25 | 0.91 | 0.49 | 0.42 | 0.13 | 0.28 |

**Table 3.1 continued**

| | |
|---|---|
| Experiment No. | AS 5 |
| Fe-C alloy wt. | 60 g |
| Initial wt.[%C] | 4.17 |
| Final wt.[%C] | 3.88 |
| Initial wt.(%$Cr_2O_3$) | 5 |
| Initial wt.[%Cr] | 0 |
| Final wt.[%Cr] | 0.50 |
| Slag wt. | 20 g |
| Slag type | 42%$SiO_2$, 38%CaO, 20%$Al_2O_3$ |
| Crucible type | 32 mm dia alumina |
| Temperature | 1470$^{o}$C |
| Furnace atmosphere | CO ( 1 atm pressure ) |

| Time (mins) | Sample-wt (g) | Slag-left (g) | (%$Cr_{tot}$) | (%$Cr^{3+}$) | (%$Cr^{2+}$) | (%$Fe^{2+}$) | [%Cr] |
|---|---|---|---|---|---|---|---|
| 0 | 0.00 | 20.00 | 3.42 | 3.42 | 0.00 | 0.00 | 0.00 |
| 10 | 3.07 | 20.00 | 2.98 | 2.49 | 0.49 | 0.06 | 0.15 |
| 20 | 1.26 | 16.93 | 2.61 | 1.91 | 0.70 | 0.10 | 0.25 |
| 30 | 0.60 | 15.67 | 2.52 | 1.61 | 0.91 | 0.12 | 0.27 |
| 40 | 0.96 | 15.07 | 2.44 | 1.37 | 1.07 | 0.13 | 0.29 |
| 60 | 1.12 | 14.11 | 2.16 | 1.13 | 1.03 | 0.14 | 0.36 |
| 80 | 1.87 | 12.99 | 1.99 | 0.93 | 1.06 | 0.15 | 0.39 |
| 120 | 1.95 | 11.12 | 1.58 | 0.66 | 0.92 | 0.16 | 0.47 |

**Table 3.1 continued**

| | |
|---|---|
| Experiment No. | AS 6 |
| Fe-C alloy wt. | 60 g |
| Initial wt.[%C] | 4.17 |
| Final wt.[%C] | 3.79 |
| Initial wt.(%$Cr_2O_3$) | 5 |
| Initial wt.[%Cr] | 0 |
| Final wt.[%Cr] | 0.43 |
| Slag wt. | 20 g |
| Slag type | 42%$SiO_2$, 38%CaO, 20%$Al_2O_3$ |
| Crucible type | 32 mm dia alumina |
| Temperature | 1470$^{o}$C |
| Furnace atmosphere | Ar ( 1 atm pressure ) |

| Time (mins) | Sample-wt (g) | Slag-left (g) | (%$Cr_{tot}$) | (%$Cr^{3+}$) | (%$Cr^{2+}$) | (%$Fe^{2+}$) | [%Cr] |
|---|---|---|---|---|---|---|---|
| 0 | 0.00 | 20.00 | 3.42 | 3.42 | 0.00 | 0.00 | 0.00 |
| 10 | 0.93 | 20.00 | 2.96 | 2.48 | 0.48 | 0.05 | 0.15 |
| 20 | 1.15 | 19.07 | 2.61 | 1.96 | 0.65 | 0.09 | 0.28 |
| 35 | 0.83 | 17.92 | 2.53 | 1.60 | 0.93 | 0.11 | 0.29 |
| 45 | 1.40 | 17.09 | 2.35 | 1.40 | 0.95 | 0.11 | 0.34 |
| 60 | 0.71 | 15.69 | 2.11 | 1.27 | 0.84 | 0.13 | 0.37 |
| 80 | 0.60 | 14.98 | 1.61 | 0.86 | 0.75 | 0.14 | 0.40 |
| 120 | 2.21 | 14.38 | 1.44 | 0.75 | 0.69 | 0.16 | 0.55 |

**Table 3.1 continued**

| | |
|---|---|
| Experiment No. | AS 7 |
| Fe-C alloy wt. | 60 g |
| Initial wt.[%C] | 4.60 |
| Final wt.[%C] | 4.11 |
| Initial wt.(%$Cr_2O_3$) | 5 |
| Initial wt.[%Cr] | 15 |
| Final wt.[%Cr] | 15.16 |
| Slag wt. | 20 g |
| Slag type | 42%$SiO_2$, 38%CaO, 20%$Al_2O_3$ |
| Crucible type | 32 mm dia alumina |
| Temperature | 1470$^{o}$C |
| Furnace atmosphere | Ar ( 1 atm pressure ) |

| Time (mins) | Sample-wt (g) | Slag-left (g) | (%$Cr_{tot}$) | (%$Cr^{3+}$) | (%$Cr^{2+}$) | (%$Fe^{2+}$) | [%Cr] |
|---|---|---|---|---|---|---|---|
| 0 | 0.00 | 20.00 | 3.42 | 3.42 | 0.00 | 0.00 | 15.00 |
| 15 | 0.74 | 20.00 | 3.39 | 2.46 | 0.93 | 0.18 | 15.01 |
| 25 | 0.75 | 19.26 | 3.36 | 2.22 | 1.14 | 0.20 | 15.02 |
| 35 | 1.60 | 18.51 | 3.26 | 1.85 | 1.41 | 0.23 | 15.05 |
| 45 | 0.86 | 16.91 | 2.84 | 1.42 | 1.42 | 0.31 | 15.17 |
| 60 | 2.10 | 16.05 | 2.51 | 1.09 | 1.42 | 0.39 | 15.26 |
| 80 | 1.36 | 13.89 | 2.01 | 0.66 | 1.35 | 0.37 | 15.37 |
| 120 | 1.72 | 12.53 | 1.95 | 0.81 | 1.14 | 0.41 | 15.39 |

**Table 3.1 continued**

| | |
|---|---|
| Experiment No. | AS 8 |
| Fe-C alloy wt. | 60 g |
| Initial wt.[%C] | 4.60 |
| Final wt.[%C] | 4.10 |
| Initial wt.(%$Cr_2O_3$) | 5 |
| Initial wt.[%Cr] | 4 |
| Final wt.[%Cr] | 4.45 |
| Slag wt. | 20 g |
| Slag type | 42%$SiO_2$, 38%CaO, 20%$Al_2O_3$ |
| Crucible type | 32 mm dia alumina |
| Temperature | 1470$^{o}$C |
| Furnace atmosphere | Ar ( 1 atm pressure ) |

| Time (mins) | Sample-wt (g) | Slag-left (g) | (%$Cr_{tot}$) | (%$Cr^{3+}$) | (%$Cr^{2+}$) | (%$Fe^{2+}$) | [%Cr] |
|---|---|---|---|---|---|---|---|
| 0 | 0.00 | 20.00 | 3.42 | 3.42 | 0.00 | 0.00 | 4.00 |
| 15 | 0.86 | 20.00 | 3.16 | 2.63 | 0.53 | 0.18 | 4.08 |
| 25 | 0.68 | 19.14 | 2.80 | 2.11 | 0.69 | 0.25 | 4.19 |
| 35 | 0.79 | 18.46 | 2.50 | 1.70 | 0.80 | 0.26 | 4.28 |
| 45 | 1.11 | 17.67 | 2.31 | 1.54 | 0.77 | 0.23 | 4.35 |
| 60 | 0.53 | 16.56 | 1.93 | 1.14 | 0.79 | 0.25 | 4.45 |
| 80 | 1.68 | 16.03 | 1.64 | 0.92 | 0.72 | 0.26 | 4.52 |
| 120 | 1.10 | 14.35 | 1.23 | 0.68 | 0.55 | 0.28 | 4.61 |

**Table 3.1 continued**

| | |
|---|---|
| Experiment No. | AS 9 |
| Slag wt. | 20 g |
| Slag type | 42%$SiO_2$, 38%CaO, 20%$Al_2O_3$ |
| Initial wt.(%$Cr_2O_3$) | 5 |
| Crucible type | 32 mm dia alumina |
| Temperature | 1470$^oC$ |
| Furnace atmosphere | Ar ( 1 atm pressure ) |

| Time (mins) | Sample-wt (g) | Slag-left (g) | (%$Cr_{tot}$) | (%$Cr^{3+}$) | (%$Cr^{2+}$) |
|---|---|---|---|---|---|
| 0 | 0.00 | 20.00 | 3.42 | 3.42 | 0.00 |
| 15 | 0.56 | 20.00 | 3.42 | 3.18 | 0.24 |
| 25 | 1.51 | 19.44 | 3.42 | 3.16 | 0.26 |
| 35 | 0.97 | 17.93 | 3.42 | 3.20 | 0.22 |
| 45 | 1.29 | 16.96 | 3.42 | 3.16 | 0.26 |
| 60 | 0.91 | 15.67 | 3.42 | 3.20 | 0.22 |
| 80 | 0.73 | 14.76 | 3.42 | 3.15 | 0.27 |
| 95 | 0.52 | 14.03 | 3.42 | 3.21 | 0.21 |

**Table 3.1 continued**

| | |
|---|---|
| Experiment No. | AS 10 |
| Slag wt. | 20 g |
| Slag type | 42%$SiO_2$, 38%CaO, 20%$Al_2O_3$ |
| Initial wt.(%$Cr_2O_3$) | 5 |
| Crucible type | 32 mm dia alumina |
| Temperature | 1470$^oC$ |
| Furnace atmosphere | CO ( 1 atm pressure ) |

| Time (mins) | Sample-wt (g) | Slag-left (g) | (%$Cr_{tot}$) | (%$Cr^{3+}$) | (%$Cr^{2+}$) |
|---|---|---|---|---|---|
| 0 | 0.00 | 20.00 | 3.42 | 3.42 | 0.00 |
| 15 | 0.91 | 20.00 | 3.42 | 3.21 | 0.21 |
| 25 | 1.04 | 19.09 | 3.42 | 3.16 | 0.26 |
| 35 | 1.58 | 18.05 | 3.42 | 3.09 | 0.33 |
| 45 | 1.15 | 16.47 | 3.42 | 3.11 | 0.31 |
| 60 | 1.25 | 15.32 | 3.42 | 3.09 | 0.33 |
| 80 | 1.02 | 14.07 | 3.42 | 3.10 | 0.32 |
| 120 | 0.94 | 13.05 | 3.42 | 3.12 | 0.30 |

**Table 3.1 continued**

| | |
|---|---|
| Experiment No. | AS 11 |
| Fe-C-S alloy wt. | 60 g |
| Initial wt.[%C] | 4.10 |
| Final wt.[%C] | 3.79 |
| Initial wt.(%$Cr_2O_3$) | 5 |
| Initial wt.[%Cr] | 0 |
| Final wt.[%Cr] | 0.76 |
| Metal addition | 0.05 wt.[%S] |
| Final wt.[%S] | 0.04 |
| Slag wt. | 20 g |
| Slag type | 42%$SiO_2$, 38%CaO, 20%$Al_2O_3$ |
| Crucible type | 32 mm dia alumina |
| Temperature | 1470$^{o}$C |
| Furnace atmosphere | CO ( 1 atm pressure ) |

| Time (mins) | Sample-wt (g) | Slag-left (g) | (%$Cr_{tot}$) | (%$Cr^{3+}$) | (%$Cr^{2+}$) | (%$Fe^{2+}$) | [%Cr] | (%S) |
|---|---|---|---|---|---|---|---|---|
| 0 | 0.00 | 20.00 | 3.42 | 3.42 | 0.00 | 0.00 | 0.00 | 0.000 |
| 15 | 0.61 | 20.00 | 2.72 | 1.61 | 1.11 | 0.61 | 0.23 | 0.013 |
| 25 | 0.76 | 19.39 | 2.35 | 1.20 | 1.15 | 0.61 | 0.25 | 0.023 |
| 35 | 0.67 | 18.63 | 1.88 | 0.75 | 1.13 | 0.61 | 0.49 | 0.022 |
| 45 | 0.64 | 17.96 | 1.76 | 0.65 | 1.11 | 0.57 | 0.53 | 0.032 |
| 60 | 1.12 | 17.32 | 1.63 | 0.60 | 1.03 | 0.53 | 0.57 | 0.032 |
| 80 | 0.78 | 16.20 | 1.27 | 0.42 | 0.85 | 0.48 | 0.66 | 0.031 |
| 120 | 1.83 | 15.42 | 0.63 | 0.07 | 0.56 | 0.40 | 0.82 | 0.034 |

**Table 3.1 continued**

| | |
|---|---|
| Experiment No. | AS 12 |
| Fe-C-S alloy wt. | 60 g |
| Initial wt.[%C] | 4.10 |
| Final wt.[%C] | 3.62 |
| Initial wt.(%$Cr_2O_3$) | 5 |
| Initial wt.[%Cr] | 0 |
| Final wt.[%Cr] | 1.04 |
| Metal addition | 0.10 wt.[%S] |
| Final wt.[%S] | 0.07 |
| Slag wt. | 20 g |
| Slag type | 42%$SiO_2$, 38%CaO, 20%$Al_2O_3$ |
| Crucible type | 32 mm dia alumina |
| Temperature | 1470$^{o}$C |
| Furnace atmosphere | CO ( 1 atm pressure ) |

| Time (mins) | Sample-wt (g) | Slag-left (g) | (%$Cr_{tot}$) | (%$Cr^{3+}$) | (%$Cr^{2+}$) | (%$Fe^{2+}$) | [%Cr] | (%S) |
|---|---|---|---|---|---|---|---|---|
| 0 | 0.00 | 20.00 | 3.42 | 3.42 | 0.00 | 0.00 | 0.00 | 0.000 |
| 15 | 1.09 | 20.00 | 1.98 | 1.04 | 0.94 | 1.59 | 0.48 | 0.032 |
| 25 | 1.84 | 18.91 | 1.03 | 0.35 | 0.68 | 1.60 | 0.73 | 0.032 |
| 35 | 1.11 | 17.07 | 0.78 | 0.26 | 0.48 | 1.64 | 0.80 | 0.038 |
| 45 | 0.63 | 15.96 | 0.63 | 0.20 | 0.43 | 1.53 | 0.87 | 0.038 |
| 60 | 1.34 | 15.33 | 0.57 | 0.13 | 0.44 | 1.33 | 0.89 | 0.044 |
| 80 | 1.01 | 13.99 | 0.40 | 0.02 | 0.38 | 1.11 | 0.93 | 0.049 |
| 120 | 0.77 | 12.98 | 0.24 | 0.00 | 0.24 | 0.82 | 0.96 | 0.050 |

**Table 3.1 continued**

| | |
|---|---|
| Experiment No. | AS 13 |
| Fe-C-S alloy wt. | 60 g |
| Initial wt.[%C] | 4.01 |
| Final wt.[%C] | 3.80 |
| Initial wt.(%$Cr_2O_3$) | 5 |
| Initial wt.[%Cr] | 0 |
| Final wt.[%Cr] | 0.88 |
| Metal addition | 0.30 wt.[%S] |
| Final wt.[%S] | 0.24 |
| Slag wt. | 20 g |
| Slag type | 42%$SiO_2$, 38%CaO, 20%$Al_2O_3$ |
| Crucible type | 32 mm dia alumina |
| Temperature | 1470$^{o}$C |
| Furnace atmosphere | CO ( 1 atm pressure ) |

| Time (mins) | Sample-wt (g) | Slag-left (g) | (%$Cr_{tot}$) | (%$Cr^{3+}$) | (%$Cr^{2+}$) | (%$Fe^{2+}$) | [%Cr] | (%S) |
|---|---|---|---|---|---|---|---|---|
| 0 | 0.00 | 20.00 | 3.42 | 3.42 | 0.00 | 0.00 | 0.00 | 0.000 |
| 15 | 0.85 | 20.00 | 2.00 | 1.12 | 0.88 | 1.83 | 0.36 | 0.065 |
| 25 | 1.19 | 19.15 | 1.22 | 0.52 | 0.70 | 2.06 | 0.69 | 0.062 |
| 35 | 1.72 | 17.96 | 1.06 | 0.47 | 0.59 | 2.01 | 0.76 | 0.064 |
| 45 | 1.06 | 16.24 | 0.85 | 0.32 | 0.53 | 1.82 | 0.81 | 0.067 |
| 60 | 0.64 | 15.18 | 0.60 | 0.21 | 0.39 | 1.68 | 0.87 | 0.076 |
| 80 | 0.90 | 14.54 | 0.47 | 0.12 | 0.35 | 1.42 | 0.90 | 0.082 |
| 110 | 1.00 | 13.64 | 0.16 | 0.00 | 0.16 | 1.11 | 0.98 | 0.085 |

**Table 3.1 continued**

| | |
|---|---|
| Experiment No. | AS 14 |
| Fe-C-S alloy wt. | 60 g |
| Initial wt.[%C] | 4.01 |
| Final wt.[%C] | 3.82 |
| Initial wt.(%$Cr_2O_3$) | 5 |
| Initial wt.[%Cr] | 0 |
| Final wt.[%Cr] | 0.94 |
| Metal addition | 0.50 wt.[%S] |
| Final wt.[%S] | 0.35 |
| Slag wt. | 20 g |
| Slag type | 42%$SiO_2$, 38%CaO, 20%$Al_2O_3$ |
| Crucible type | 32 mm dia alumina |
| Temperature | 1470$^{o}$C |
| Furnace atmosphere | CO ( 1 atm pressure ) |

| Time (mins) | Sample-wt (g) | Slag-left (g) | (%$Cr_{tot}$) | (%$Cr^{3+}$) | (%$Cr^{2+}$) | (%$Fe^{2+}$) | [%Cr] | (%S) |
|---|---|---|---|---|---|---|---|---|
| 0 | 0.00 | 20.00 | 3.42 | 3.42 | 0.00 | 0.00 | 0.00 | 0.00 |
| 15 | 1.53 | 20.00 | 1.94 | 1.09 | 0.85 | 1.91 | 0.46 | 0.06 |
| 25 | 1.05 | 18.47 | 1.19 | 0.52 | 0.67 | 1.91 | 0.69 | 0.08 |
| 35 | 0.93 | 17.42 | 0.88 | 0.44 | 0.44 | 1.81 | 0.78 | 0.12 |
| 45 | 0.80 | 16.49 | 0.73 | 0.33 | 0.40 | 1.69 | 0.84 | 0.13 |
| 60 | 1.00 | 15.69 | 0.56 | 0.21 | 0.35 | 1.48 | 0.88 | 0.13 |
| 80 | 0.91 | 14.69 | 0.49 | 0.20 | 0.29 | 1.27 | 0.91 | 0.13 |

**Table 3.1 continued**

| | |
|---|---|
| Experiment No. | AS 15 |
| Fe-C alloy wt. | 60 g |
| Initial wt.[%C] | 4.10 |
| Final wt.[%C] | 3.71 |
| Initial wt.(%$Cr_2O_3$) | 5 |
| Initial wt.[%Cr] | 0 |
| Final wt.[%Cr] | 0.78 |
| Slag addition-wt.(%S) | 0.20 as CaS |
| Final wt.[%S] | 0.03 |
| Slag wt. | 20 g |
| Slag type | 42%$SiO_2$, 38%CaO, 20%$Al_2O_3$ |
| Crucible type | 32 mm dia alumina |
| Temperature | 1470°C |
| Furnace atmosphere | CO ( 1 atm pressure ) |

| Time (mins) | Sample-wt (g) | Slag-left (g) | (%$Cr_{tot}$) | (%$Cr^{3+}$) | (%$Cr^{2+}$) | (%$Fe^{2+}$) | [%Cr] | (%S) |
|---|---|---|---|---|---|---|---|---|
| 0 | 0.00 | 20.00 | 3.42 | 3.42 | 0.00 | 0.00 | 0.00 | 0.200 |
| 15 | 1.90 | 20.00 | 2.19 | 0.55 | 1.64 | 0.19 | 0.44 | 0.106 |
| 25 | 1.49 | 18.10 | 1.91 | 0.48 | 1.43 | 0.26 | 0.49 | 0.098 |
| 35 | 1.38 | 16.61 | 1.74 | 0.39 | 1.35 | 0.34 | 0.54 | 0.092 |
| 45 | 1.50 | 15.23 | 1.48 | 0.23 | 1.25 | 0.39 | 0.61 | 0.084 |
| 60 | 1.23 | 13.73 | 1.13 | 0.10 | 1.03 | 0.46 | 0.68 | 0.049 |
| 80 | 1.24 | 12.50 | 0.88 | 0.05 | 0.83 | 0.51 | 0.75 | 0.048 |
| 120 | 1.30 | 11.26 | 0.67 | 0.00 | 0.67 | 0.34 | 0.81 | 0.048 |

**Table 3.1 continued**

| | |
|---|---|
| Experiment No. | AS 16 |
| Fe-C alloy wt. | 60 g |
| Initial wt.[%C] | 4.10 |
| Final wt.[%C] | 3.63 |
| Initial wt.(%$Cr_2O_3$) | 5 |
| Initial wt.[%Cr] | 0 |
| Final wt.[%Cr] | 0.87 |
| Slag addition-wt.(%S) | 0.20 as FeS |
| Final wt.[%S] | 0.038 |
| *Slag wt.* | *20 g* |
| Slag type | 42%$SiO_2$, 38%CaO, 20%$Al_2O_3$ |
| Crucible type | 32 mm dia alumina |
| Temperature | 1470$^{o}$C |
| Furnace atmosphere | CO ( 1 atm pressure ) |

| Time (mins) | Sample-wt (g) | Slag-left (g) | (%$Cr_{tot}$) | (%$Cr^{3+}$) | (%$Cr^{2+}$) | (%$Fe^{2+}$) | [%Cr] | (%S) |
|---|---|---|---|---|---|---|---|---|
| 0 | 0.00 | 20.00 | 3.42 | 3.42 | 0.00 | 0.35 | 0.00 | 0.200 |
| 15 | 1.90 | 20.00 | 1.76 | 0.40 | 1.36 | 0.49 | 0.55 | 0.085 |
| 25 | 1.09 | 18.10 | 1.66 | 0.27 | 1.39 | 0.65 | 0.58 | 0.084 |
| 35 | 1.04 | 17.01 | 1.47 | 0.17 | 1.30 | 0.75 | 0.63 | 0.085 |
| 45 | 1.29 | 15.97 | 1.22 | 0.07 | 1.15 | 0.73 | 0.69 | 0.074 |
| 60 | 1.05 | 14.68 | 0.87 | 0.04 | 0.83 | 0.65 | 0.78 | 0.052 |
| 80 | 1.43 | 13.63 | 0.72 | 0.00 | 0.72 | 0.70 | 0.86 | 0.041 |
| 120 | 1.30 | 12.20 | 0.53 | 0.00 | 0.53 | 0.59 | 0.88 | 0.038 |

**Table 3.1 continued**

| | |
|---|---|
| Experiment No. | AS 17 |
| Fe-C alloy wt. | 60 g |
| Initial wt.[%C] | 4.01 |
| Final wt.[%C] | 3.61 |
| Slag wt. | 20 g |
| Slag type | 42%$SiO_2$, 38%CaO, 20%$Al_2O_3$ |
| Crucible type | 32 mm dia alumina |
| Temperature | 1470$^{o}$C |
| Furnace atmosphere | CO ( 1 atm pressure ) |

| Time (mins) | Sample-wt (g) | Slag-left (g) | (%$Fe^{2+}$) |
|---|---|---|---|
| 0 | 0.00 | 20.00 | 0.00 |
| 10 | 0.56 | 20.00 | 0.06 |
| 25 | 1.83 | 19.44 | 0.08 |
| 35 | 1.19 | 17.61 | 0.11 |
| 45 | 1.84 | 16.42 | 0.11 |
| 60 | 1.40 | 14.58 | 0.10 |
| 80 | 1.02 | 13.18 | 0.11 |

**Table 3.1 continued**

| | |
|---|---|
| Experiment No. | AS 18 |
| Fe-C alloy wt | 60 g |
| Initial wt.[%C] | 4.01 |
| Initial wt.(%$Cr_2O_3$) | 5 |
| Initial wt.[%Cr] | 0 |
| Final wt.[%Cr] | 0.30 |
| No Metal or Slag addition | |
| Slag wt. | 20 g |
| Slag type | 42%$SiO_2$, 38%CaO, 20%$Al_2O_3$ |
| Crucible type | 32 mm dia alumina |
| Temperature | 1470$^{o}$C |
| Furnace atmosphere | CO ( 1 atm pressure ) |

| Time (mins) | Slag-wt (g) | Metal beads (g) | (%$Cr_{tot}$) | (%$Cr^{3+}$) | (%$Cr^{2+}$) | (%$Fe^{2+}$) | [%Cr] |
|---|---|---|---|---|---|---|---|
| 0 | 20.00 | 0.00 | 3.42 | 3.42 | 0.00 | 0.00 | 0.00 |
| 25 | 20.00 | 0.03 | 2.53 | 1.65 | 0.88 | 0.34 | 0.30 |

Terminated after 25 minutes

**Table 3.1 continued**

| | |
|---|---|
| Experiment No. | AS 19 |
| Fe-C-S alloy wt | 60 g |
| Initial wt.[%C] | 4.01 |
| Initial wt. ($\%Cr_2O_3$) | 5 |
| Final wt.[%Cr] | 0.72 |
| Metal addition | 0.10 wt.[%S] |
| Slag wt. | 20 g |
| Slag type | 42%$SiO_2$, 38%CaO, 20%$Al_2O_3$ |
| Crucible type | *32 mm dia alumina* |
| Temperature | 1470$^{o}$C |
| Furnace atmosphere | CO ( 1 atm pressure ) |

| Time (mins) | Slag-wt (g) | Metal beads (g) | ($\%Cr_{tot}$) | ($\%Cr^{3+}$) | ($\%Cr^{2+}$) | ($\%Fe^{2+}$) | [%Cr] |
|---|---|---|---|---|---|---|---|
| 0 | 20.00 | 0.00 | 3.42 | 3.42 | 0.00 | 0.00 | 0.00 |
| 25 | 20.00 | 0.36 | 1.23 | 0.55 | 0.68 | 1.52 | 0.72 |

Terminated after 25 minutes

**Table 3.1 continued**

| | |
|---|---|
| Experiment No. | AS 20 |
| Fe-C-Se alloy wt. | 60 g |
| Initial wt.[%C] | 4.23 |
| Final wt.[%C] | 3.72 |
| Initial wt.(%$Cr_2O_3$) | 5 |
| Initial wt.[%Cr] | 0 |
| Final wt.[%Cr] | 0.86 |
| Metal addition | 0.005 wt.[%Se] |
| Slag wt. | 20 g |
| Slag type | 42%$SiO_2$, 38%CaO, 20%$Al_2O_3$ |
| Crucible type | 32 mm dia alumina |
| Temperature | 1470$^{o}$C |
| Furnace atmosphere | CO ( 1 atm pressure ) |

| Time (mins) | Sample-wt (g) | Slag-left (g) | (%$Cr_{tot}$) | (%$Cr^{3+}$) | (%$Cr^{2+}$) | (%$Fe^{2+}$) | [%Cr] |
|---|---|---|---|---|---|---|---|
| 0 | 0.00 | 20.00 | 3.42 | 3.42 | 0.00 | 0.00 | 0.00 |
| 15 | 0.81 | 20.00 | 2.56 | 1.17 | 1.39 | 1.32 | 0.28 |
| 25 | 1.56 | 19.19 | 1.26 | 0.67 | 0.59 | 1.48 | 0.69 |
| 35 | 0.96 | 17.63 | 1.02 | 0.58 | 0.44 | 1.36 | 0.76 |
| 45 | 1.34 | 16.67 | 0.86 | 0.46 | 0.40 | 1.26 | 0.81 |
| 60 | 1.07 | 15.33 | 0.71 | 0.43 | 0.28 | 1.04 | 0.84 |
| 80 | 1.10 | 14.26 | 0.54 | 0.26 | 0.28 | 0.93 | 0.88 |
| 120 | 0.88 | 13.16 | 0.26 | 0.24 | 0.02 | 0.64 | 0.95 |

**Table 3.1 continued**

| | |
|---|---|
| Experiment No. | AS 21 |
| Fe-C-Se alloy wt. | 60 g |
| Initial wt.[%C] | 4.10 |
| Final wt.[%C] | 3.67 |
| Initial wt.($\%Cr_2O_3$) | 5 |
| Initial wt.[%Cr] | 0 |
| Final wt.[%Cr] | 0.92 |
| Metal addition | 0.02 wt.[%Se] |
| Slag wt. | 20 g |
| Slag type | $42\%SiO_2$, 38%CaO, $20\%Al_2O_3$ |
| Crucible type | 32 mm dia alumina |
| Temperature | $1470^oC$ |
| Furnace atmosphere | CO ( 1 atm pressure ) |

| Time (mins) | Sample-wt (g) | Slag-left (g) | ($\%Cr_{tot}$) | ($\%Cr^{3+}$) | ($\%Cr^{2+}$) | ($\%Fe^{2+}$) | [%Cr] |
|---|---|---|---|---|---|---|---|
| 0 | 0.00 | 20.00 | 3.42 | 3.42 | 0.00 | 0.00 | 0.00 |
| 15 | 1.92 | 20.00 | 1.60 | 0.71 | 0.89 | 1.56 | 0.60 |
| 25 | 0.49 | 18.08 | 1.15 | 0.51 | 0.64 | 1.45 | 0.74 |
| 35 | 0.94 | 17.59 | 0.74 | 0.34 | 0.40 | 1.34 | 0.85 |
| 45 | 1.82 | 16.65 | 0.58 | 0.23 | 0.35 | 1.20 | 0.90 |
| 60 | 0.77 | 14.83 | 0.42 | 0.22 | 0.20 | 1.02 | 0.94 |
| 80 | 1.02 | 14.06 | 0.30 | 0.14 | 0.16 | 0.80 | 0.96 |

**Table 3.1 continued**

| | |
|---|---|
| Experiment No. | AS 22 |
| Fe-C alloy wt. | 60 g |
| Initial wt.[%C] | 4.23 |
| Final wt.[%C] | 3.96 |
| Initial wt.(%$Cr_2O_3$) | 5 |
| Initial wt.[%Cr] | 0 |
| Final wt.[%Cr] | 0.50 |
| Slag addition | 2.0 wt% $CaF_2$ |
| Slag wt. | 20 g |
| Slag type | 42%$SiO_2$, 38%CaO, 20%$Al_2O_3$ |
| Crucible type | 32 mm dia alumina |
| Temperature | 1470$^{o}$C |
| Furnace atmosphere | CO ( 1 atm pressure ) |

| Time (mins) | Sample-wt (g) | Slag-left (g) | (%$Cr_{tot}$) | (%$Cr^{3+}$) | (%$Cr^{2+}$) | (%$Fe^{2+}$) | [%Cr] |
|---|---|---|---|---|---|---|---|
| 0 | 0.00 | 20.00 | 3.42 | 3.42 | 0.00 | 0.00 | 0.00 |
| 15 | 1.90 | 20.00 | 2.90 | 2.10 | 0.80 | 0.20 | 0.17 |
| 25 | 0.82 | 18.10 | 2.55 | 1.62 | 0.93 | 0.18 | 0.27 |
| 35 | 1.53 | 17.28 | 2.40 | 1.50 | 0.90 | 0.15 | 0.31 |
| 45 | 1.50 | 15.75 | 2.22 | 1.30 | 0.92 | 0.18 | 0.36 |
| 60 | 1.18 | 14.25 | 1.87 | 0.99 | 0.88 | 0.17 | 0.45 |
| 80 | 0.94 | 13.07 | 1.61 | 0.89 | 0.72 | 0.32 | 0.53 |

**Table 3.1 continued**

| | |
|---|---|
| Experiment No. | AS 22R |
| Fe-C alloy wt. | 60 g |
| Initial wt.[%C] | 4.23 |
| Final wt.[%C] | 3.98 |
| Initial wt.(%$Cr_2O_3$) | 5 |
| Initial wt.[%Cr] | 0 |
| Final wt.[%Cr] | 0.64 |
| Slag addition | 2.0 wt% $CaF_2$ |
| Slag wt. | 20 g |
| Slag type | 42%$SiO_2$, 38%CaO, 20%$Al_2O_3$ |
| Crucible type | 32 mm dia alumina |
| Temperature | 1470°C |
| Furnace atmosphere | CO ( 1 atm pressure ) |

| Time (mins) | Sample-wt (g) | Slag-left (g) | (%$Cr_{tot}$) | (%$Cr^{3+}$) | (%$Cr^{2+}$) | (%$Fe^{2+}$) | [%Cr] |
|---|---|---|---|---|---|---|---|
| 0 | 0.00 | 20.00 | 3.42 | 3.42 | 0.00 | 0.00 | 0.00 |
| 15 | 0.88 | 20.00 | 3.00 | 2.16 | 0.84 | 0.16 | 0.14 |
| 25 | 0.85 | 19.12 | 2.60 | 1.50 | 1.10 | 0.16 | 0.27 |
| 35 | 0.84 | 18.27 | 2.49 | 1.43 | 1.06 | 0.14 | 0.30 |
| 45 | 0.96 | 17.43 | 2.33 | 1.31 | 1.02 | 0.15 | 0.35 |
| 60 | 1.61 | 16.47 | 1.99 | 0.99 | 1.00 | 0.16 | 0.44 |
| 80 | 1.21 | 14.86 | 1.64 | 0.81 | 0.83 | 0.17 | 0.53 |
| 100 | 0.77 | 13.65 | 1.49 | 0.70 | 0.79 | 0.16 | 0.59 |

**Table 3.1 continued**

| | |
|---|---|
| Experiment No. | AS 23 |
| Fe-C alloy wt. | 60 g |
| Initial wt.[%C] | 4.23 |
| Final wt.[%C] | 3.90 |
| Initial wt.(%$Cr_2O_3$) | 5 |
| Initial wt.[%Cr] | 0 |
| Final wt.[%Cr] | 0.81 |
| Slag addition | 3.5 wt% $CaF_2$ |
| Slag wt. | 20 g |
| Slag type | 42%$SiO_2$, 38%CaO, 20%$Al_2O_3$ |
| Crucible type | 32 mm dia alumina |
| Temperature | 1470$^{o}$C |
| Furnace atmosphere | CO ( 1 atm pressure ) |

| Time (mins) | Sample-wt (g) | Slag-left (g) | (%$Cr_{tot}$) | (%$Cr^{3+}$) | (%$Cr^{2+}$) | (%$Fe^{2+}$) | [%Cr] |
|---|---|---|---|---|---|---|---|
| 0 | 0.00 | 20.00 | 3.42 | 3.42 | 0.00 | 0.00 | 0.00 |
| 15 | 0.83 | 20.00 | 2.38 | 1.43 | 0.95 | 0.41 | 0.14 |
| 25 | 1.30 | 19.17 | 2.04 | 1.14 | 0.90 | 0.51 | 0.45 |
| 35 | 1.46 | 17.87 | 1.44 | 0.64 | 0.80 | 0.48 | 0.53 |
| 45 | 0.94 | 16.41 | 1.22 | 0.54 | 0.68 | 0.44 | 0.63 |
| 60 | 1.21 | 15.47 | 1.02 | 0.43 | 0.59 | 0.36 | 0.73 |
| 80 | 1.03 | 14.26 | 0.78 | 0.41 | 0.37 | 0.33 | 0.78 |
| 110 | 0.81 | 13.23 | 0.57 | 0.22 | 0.35 | 0.27 | 0.83 |

**Table 3.1 continued**

| | |
|---|---|
| Experiment No. | AS 24 |
| Fe-C alloy wt. | 60 g |
| Initial wt.[%C] | 4.23 |
| Final wt.[%C] | 3.87 |
| Initial wt.(%$Cr_2O_3$) | 5 |
| Initial wt.[%Cr] | 0 |
| Final wt.[%Cr] | 0.86 |
| Slag addition | 5.0 wt% $CaF_2$ |
| Slag wt. | 20 g |
| Slag type | 42%$SiO_2$, 38%CaO, 20%$Al_2O_3$ |
| Crucible type | 32 mm dia alumina |
| Temperature | 1470$^{o}$C |
| Furnace atmosphere | CO ( 1 atm pressure ) |

| Time (mins) | Sample-wt (g) | Slag-left (g) | (%$Cr_{tot}$) | (%$Cr^{3+}$) | (%$Cr^{2+}$) | (%$Fe^{2+}$) | [%Cr] |
|---|---|---|---|---|---|---|---|
| 0 | 0.00 | 20.00 | 3.42 | 3.42 | 0.00 | 0.00 | 0.00 |
| 15 | 1.03 | 20.00 | 1.30 | 0.72 | 0.58 | 1.16 | 0.67 |
| 20 | 0.75 | 18.97 | 1.02 | 0.67 | 0.45 | 1.16 | 0.74 |
| 25 | 2.03 | 18.22 | 0.74 | 0.49 | 0.25 | 0.99 | 0.86 |
| 35 | 0.87 | 16.19 | 0.55 | 0.37 | 0.18 | 0.77 | 0.91 |
| 50 | 1.99 | 15.32 | 0.43 | 0.30 | 0.13 | 0.60 | 0.94 |
| 60 | 0.97 | 13.33 | 0.31 | 0.21 | 0.10 | 0.53 | 0.97 |

**Table 3.1 continued**

| | |
|---|---|
| *Experiment No.* | *AS 25* |
| Fe-C alloy wt. | 60 g |
| Initial wt.[%C] | 4.23 |
| Final wt.[%C] | 3.81 |
| Initial wt.(%$Cr_2O_3$) | 10 |
| Initial wt.[%Cr] | 0 |
| Final wt.[%Cr] | 1.86 |
| Slag addition | 5.0 wt% $CaF_2$ |
| Slag wt. | 20 g |
| Slag type | 42%$SiO_2$, 38%CaO, 20%$Al_2O_3$ |
| Crucible type | 32 mm dia alumina |
| Temperature | 1470$^{o}$C |
| Furnace atmosphere | CO ( 1 atm pressure ) |

| Time (mins) | Sample-wt (g) | Slag-left (g) | (%$Cr_{tot}$) | (%$Cr^{3+}$) | (%$Cr^{2+}$) | (%$Fe^{2+}$) | [%Cr] |
|---|---|---|---|---|---|---|---|
| 0 | 0.00 | 20.00 | 6.84 | 6.84 | 0.00 | 0.00 | 0.00 |
| 15 | 1.98 | 20.00 | 3.18 | 1.94 | 1.24 | 3.22 | 1.21 |
| 25 | 0.52 | 18.02 | 2.01 | 1.30 | 0.71 | 2.94 | 1.63 |
| 35 | 0.91 | 17.50 | 1.49 | 0.94 | 0.55 | 2.71 | 1.86 |
| 45 | 0.95 | 16.59 | 1.35 | 0.90 | 0.45 | 2.54 | 1.87 |
| 60 | 1.54 | 15.64 | 1.21 | 0.85 | 0.36 | 2.41 | 1.90 |
| 80 | 1.09 | 14.10 | 1.05 | 0.74 | 0.31 | 2.17 | 1.94 |
| 120 | 0.82 | 13.01 | 0.96 | 0.66 | 0.30 | 1.85 | 1.96 |

**Table 3.1 continued**

| | |
|---|---|
| Experiment No. | AS26 |
| Fe-C alloy wt. | 60 g |
| Initial wt [%C] | 4.10 |
| Final wt [%C] | 3.57 |
| Initial wt (%$Cr_2O_3$) | 5 |
| Initial wt [%Cr] | 0 |
| Final wt [%Cr] | 0.62 |
| Slag addition - wt (%FeO) | 0.45 |
| Slag wt. | 20 g |
| Slag type | 42%$SiO_2$, 38%CaO, 20%$Al_2O_3$ |
| Crucible type | 32 mm dia alumina |
| Temperature | 1470°C |
| Furnace atmosphere | CO (1 atm pressure) |

| Time (mins) | Sample-wt (g) | Slag-left (g) | (%$Cr_{tot}$) | (%$Cr^{3+}$) | (%$Cr^{2+}$) | (%$Fe^{2+}$) | [%Cr] |
|---|---|---|---|---|---|---|---|
| 0 | 0.00 | 20.00 | 3.42 | 3.42 | 0.00 | 0.35 | 0.00 |
| 15 | 1.92 | 20.00 | 3.18 | 3.04 | 0.14 | 0.40 | 0.08 |
| 25 | 0.62 | 18.08 | 2.79 | 2.40 | 0.39 | 0.42 | 0.20 |
| 35 | 1.38 | 17.46 | 2.33 | 1.97 | 0.36 | 0.41 | 0.33 |
| 45 | 0.79 | 16.08 | 2.11 | 1.74 | 0.37 | 0.39 | 0.39 |
| 60 | 0.79 | 15.29 | 2.00 | 1.62 | 0.38 | 0.37 | 0.42 |
| 80 | 0.90 | 14.50 | 1.52 | 1.17 | 0.35 | 0.30 | 0.53 |
| 120 | 1.43 | 13.60 | 0.92 | 0.72 | 0.20 | 0.29 | 0.66 |

**Table 3.1 continued**

| | |
|---|---|
| Experiment No. | AS27 |
| Fe-C alloy wt. | 60 g |
| Initial wt [%C] | 4.10 |
| Final wt [%C] | 3.89 |
| Initial wt (%FeO) | 0.45 |
| Slag wt. | 20 g |
| Slag type | 42%$SiO_2$, 38%CaO, 20%$Al_2O_3$ |
| Crucible type | 32 mm dia alumina |
| Temperature | 1470$^{o}$C |
| Furnace atmosphere | CO (1 atm pressure) |

| Time (mins) | Sample-wt (g) | Slag-left (g) | (%$Fe^{2+}$) | (%FeO) |
|---|---|---|---|---|
| 0 | 0.00 | 20.00 | 0.35 | 0.45 |
| 10 | 0.82 | 20.00 | 0.27 | 0.35 |
| 20 | 0.62 | 19.18 | 0.25 | 0.32 |
| 30 | 0.61 | 18.56 | 0.23 | 0.30 |
| 40 | 0.68 | 17.95 | 0.20 | 0.25 |
| 50 | 0.93 | 17.27 | 0.18 | 0.23 |

**Table 3.2: Summary of experimental conditions for the reduction of $Cr_2O_3$ by carbon.**

| Run No. | Temp, °C | Furnace atm. | Metal wt,g | Slag wt,g | (%$Cr_2O_3$) | Metal (addition) | Slag |
|---|---|---|---|---|---|---|---|
| AS1 | 1470 | Ar | 60 | 20 | 5 | - | - |
| AS2 | 1470 | Ar | 60 | 20 | 8 | - | - |
| AS3 | 1470 | Ar | 60 | 20 | 10 | - | - |
| AS4 | 1470 | Ar | 60 | 20 | 3 | - | - |
| AS5 | 1470 | CO | 60 | 20 | 5 | - | - |
| AS6 | 1470 | Ar | 60 | 20 | 5 | - | - |
| AS7 | 1470 | Ar | 60 | 20 | 5 | 15 %Cr | - |
| AS8 | 1470 | Ar | 60 | 20 | 5 | 4 %Cr | - |
| AS9 | 1470 | Ar | - | 20 | 5 | - | - |
| AS10 | 1470 | CO | - | 20 | 5 | - | - |
| AS11 | 1470 | CO | 60 | 20 | 5 | 0.05 %S | - |
| AS12 | 1470 | CO | 60 | 20 | 5 | 0.10 %S | - |
| AS13 | 1470 | CO | 60 | 20 | 5 | 0.30 %S | - |
| AS14 | 1470 | CO | 60 | 20 | 5 | 0.50 %S | - |
| AS15 | 1470 | CO | 60 | 20 | 5 | - | 0.2 %S (as CaS) |
| AS16 | 1470 | CO | 60 | 20 | 5 | - | 0.2 %S (as FeS) |
| AS17 | 1470 | CO | 60 | 20 | - | - | - |
| AS18 | 1470 | CO | 60 | 20 | 5 | - | - |
| AS19 | 1470 | CO | 60 | 20 | 5 | 0.10 %S | - |

**Table 3.2 continued**

| Run No. | Temp, °C | Furnace atm. | Metal wt,g | Slag wt,g | Slag ($\%Cr_2O_3$) | Metal (addition) | Slag (addition) |
|---|---|---|---|---|---|---|---|
| AS20 | 1470 | CO | 60 | 20 | 5 | 0.005 %Se | - |
| AS21 | 1470 | CO | 60 | 20 | 5 | 0.02 %Se | - |
| AS22 | 1470 | CO | 60 | 20 | 5 | - | 2 $\%CaF_2$ |
| AS22R | 1470 | CO | 60 | 20 | 5 | - | 2 $\%CaF_2$ |
| AS23 | 1470 | CO | 60 | 20 | 5 | - | 3.5 $\%CaF_2$ |
| AS24 | 1470 | CO | 60 | 20 | 5 | - | 5 $\%CaF_2$ |
| AS25 | 1470 | CO | 60 | 20 | 10 | - | 5 $\%CaF_2$ |
| AS26 | 1470 | CO | 60 | 20 | 5 | - | 0.45 %FeO |
| AS27 | 1470 | CO | 60 | 20 | - | - | 0.45 %FeO |

# CHAPTER 4

# DEVELPOMENT OF A FIRST - ORDER CONSECUTIVE TWO - STAGE REACTION MODEL FOR $Cr_2O_3$ REDUCTION

# CHAPTER 4

# DEVELOPMENT OF A FIRST-ORDER CONSECUTIVE TWO-STAGE REACTION MODEL FOR $Cr_2O_3$ REDUCTION.

## 4.1 Intoduction

This chapter is concerned with the development of a first-order consecutive two-stage reaction model for the reduction of $Cr_2O_3$ from slag. Before moving on to a discussion of the development of the model, results on the reaction site of the reduction reactions, the effect of furnace atmosphere and oxide concentration are discussed. These results are later used in the development of the model.

## 4.2 Reaction site

There is the possibility of gaseous reduction of $Cr_2O_3$ taking place at the slag/gas interface, especially if the furnace has a CO atmosphere. To explore this possibility, runs AS9 and AS10 were carried out under an argon and carbon monoxide atmosphere, respectively, with no metallic phase. The results from these runs are presented in Fig. 4.1. The figure shows that there is a small difference in the concentrations of $(Cr^{3+})$ and

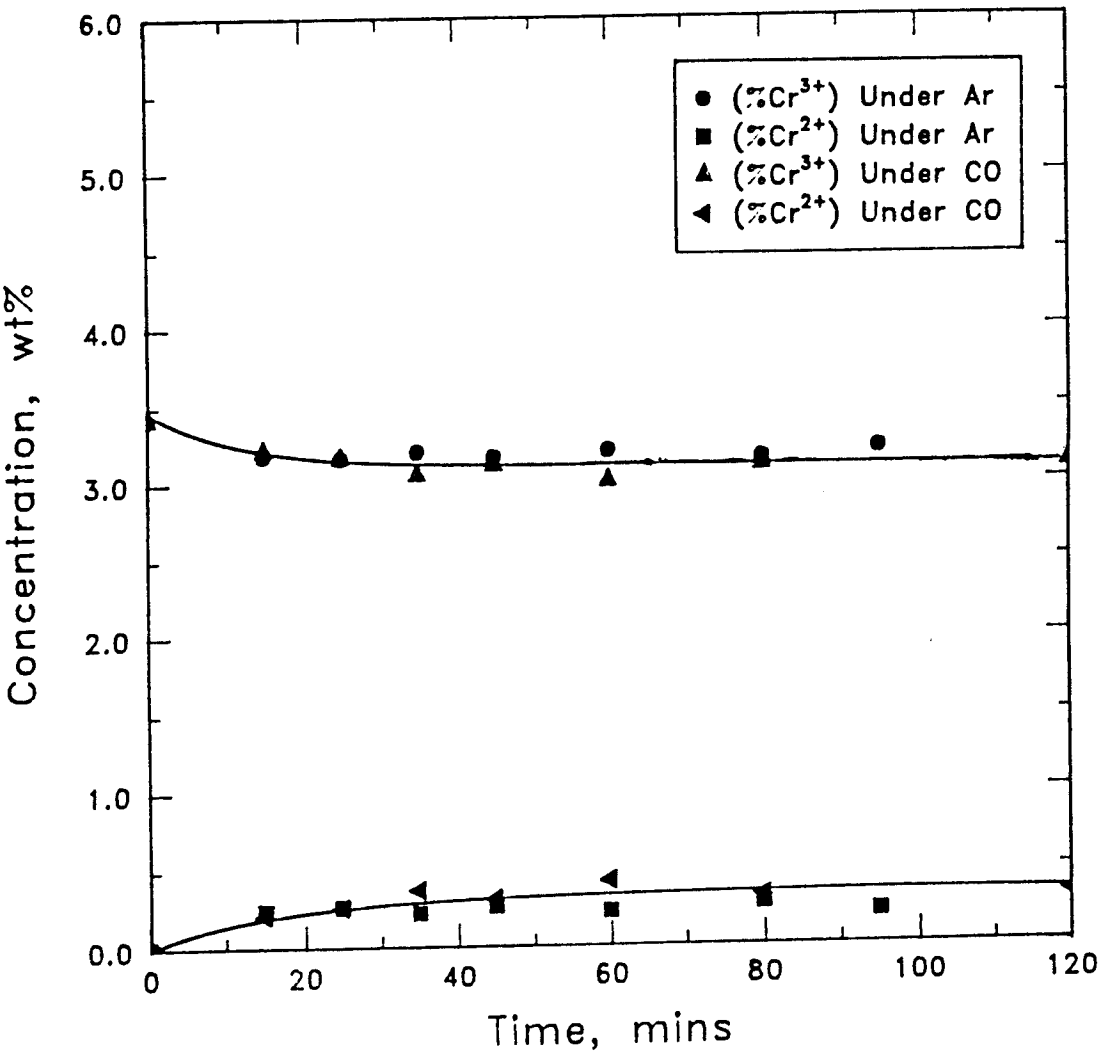


Fig. 4.1 Rate curves for ($Cr^{3+}$) and ($Cr^{2+}$) reduction in argon and carbon monoxide without metal ( AS9 and AS10).

$(Cr^{2+})$ obtained from the different atmospheres used. A slight reduction of $(Cr^{3+})$ to $(Cr^{2+})$ in the first 15 minutes occurs in both cases, after which the $(Cr^{3+})$ and $(Cr^{2+})$ concentrations remain constant throughout the runs. This may be attributable to the formation of a diffusion layer above the slag which becomes saturated with oxygen or $CO_2$, in the case of CO atmosphere, thereby inhibiting further reduction.

Fig. 4.2 shows rate curves for the reduction of $(Cr^{3+})$ and $(Cr^{2+})$ with (run AS1) and without (run AS9) a metal phase. The figure shows that the rate of $(Cr^{3+})$ reduction and $(Cr^{2+})$ production is decreased when the metallic phase is removed. This indicates that the reduction of $Cr_2O_3$ from slag takes place primarily at the slag/metal interface, and that a metal surface is needed for the reaction to take place at all. Philbrook and Kirkbride[49] obtained similar results in their study of the rate of FeO reduction from a $CaO-SiO_2-Al_2O_3$ slag by carbon-saturated iron. They found the rate of FeO reduction to decrease when the metallic phase was removed even though the slag-graphite interface was trebled in area.

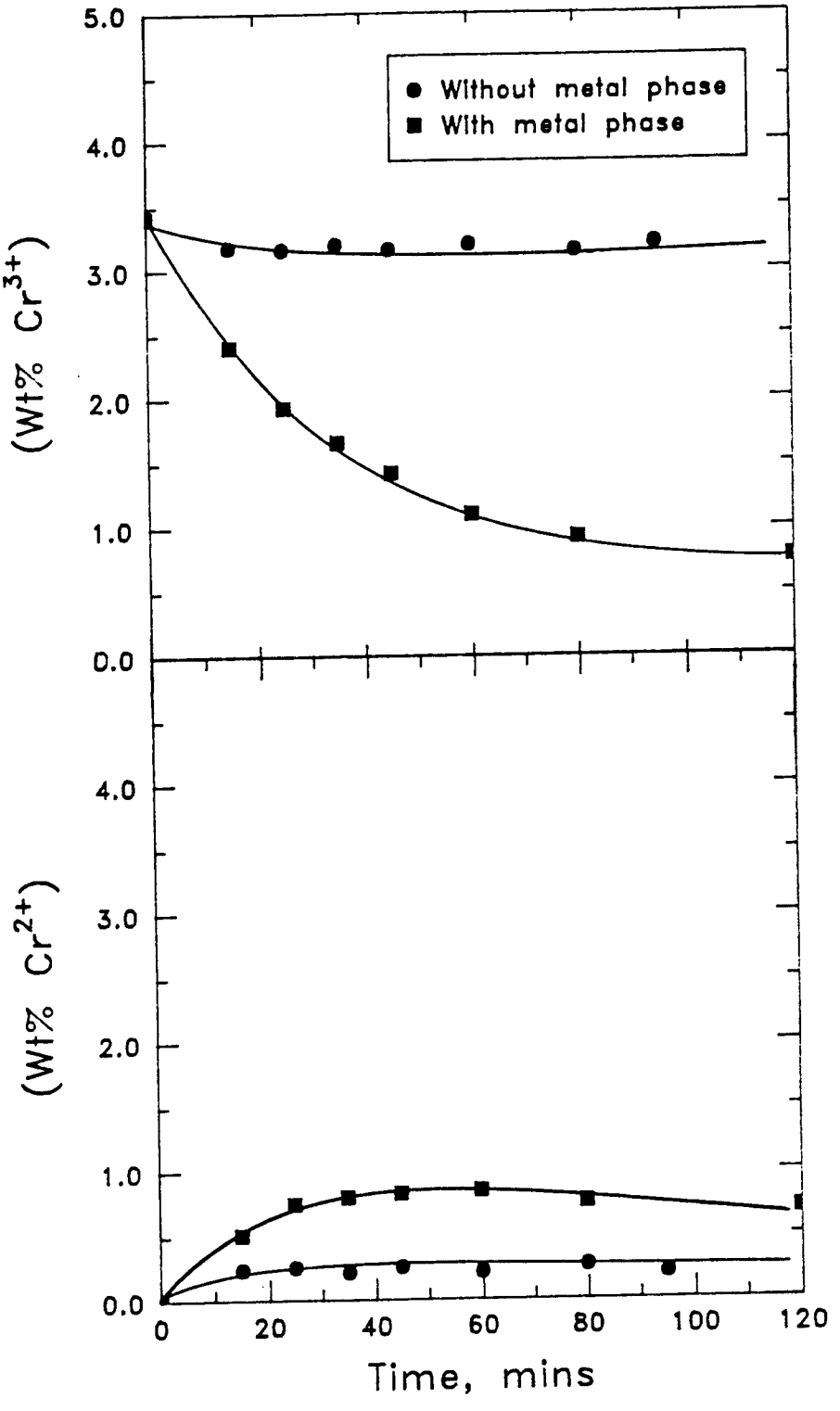


Fig. 4.2 Rate curves for ($Cr^{3+}$) and ($Cr^{2+}$) reduction in argon with slag/metal interface and without metal ( AS1 and AS9).

## 4.3 Effect of furnace atmosphere

For the purpose of examining the effect of furnace atmosphere on the rate of reduction of $Cr_2O_3$, runs AS1 and AS5 were carried out under an argon and a carbon monoxide atmosphere, respectively. The runs were conducted in the presence of a metallic phase to provide a slag/metal interface required for the reduction reactions to proceed, as outlined in Section 4.2. Except for the different atmospheres, all other experimental conditions remained the same.

The results are shown in Fig. 4.3. The figure shows that the furnace atmosphere does not affect the rate of reduction of $(Cr^{3+})$, this is shown by the similarity in the concentrations of $(Cr^{3+})$ from the two runs. An argon atmosphere, however, seems to increase the reduction rate of $(Cr^{2+})$. Anyakwo[37], in a similar study, also found no change in the reduction rate of $(Cr^{3+})$ in runs conducted under an argon and a carbon monoxide atmosphere. He observed an increase in the rate of $(Cr^{2+})$ reduction in experiments carried out under an argon atmosphere, as shown in Fig. 4.4 (at $1500^{o}C$).

Similar effects have been noted previously in silica reduction studies[26,50,51]. Silica was reduced from

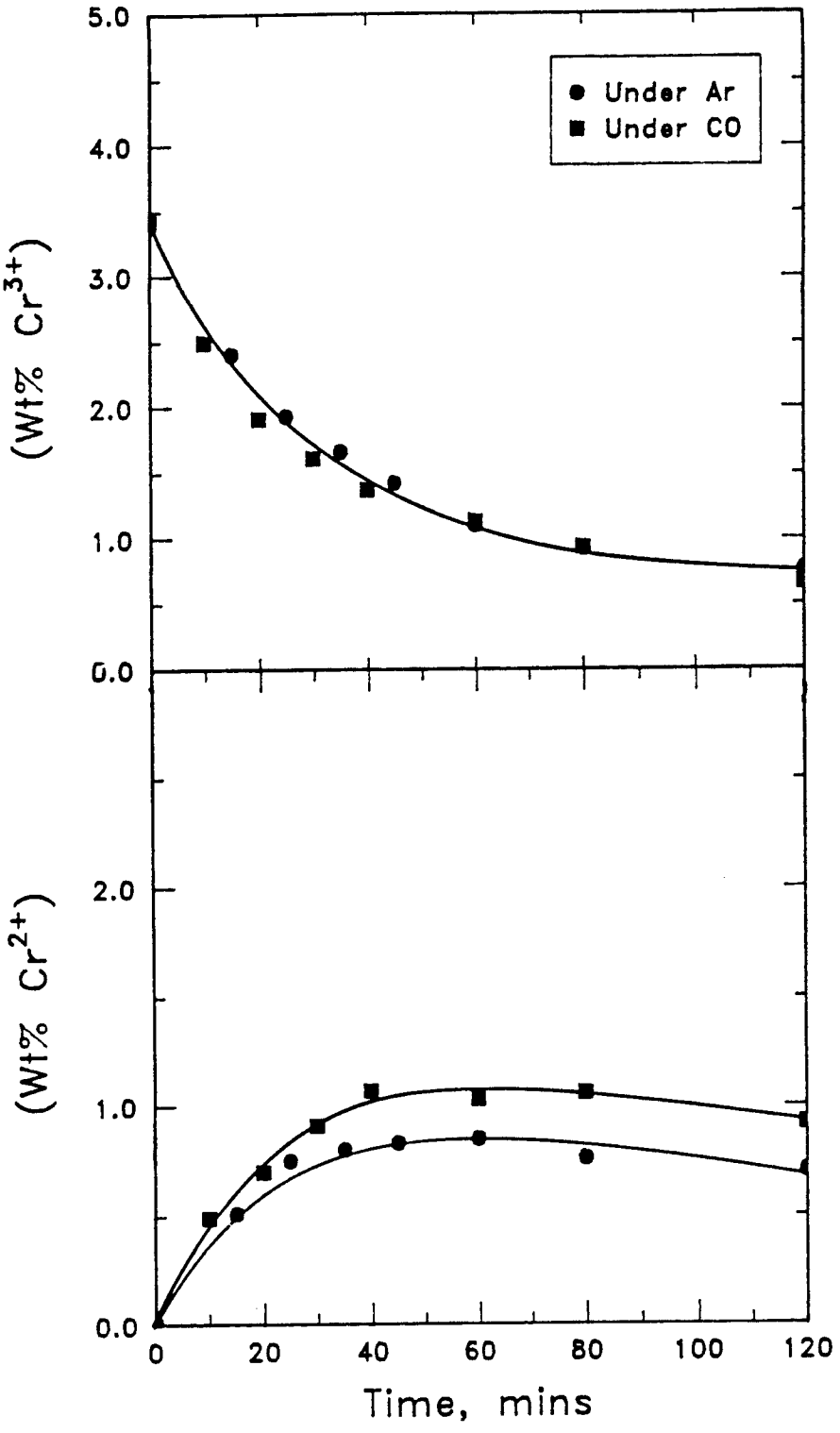


Fig. 4.3 Rate curves for ($Cr^{3+}$) and ($Cr^{2+}$) reduction showing effect of furnace atmosphere ( AS1 and AS5).

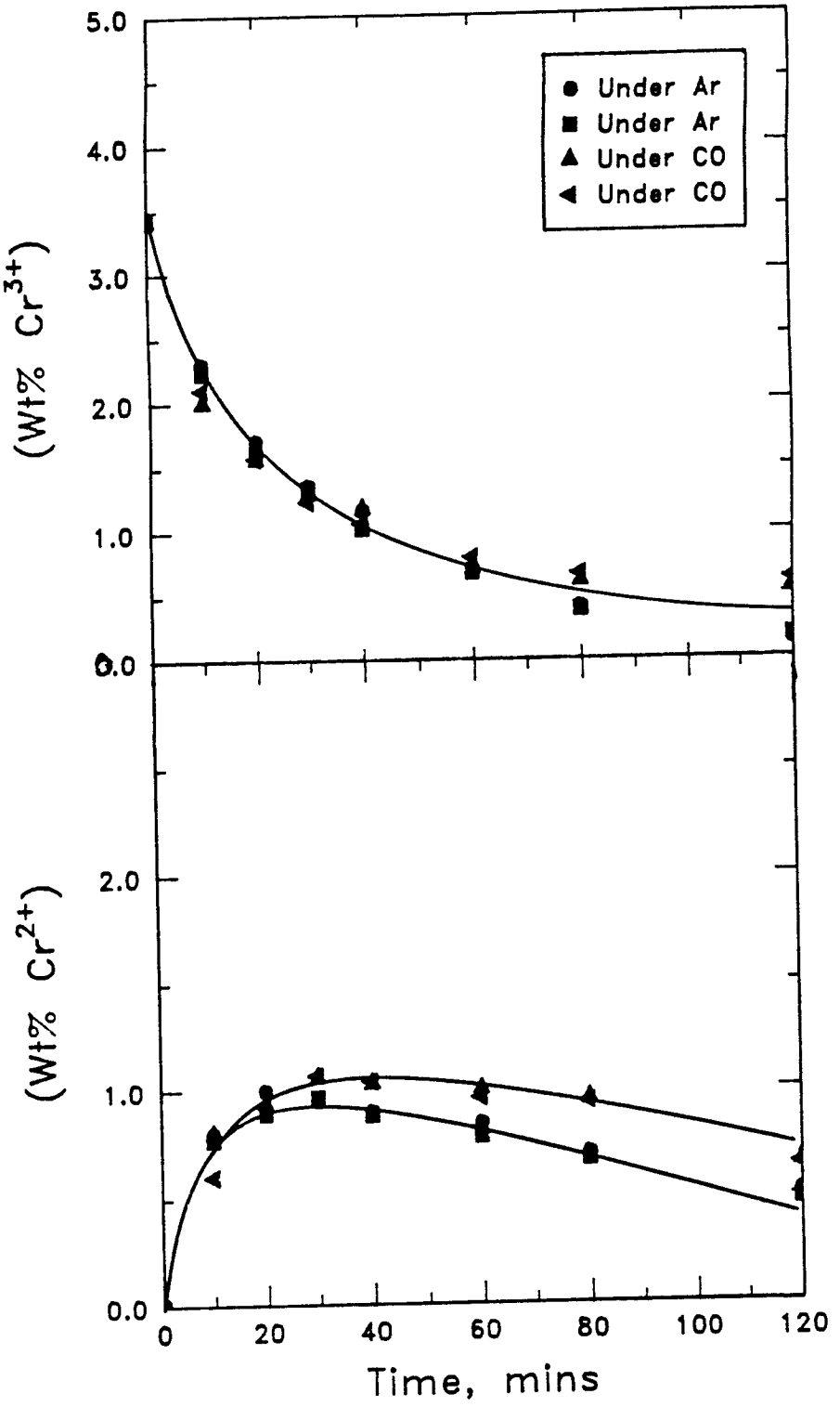


Fig. 4.4 Rate curves for ($Cr^{3+}$) and ($Cr^{2+}$) reduction showing effect of furnace atmosphere (Ref. 37).

calcium silicate slags by carbon saturated iron in graphite crucibles, twice as fast under argon than under carbon monoxide, and it was observed that the slag wetted the crucible under argon but not under a carbon monoxide atmosphere. It was proposed that there was some change in the physical properties of the slag and that this affected the rate of the reduction reaction which takes place at the slag/crucible/metal interface. However, in the present study, alumina crucibles were used and the inner walls of the crucibles were wetted by slag in both cases. It may be that the relative degree of wetting was different. This was not possible to substantiate in this study. It is not immediately clear why the rate of reduction of $(Cr^{2+})$ increases under an argon atmosphere.

## 4.4 Effect of oxide concentration

Changes in concentration alter the rate of reaction by altering the driving force for the reaction. For mass transfer control, changes in the bulk concentration will increase or decrease the concentration (and activity) gradient for diffusion through the interfacial boundary layer. For chemical reaction rate control, changes in composition alter the free energy driving the reaction. This can be reflected in a change of reaction rate, but

not in rate constant or mass transfer coefficient.

In order to examine whether changes in $Cr_2O_3$ concentration would affect its reduction rate, runs AS1, AS2 and AS3 were carried out in which the initial concentration was 5, 8 and 10 wt% $Cr_2O_3$, respectively, under an argon atmosphere. Fig. 4.5 shows the results obtained for the reduction of $(Cr^{3+})$ and $(Cr^{2+})$ from these runs. It is clear from the rate curves that at higher initial concentrations of $Cr_2O_3$ in slag, i.e. higher driving force, the reduction rate of $(Cr^{3+})$ is high leading to high production rates of $(Cr^{2+})$. At low initial concentrations of $Cr_2O_3$, the reduction rate of $(Cr^{3+})$ and production rate of $(Cr^{2+})$ are low. These rates are, therefore, proportional to the concentration of $Cr_2O_3$ in slag.

To satisfy the general first-order theory, which states that the reaction rate is proportional to the concentration of the reactant, the rate constants for the reactions involving the reduction of $(Cr^{3+})$ and $(Cr^{2+})$ must be the same for the different $Cr_2O_3$ concentrations in slag. Supporting evidence comes from the results of Robison and Pehlke[31] who found no change in $D/\delta$ for mass transfer of $(Cr^{3+})$ across the interface between the results from an unsaturated slag run, with an initial $Cr_2O_3$ content below

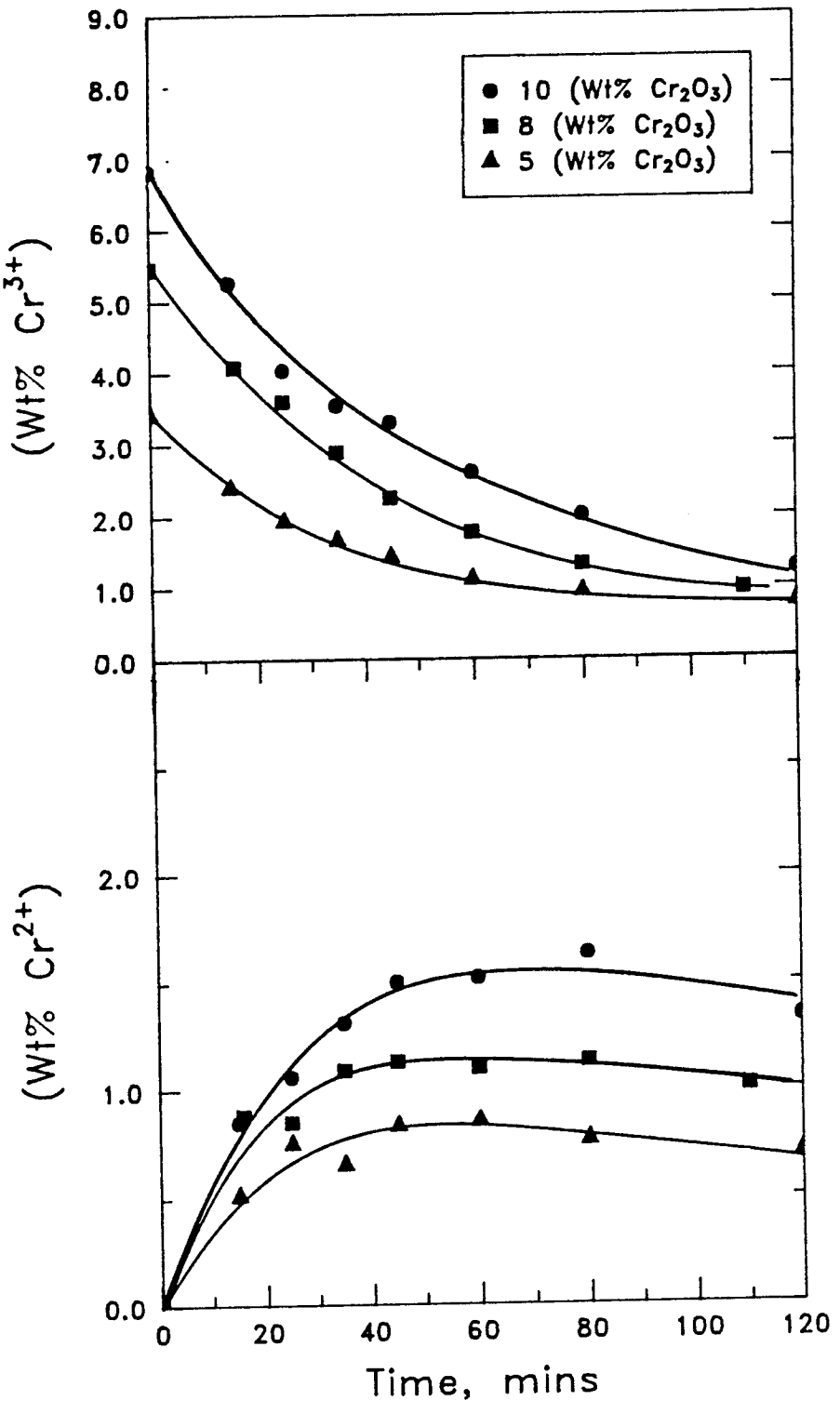


Fig. 4.5 Effect of $Cr_2O_3$ concentration on ($Cr^{3+}$) and ($Cr^{2+}$) reduction ( AS1, AS2 and AS3, under argon atm ).

saturation, and saturated slag runs. The excellent agreement of the unsaturated-slag runs is indicative of no change in mechanism. The change in the rate of reduction is, therefore, due to changes in the initial concentration of $Cr_2O_3$. The mechanism of reduction remains the same and as such the rate constants for the reduction reactions are expected to be similar for the different concentrations of $Cr_2O_3$. This will be discussed later after the model is developed.

## 4.5 MODEL DEVELOPMENT AND TESTING

### 4.5.1 Introduction

The reduction of $Cr_2O_3$ from slag by carbon can be described by the reactions:

$$(Cr_2O_3) + CO(g) \rightleftharpoons 2(CrO) + CO_2(g) \qquad (4.1)$$

and

$$(CrO) + CO(g) \rightleftharpoons [Cr] + CO_2(g) \qquad (4.2)$$

These reactions show that the reduction of $Cr_2O_3$ from slag follows a consecutive reaction mechanism in which $Cr_2O_3$ is reduced to CrO in the slag phase; and CrO reduced to Cr in the metal phase. From these reactions, it is clear that the product of the first reaction

becomes itself a reactant of the second reaction, both reactions taking place simultaneously. The reactions also show that the production of [Cr] is dependent on the concentration of $Cr_2O_3$ and as such any kinetic analysis of the system which separates the two reactions would not truly represent the events occurring during the reduction of $Cr_2O_3$ from slag.

Previous studies[20,31,35,37] on the reduction of $Cr_2O_3$ from slag have shown that there is a colour change of slag from bright green to deep blue during the initial stages of reduction, suggesting that chromic ($Cr^{3+}$) is reduced to chromous ($Cr^{2+}$) ion. This phenomenon was also observed in this study. In some studies into the reduction of chromic oxide from slag, the chromium in the slag is analysed as total chromium and used in the kinetic analysis of the system as such[32,33,41]. No mention is made of the existence of two valence states of chromium in slag. Although McCoy and Philbrook[20] recognised the presence of ($Cr^{3+}$) and ($Cr^{2+}$) in slag, they analysed their results by considering chromium to be present mainly as ($Cr^{2+}$). Robison and Pehlke[31] and recently Anyakwo[37] managed to split the total chromium in slag into ($Cr^{3+}$) and ($Cr^{2+}$) ions. They recognised the fact that the reduction of chromic oxide from slag takes place in two stages. However, in both cases, the two reactions were considered separately when analysing the

kinetics of the system.

Consecutive reaction schemes of varying complexity can be used to determine whether the reactions are of the kinetic type being considered and to evaluate the rate constants. Consecutive reactions in which an intermediate is involved can be represented by a general reaction:

$$A \underset{k_2}{\overset{k_1}{\rightleftharpoons}} B \underset{k_4}{\overset{k_3}{\rightleftharpoons}} C \qquad (4.3)$$

Depending on the reaction scheme being considered $k_2$ and $k_4$ can be zero. The scheme above can be extended to more complicated cases as for example when A directly reacts to produce C, as shown in equation (4.4).

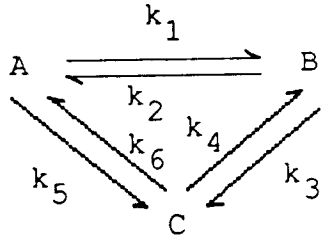


(4.4)

The use of consecutive reaction schemes has been applied in chemistry to evaluate rate constants and to determine the kinetic types of various reactions. Los et al[52] studied the kinetics of Mutarotation of D-Glucose

with consideration of an intermediate free-aldehyde form. Their results show that the Mutarotation equilibrium reaction can be represented by the reaction type shown in equation (4.3). In their study of P-Phenylene-bis-diazonium ion with water, Lewis et al[53] used similar reaction schemes to determine the rate constants. They found the reactions to follow a scheme similar to the one in equation (4.4).

### 4.5.2 Consecutive reaction schemes for $Cr_2O_3$ reduction

As outlined in section 4.5.1, the oxide being reduced in this study does not exhibit a single valence state, but instead exhibits two valence states in slag. Because of the valence change after reduction, the reduction of chromic oxide does not involve one reaction, but several. For example, $(Cr^{3+})$ may be reduced directly to [Cr] in the metal phase; $(Cr^{3+})$ may be reduced to $(Cr^{2+})$ in the slag phase; and $(Cr^{2+})$ may be reduced to [Cr] in the metal phase. The reverse reactions are also possible. In view of this complexity, a number of possible reaction models are derived. The problem is to determine which of these can best describe the reactions occurring during the reduction of $Cr_2O_3$. Four reaction schemes are initially considered in the analysis of the experimental results:

(1) that in which the reactions proceed irreversibly

$$(Cr^{3+}) \longrightarrow (Cr^{2+}) \longrightarrow [Cr] \qquad (4.5)$$

(2) that in which the first reaction is reversible and the second irreversible

$$(Cr^{3+}) \rightleftharpoons (Cr^{2+}) \longrightarrow [Cr] \qquad (4.6)$$

(3) that in which the first reaction is irreversible and the second reversible

$$(Cr^{3+}) \longrightarrow (Cr^{2+}) \rightleftharpoons [Cr] \qquad (4.7)$$

(4) and that in which both reactions are reversible

$$(Cr^{3+}) \rightleftharpoons (Cr^{2+}) \rightleftharpoons [Cr] \qquad (4.8)$$

Solutions to the differential equations showing the rate of change of the chromium species with time derived from the equations above can be obtained. Several investigators[54-62] have given methods of determining solutions to differential equations obtained from consecutive reactions. The method of Capellos et al[62] where Laplace Transforms are used is applied here. Appendix A shows an example of the application of this method. The first reaction scheme to be considered is that in which the reactions proceed irreversibly.

### 4.5.2.1 Scheme 1: First-order consecutive irreversible two-stage reactions.

Using this scheme the reduction of $Cr_2O_3$ can be represented as:

$$(Cr^{3+}) \xrightarrow{k_1} (Cr^{2+}) \xrightarrow{k_3} [Cr] \qquad (4.9)$$

The rate constant for the second reaction is represented by $k_3$ for convenience as will become clear when more complex schemes are considered. The differential equations describing this reaction scheme are:

$$\frac{d(Cr^{3+})}{dt} = -\frac{k_1}{h}(Cr^{3+}) \qquad (4.10)$$

$$\frac{d(Cr^{2+})}{dt} = \frac{k_1}{h}(Cr^{3+}) - \frac{k_3}{h}(Cr^{2+}) \qquad (4.11)$$

$$\frac{d[Cr]}{dt} = \frac{k_3}{h}(Cr^{2+}) \qquad (4.12)$$

where h is the slag height in cm. The solutions to equations (4.10), (4.11) and (4.12) after applying the boundary conditions; at $t = 0$, $(Cr^{3+}) = (Cr^{3+})_o$, $(Cr^{2+}) = [Cr] = 0$, are:

$$(Cr^{3+}) = (Cr^{3+})_o \exp(-K_1 t) \qquad (4.13)$$

$$(Cr^{2+}) = \frac{K_1 (Cr^{3+})_o}{K_3 - K_1} \left\{ \exp(-K_1 t) - \exp(-K_3 t) \right\} \qquad (4.14)$$

$$[Cr] = (Cr^{3+})_o \left\{ 1 + \frac{K_3}{K_1 - K_3} \exp(-K_1 t) - \frac{K_1}{K_1 - K_3} \exp(-K_3 t) \right\} \qquad (4.15)$$

where $K_1 = \frac{k_1}{h}$ etc. The units for K's are $min^{-1}$ and those for the k's are $cm.min^{-1}$. Equations (4.13), (4.14) and (4.15) show the dependence of the concentrations of the chromium species on rate constants and time for a first-order consecutive irreversible two-stage reaction scheme.

The rate constants for a particular set of data were determined by use of a computer program shown in appendix B. The program is for a general case when both reactions are reversible. The situation when both reactions are irreversible is obtained by taking the rate constants $k_2$ and $k_4$ equal to zero. The height of the slag is assumed constant, for simplicity, though it

changes due to slag sampling during the course of the experiment. The sensitivity of the concentrations of the chromium species to changes in slag height will be discussed later when the variation in slag height is taken into account.

The program in appendix B minimises the sums of squares of deviations, shown by equation (4.16), between the observed and calculated concentrations of the chromium species by changing the rate constant values.

$$F^2 = \sum_{i=1}^{n} (X_i - X_{pred})^2 \text{ minimised} \qquad (4.16)$$

where $F^2$ = index of disagreement

$X_i$ = observed concentration

$X_{pred}$ = predicted concentration

n = number of values at spaced time intervals

Basically, an initial guess of the rate constants is made and the concentrations of the chromium species calculated. These are then compared with the observed concentrations using equation (4.16) to determine the sums of squares of deviations. One of the rate constants is then changed and the process repeated until the sums of squares of deviations are a minimum. The rate constants giving the minimum sums of squares of deviations after a number of loops are taken as the rate

constants for a particular set of data.

To determine the rate constant to change for each loop, the program generates a random number between 0 and 1 using the NAG subroutine G05CAF. This is then multiplied by the number of rate constants being considered, the result of which when scaled down gives a whole number. If the result is equal to 0 then $k_1$ is to be changed, if it is equal to 1 then $k_2$ is to be changed and so on. The amount by which a rate constant is varied is also determined by random number generation using the same subroutine as above. The random number, which is between 0 and 1, is subtracted by 0.5 so that the result is between -0.5 and 0.5. This takes care of the fact that we can either increase or decrease the value of a rate constant. The value from the above operation is then multiplied by a factor, depending on the rate constant being varied, and the result added to the previous value of the rate constant. The factors used were 0.001, 0.0001, 0.001 and 0.0001 for $k_1$, $k_2$, $k_3$ and $k_4$, respectively. This procedure is repeated until the rate constants giving the minimum sums of squares of deviations are determined, after a number of loops.

The number of loops necessary to arrive at a minimum in the sums of squares of deviations were determined by carrying out loops for minimisation of the sums of

squares of deviations 1000, 10000 and 100000 times. Fig 4.6 shows an example of a graph showing the change in the sums of squares of deviations with number of loops. The figure shows that after about 10000 loops the sums of squares of deviations remain constant, an indication that a minimum has been reached. This was the case for all the data in this study. In terms of computing time, 10000 loops were considered adequate to give a minimum in the sums of squares of deviations and thus the rate constants.

The concentrations of the chromium species at various times were calculated using a computer program shown in appendix C and rate constants obtained from appendix B. The observed concentrations from run AS1 were used for comparison with the calculated values. Table 4.1 shows the observed concentrations and those calculated from this reaction scheme. Figure 4.7 shows a plot of the calculated concentration rate curves for a first-order consecutive-irreversible two-stage reaction scheme with the corresponding experimental results from run AS1. As can be seen from the figure, the calculated curves do not fit the observed results satisfactorily especially at times longer than 50 minutes. One can deduce from this that the reactions for the reduction of $Cr_2O_3$ from slag cannot be represented by a first-order consecutive irreversible two-stage reaction scheme.

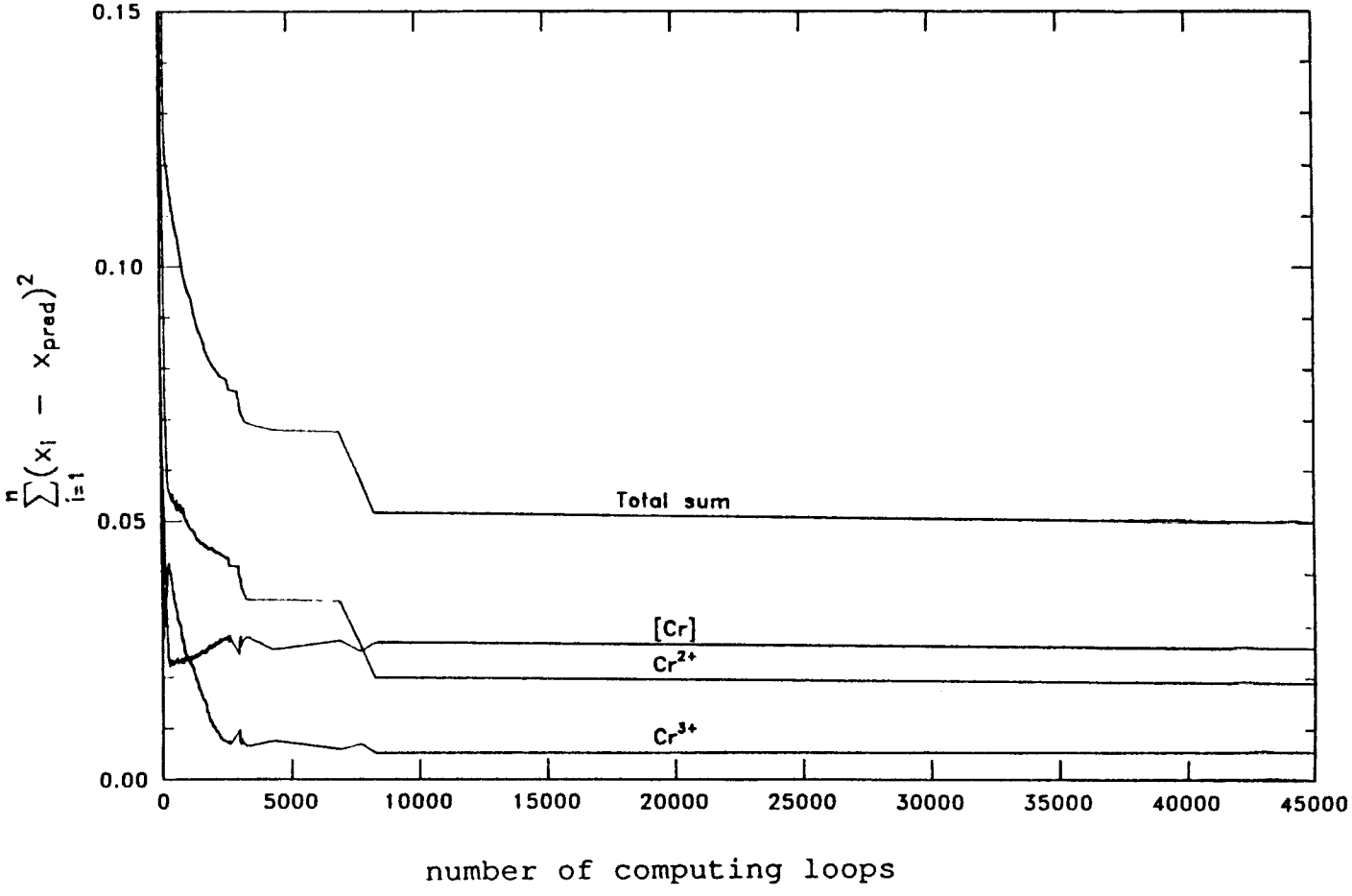


Fig. 4.6 Variation of sums of squares of deviations of the chromium species with number of computing loops.

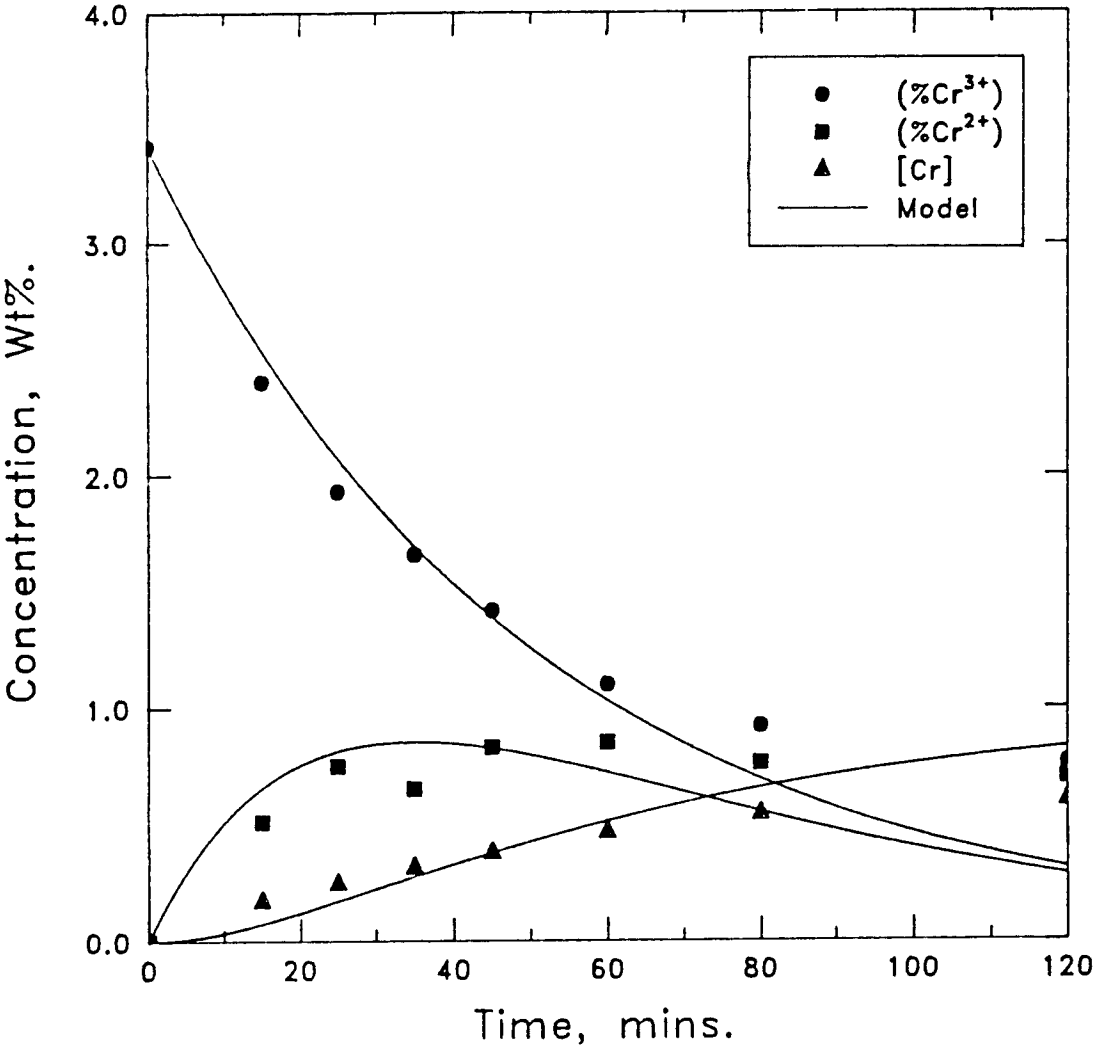


$k_1 = 0.0195\ cm \cdot min^{-1}$.
$k_3 = 0.0390\ cm \cdot min^{-1}$.

Sums of squares of deviations are:
$Cr^{3+} = 0.301$, $Cr^{2+} = 0.303$, $Cr_{Met.} = 0.087$.

Fig. 4.7 Time variation in concentration of $(Cr^{3+})$, $(Cr^{2+})$ and [Cr]. The curves are calculated from Scheme 1 and the points are observed values from run AS1.

*Table 4.1. Observed and calculated concentrations for ($Cr^{3+}$), ($Cr^{2+}$) and [Cr] from scheme 1.*

| Time (mins) | ($Cr^{3+}$), wt% | | ($Cr^{2+}$), wt% | | [Cr], wt% | |
|---|---|---|---|---|---|---|
| | Obsd. | Calc. | Obsd. | Calc. | Obsd. | Calc |
| 0 | 3.42 | 3.42 | 0.00 | 0.00 | 0.00 | 0.00 |
| 15 | 2.40 | 2.53 | 0.51 | 0.66 | 0.17 | 0.08 |
| 25 | 1.93 | 2.07 | 0.75 | 0.81 | 0.24 | 0.17 |
| 35 | 1.66 | 1.69 | 0.65 | 0.85 | 0.36 | 0.28 |
| 45 | 1.42 | 1.39 | 0.83 | 0.82 | 0.38 | 0.38 |
| 60 | 1.10 | 1.03 | 0.85 | 0.72 | 0.46 | 0.52 |
| 80 | 0.92 | 0.69 | 0.76 | 0.55 | 0.54 | 0.66 |
| 120 | 0.76 | 0.31 | 0.70 | 0.28 | 0.60 | 0.83 |

### 4.5.2.2 Scheme 2: Fisrt-order consecutive reversible and irreversible two-stage reactions.

Using a first-order consecutive two-stage reaction scheme in which the first reaction is reversible and the second irreversible, the reactions for the reduction of $Cr_2O_3$ can be represented as:

$$(Cr^{3+}) \underset{k_2}{\overset{k_1}{\rightleftharpoons}} (Cr^{2+}) \xrightarrow{k_3} [Cr] \qquad (4.17)$$

The differential equations describing this scheme are:

$$\frac{d(Cr^{3+})}{dt} = \frac{k_2}{h}(Cr^{2+}) - \frac{k_1}{h}(Cr^{3+}) \qquad (4.18)$$

$$\frac{d(Cr^{2+})}{dt} = \frac{k_1}{h}(Cr^{3+}) - \frac{k_2 + k_3}{h}(Cr^{2+}) \qquad (4.19)$$

$$\frac{d[Cr]}{dt} = \frac{k_3}{h}(Cr^{2+}) \qquad (4.20)$$

where h is the height of slag in cm. For the boundary conditions; at $t = 0$, $(Cr^{3+}) = (Cr^{3+})_o$, $(Cr^{2+}) = [Cr] = 0$, the solutions to equations (4.18), (4.19) and (4.20) are:

$$(Cr^{3+}) = (Cr^{3+})_o \left\{ \frac{K_2 + K_3 - m_1}{m_2 - m_1} \exp(-m_1 t) + \frac{K_2 + K_3 - m_2}{m_1 - m_2} \exp(-m_2 t) \right\} \qquad (4.21)$$

$$(Cr^{2+}) = K_1 (Cr^{3+})_o \left\{ \frac{1}{m_2 - m_1} \exp(-m_1 t) + \frac{1}{m_1 - m_2} \exp(-m_2 t) \right\} \qquad (4.22)$$

$$[Cr] = K_1 K_3 (Cr^{3+})_o \left\{ \frac{1}{m_1 m_2} - \frac{1}{m_1(m_2 - m_1)} \right.$$

$$\left. \exp(-m_1 t) - \frac{1}{m_2(m_1 - m_2)} \exp(-m_2 t) \right\} \qquad (4.23)$$

where $K_1 = \frac{k_1}{h}$ etc. The expressions for the m functions are:

$$m_1 = 0.5 \left[ (K_1 + K_2 + K_3) + \sqrt{(K_1 + K_2 + K_3)^2 - 4 K_1 K_3} \right] \qquad (4.24)$$

$$m_2 = 0.5 \left[ (K_1 + K_2 + K_3) - \sqrt{(K_1 + K_2 + K_3)^2 - 4 K_1 K_3} \right] \qquad (4.25)$$

Equations (4.21), (4.22) and (4.23) give the dependence of the concentrations of the chromium species on rate constants and time for a first-order consecutive two-stage reaction scheme in which the first reaction is reversible and the second irreversible. Table 4.2 shows the calculated concentrations from this reaction scheme and the corresponding observed values from run AS1. In this case the rate constant $k_4$ is taken as being equal to zero when using the computer programs in appendices B and C, so that the general scheme is reduced to the one

under consideration.

**Table 4.2: Observed and calculated concentrations for ($Cr^{3+}$), ($Cr^{2+}$) and [Cr] from scheme 2.**

| Time | ($Cr^{3+}$), wt% | | ($Cr^{2+}$), wt% | | [Cr], wt% | |
|---|---|---|---|---|---|---|
| (mins) | Obsd. | Calc. | Obsd. | Calc. | Obsd. | Calc |
| 0 | 3.42 | 3.42 | 0.00 | 0.00 | 0.00 | 0.00 |
| 15 | 2.40 | 2.56 | 0.51 | 0.64 | 0.17 | 0.08 |
| 25 | 1.93 | 2.12 | 0.75 | 0.78 | 0.24 | 0.17 |
| 35 | 1.66 | 1.78 | 0.65 | 0.81 | 0.36 | 0.28 |
| 45 | 1.42 | 1.49 | 0.83 | 0.78 | 0.38 | 0.36 |
| 60 | 1.10 | 1.15 | 0.85 | 0.68 | 0.46 | 0.49 |
| 80 | 0.92 | 0.82 | 0.76 | 0.53 | 0.54 | 0.63 |
| 120 | 0.76 | 0.42 | 0.70 | 0.29 | 0.60 | 0.80 |

Figure 4.8 shows a plot of the calculated rate curves for ($Cr^{3+}$), ($Cr^{2+}$) and [Cr] with the corresponding observed values from run AS1. Table 4.3 shows a comparison of the sums of squares of deviations between schemes 1 and 2.

The table shows that there is a decrease in the sums of squares of deviations of all the chromium species using scheme 2 as opposed to scheme 1. Examination of Fig. 4.8 shows that there is a slight improvement in the fit for the ($Cr^{3+}$) curve compared to the simpler model above.

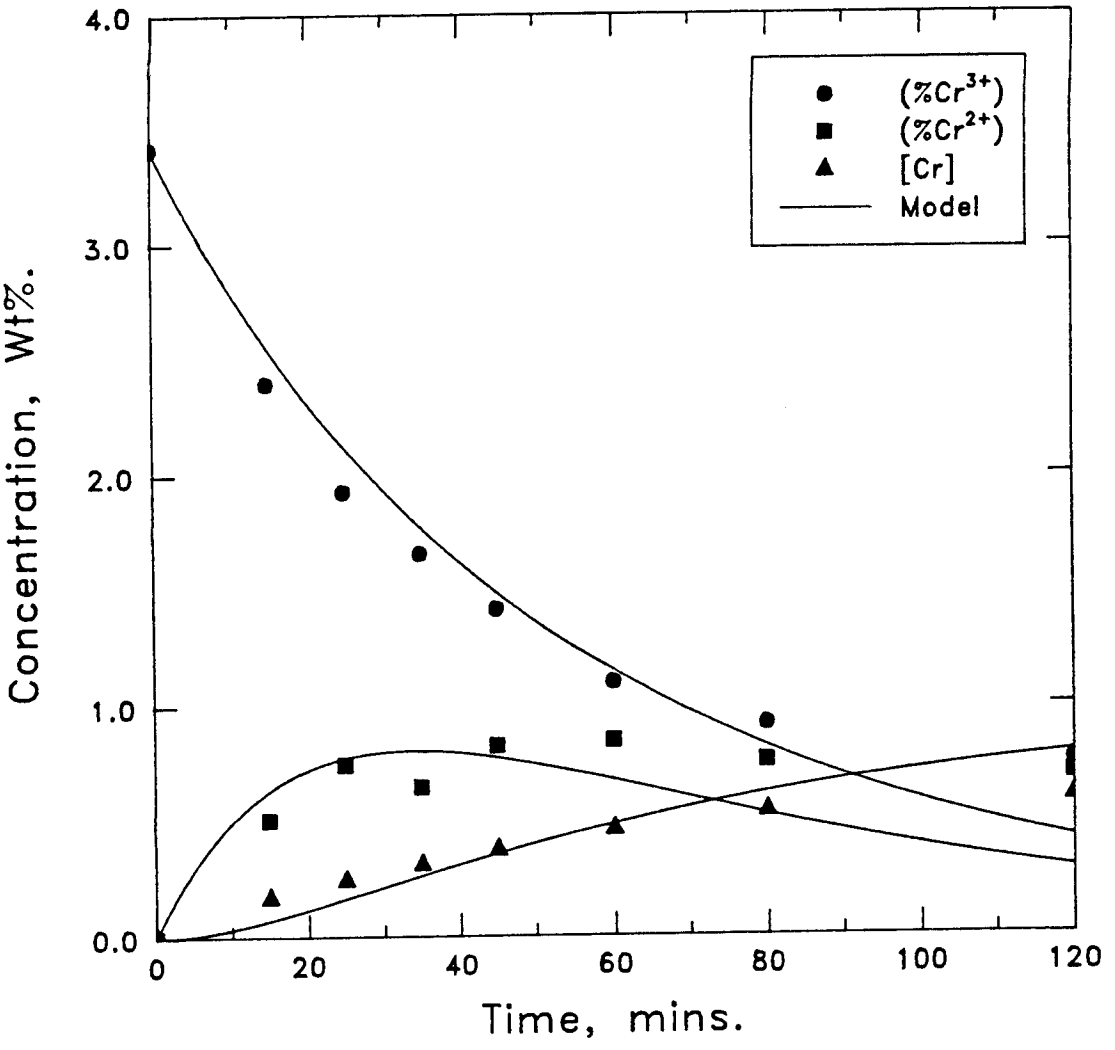


$k_1 = 0.0195\ cm \cdot min^{-1}$. $k_2 = 0.0049\ cm \cdot min^{-1}$.
$k_3 = 0.0390\ cm \cdot min^{-1}$.

Sums of squares of deviations are:
$Cr^{3+} = 0.210$, $Cr^{2+} = 0.298$, $Cr_{Met.} = 0.065$.

Fig. 4.8 Time variation in concentration of ($Cr^{3+}$), ($Cr^{2+}$) and [Cr]. The curves are calculated from scheme 2 and the points are observed values from run AS1.

**Table 4.3: Sums of squares of deviations for schemes 1 and 2.**

| Scheme | $(Cr^{3+})$ | $(Cr^{2+})$ | [Cr] |
|---|---|---|---|
| 1 | 0.301 | 0.303 | 0.087 |
| 2 | 0.210 | 0.298 | 0.065 |

The shapes of the $(Cr^{2+})$ and [Cr] curves remain unchanged, though there is a reduction in the sum of squares of deviations. It follows from the above that this reaction scheme does not represent the kinetics of reduction of $Cr_2O_3$ from slag.

In contrast to scheme 2, a consecutive two-stage reaction scheme in which the first reaction is irreversible and the second reversible is considered in the next section.

### 4.5.2.3 Scheme 3: First-order consecutive irreversible and reversible two-stage reactions.

Using this scheme in which the first reaction is irreversible and the second reversible, the reactions for *the reduction of $Cr_2O_3$ can be represented as:*

$$(Cr^{3+}) \xrightarrow{k_1} (Cr^{2+}) \underset{k_4}{\overset{k_3}{\rightleftharpoons}} [Cr] \qquad (4.26)$$

The differential equations are:

$$\frac{d(Cr^{3+})}{dt} = -\frac{k_1}{h}(Cr^{3+}) \qquad (4.27)$$

$$\frac{d(Cr^{2+})}{dt} = \frac{k_1}{h}(Cr^{3+}) - \frac{k_3}{h}(Cr^{2+}) + \frac{k_4}{h}[Cr] \qquad (4.28)$$

$$\frac{d[Cr]}{dt} = \frac{k_3}{h}(Cr^{2+}) - \frac{k_4}{h}[Cr] \qquad (4.29)$$

where h is the height of slag in cm. For the boundary conditions; at $t = 0$, $(Cr^{3+}) = (Cr^{3+})_o$, $(Cr^{2+}) = [Cr] = 0$ the solutions to equations (4.27), (4.28) and (4.29) are

$$(Cr^{3+}) = (Cr^{3+})_o \exp(-K_1 t) \qquad (4.30)$$

$$(Cr^{2+}) = K_1 (Cr^{3+})_o \left\{ \frac{K_4}{m_1 m_2} - \frac{K_4 - m_1}{m_1(m_2 - m_1)} \exp(-m_1 t) - \frac{K_4 - m_2}{m_2(m_1 - m_2)} \exp(-m_2 t) \right\} \qquad (4.31)$$

$$[Cr] = K_1K_3\,(Cr^{3+})_o \left\{ \frac{1}{m_1m_2} - \frac{1}{m_1(m_2 - m_1)} \exp(-m_1t) - \frac{1}{m_2(m_1 - m_2)} \exp(-m_2t) \right\} \quad (4.32)$$

where $K_1 = \frac{k_1}{h}$ etc. The expressions for the m functions are:

$$m_1 = 0.5 \left[ (K_1 + K_3 + K_4) + \sqrt{(K_1 + K_3 + K_4)^2 - 4(K_1K_3 + K_1K_4)} \right] \quad (4.33)$$

$$m_2 = 0.5 \left[ (K_1 + K_3 + K_4) - \sqrt{(K_1 + K_3 + K_4)^2 - 4(K_1K_3 + K_1K_4)} \right] \quad (4.34)$$

Equations (4.30), (4.31) and (4.32) give the concentration dependence of the chromium species on rate constants and time for a first-order consecutive two-stage reaction scheme in which the first reaction is irreversible and the second reversible. It is to be noted that although equation (4.32) may seem to be similar to equation (4.23), they are actually different. The difference lies in the values of $m_1$ and $m_2$. In equation (4.23), $m_1$ and $m_2$ are determined from the rate constants $K_1$, $K_2$ and $K_3$ whereas in equation (4.32), they

are determined from $K_1$,$K_3$ and $K_4$. In addition, an extra term $K_1K_4$, appears under the square root when determining $m_1$ and $m_2$ in equation (4.32).

As in schemes 1 and 2, the concentrations of the chromium species were calculated using the programs in appendices B and C by taking $k_2 = 0$. The calculated and corresponding observed values from run AS1 are shown in Table 4.4.

**Table 4.4: Observed and calculated concentrations for ($Cr^{3+}$), ($Cr^{2+}$) and [Cr] from scheme 3.**

| Time | ($Cr^{3+}$), wt% | | ($Cr^{2+}$), wt% | | [Cr], wt% | |
|---|---|---|---|---|---|---|
| (mins) | Obsd. | Calc. | Obsd. | Calc. | Obsd. | Calc. |
| 0 | 3.42 | 3.42 | 0.00 | 0.00 | 0.00 | 0.00 |
| 15 | 2.40 | 2.54 | 0.51 | 0.61 | 0.17 | 0.08 |
| 25 | 1.93 | 2.09 | 0.75 | 0.77 | 0.24 | 0.18 |
| 35 | 1.66 | 1.72 | 0.65 | 0.83 | 0.36 | 0.28 |
| 45 | 1.42 | 1.41 | 0.83 | 0.84 | 0.38 | 0.37 |
| 60 | 1.10 | 1.05 | 0.85 | 0.82 | 0.46 | 0.48 |
| 80 | 0.92 | 0.71 | 0.76 | 0.78 | 0.54 | 0.59 |
| 120 | 0.76 | 0.32 | 0.70 | 0.72 | 0.60 | 0.71 |

Fig 4.9 shows a plot of the calculated rate curves from scheme 3 with the observed values. The figure shows that when the second reaction is considered reversible, there seems to be an improvement in the fits for the ($Cr^{2+}$) and [Cr] curves compared to those in schemes 1 and

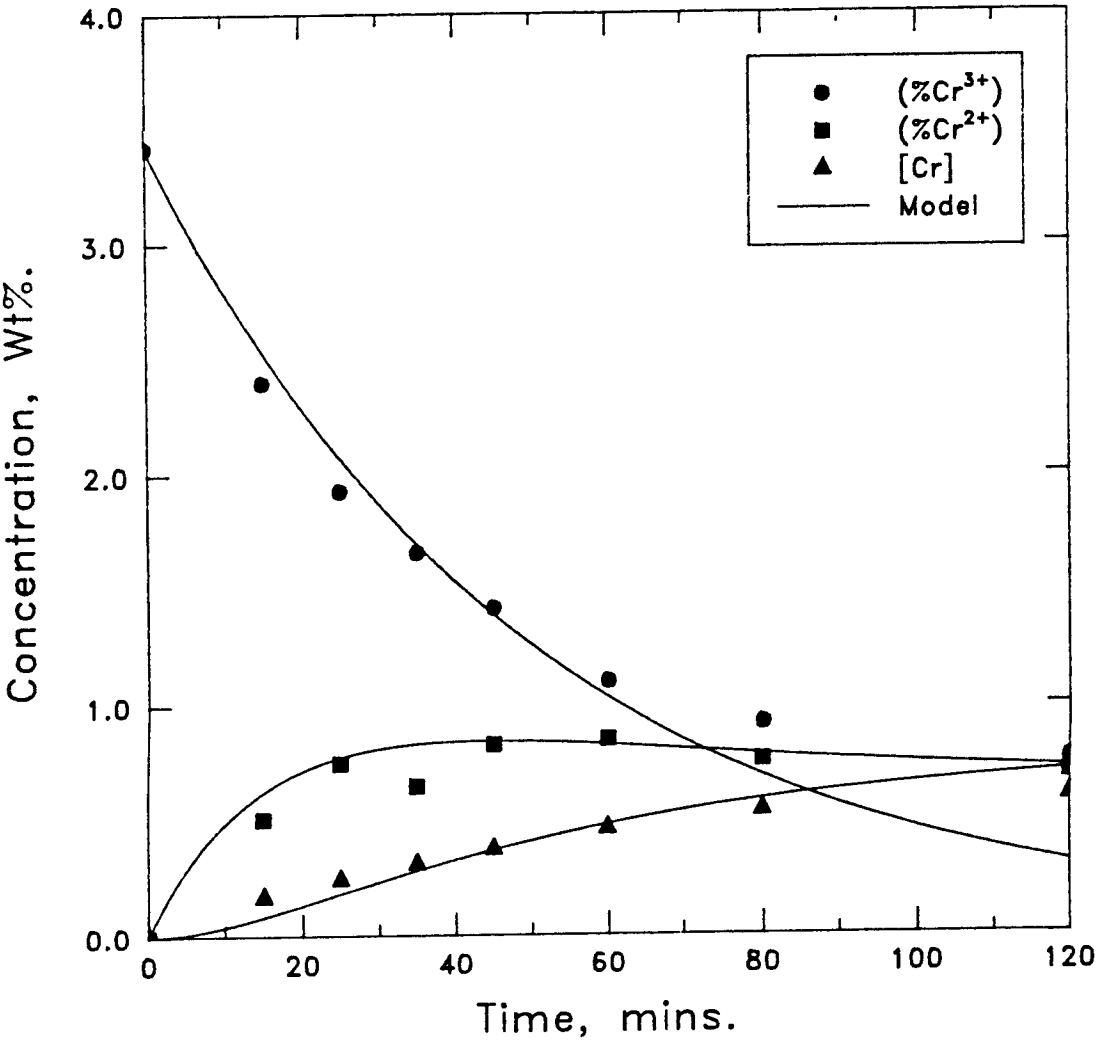


$k_1 = 0.0195\ cm \cdot min^{-1}$.

$k_3 = 0.0488\ cm \cdot min^{-1}$. $k_4 = 0.0117\ cm \cdot min^{-1}$.

Sums of squares of deviations are:

$Cr^{3+} = 0.301$, $Cr^{2+} = 0.051$, $Cr_{Met.} = 0.027$.

Fig. 4.9 Time variation in concentration of ($Cr^{3+}$), ($Cr^{2+}$) and [Cr]. The curves are calculated from scheme 3 and the points are observed values from run AS1.

2. This is also evidenced by the reduction in the sum of squares of deviations for these chromium species, as shown in Table 4.5

**Table 4.5: Sums of squares of deviations for schemes 1, 2 and 3.**

| Scheme | $(Cr^{3+})$ | $(Cr^{2+})$ | [Cr] |
|---|---|---|---|
| 1 | 0.301 | 0.303 | 0.087 |
| 2 | 0.210 | 0.298 | 0.065 |
| 3 | 0.301 | 0.051 | 0.027 |

It is evident from the figure that there is a large deviation of the $(Cr^{3+})$ curve from the observed values especially at longer times. This is shown by the increase in the sum of squares of deviations for this curve compared to that in scheme 2 where the first reaction is reversible. Therefore, this scheme can not be considered to represent the kinetics of reduction of $Cr_2O_3$ from slag.

It has been seen so far that if one considers the first reaction to be reversible and the second irreversible, the $(Cr^{3+})$ curve fits the observed values satisfactorily, within experimental error, whereas the $(Cr^{2+})$ and [Cr] curves markedly deviate from their corresponding observed values. On the other hand, consideration of the first

reaction to be irreversible and the second reversible improves the fits for the ($Cr^{2+}$) and [Cr] curves whereas that for ($Cr^{3+}$) deviates from the observed values. A compromise is reached when both reactions are considered to be reversible. A reaction scheme describing this type of consecutive reactions is discussed in the next section.

### 4.5.2.4 Scheme 4: First-order consecutive reversible two-stage reactions.

Using this scheme the reactions can be represented as:

$$(Cr^{3+}) \underset{k_2}{\overset{k_1}{\rightleftharpoons}} (Cr^{2+}) \underset{k_4}{\overset{k_3}{\rightleftharpoons}} [Cr] \qquad (4.35)$$

The differential equations describing this scheme are:

$$\frac{d(Cr^{3+})}{dt} = \frac{k_2}{h}(Cr^{2+}) - \frac{k_1}{h}(Cr^{3+}) \qquad (4.36)$$

$$\frac{d(Cr^{2+})}{dt} = \frac{k_1}{h}(Cr^{3+}) - \frac{k_2 + k_3}{h}(Cr^{2+}) + \frac{k_4}{h}[Cr] \qquad (4.37)$$

$$\frac{d[Cr]}{dt} = \frac{k_3}{h}(Cr^{2+}) - \frac{k_4}{h}[Cr] \qquad (4.38)$$

where h is the height of slag in cm. For the boundary conditions; at t = 0, $(Cr^{3+}) = (Cr^{3+})_o$, $(Cr^{2+}) = [Cr] = 0$, the solutions to equations (4.36), (4.37) and (4.38) are:

$$(Cr^{3+}) = (Cr^{3+})_o \left\{ \frac{K_2K_4}{m_1m_2} + \frac{m_1^2 - m_1(K_2+ K_3+ K_4) + K_2K_4}{m_1(m_1 - m_2)} \exp(-m_1t) + \frac{m_2^2 - m_2(K_2+ K_3+ K_4) + K_2K_4}{m_2(m_2 - m_1)} \exp(-m_2t) \right\} \qquad (4.39)$$

$$(Cr^{2+}) = K_1 (Cr^{3+})_o \left\{ \frac{K_4}{m_1m_2} - \frac{K_4 - m_1}{m_1 (m_2 - m_1)} \exp(-m_1t) - \frac{K_4 - m_2}{m_2(m_1 - m_2)} \exp(-m_2t) \right\} \qquad (4.40)$$

$$[Cr] = K_1K_3 (Cr^{3+})_o \left\{ \frac{1}{m_1m_2} - \frac{1}{m_1(m_2 - m_1)} \exp(-m_1t) - \frac{1}{m_2(m_1 - m_2)} \exp(-m_2t) \right\} \qquad (4.41)$$

where $K_1 = \frac{k_1}{h}$ etc. The expressions for the m functions are:

$$m_1 = 0.5 \left[ (K_1 + K_2 + K_3 + K_4) + \sqrt{(K_1 + K_2 + K_3 + K_4)^2 - 4 (K_1K_3 + K_2K_4 + K_1K_4)} \right] \quad (4.42)$$

$$m_2 = 0.5 \left[ ( K_1 + K_2 + K_3 + K_4 ) - \sqrt{(K_1 + K_2 + K_3 + K_4)^2 - 4 ( K_1K_3 + K_2K_4 + K_1K_4 )} \right] \quad (4.43)$$

Equations (4.39), (4.40) and (4.41) give the dependence of the concentrations of the chromium species on rate constants and time for a consecutive two-stage reaction scheme in which both reactions are reversible. Again a similarity in equations (4.41), (4.32) and (4.23) on one hand and equations (4.40) and (4.31) on the other is apparent. As outlined in section 4.5.2.3, these equations are different, the difference being in the determination of the m functions. For example, in equations (4.40) and (4.41) the m functions are determined from the rate constants $K_1$, $K_2$, $K_3$ and $K_4$ and they have an extra term, $K_2K_4$, under the square root compared to the m functions in equation (4.31) where they are determined from $K_1$, $K_3$ and $K_4$. The difference between equations (4.32) and (4.23) has been outlined in

section 4.5.2.3.

The concentrations of the chromium species were calculated as before using the computer programs in appendices B and C. Here all the four rate constants were used in the calculation. Table 4.6 shows the observed and calculated values.

**Table 4.6: Observed and calculated concentrations for ($Cr^{3+}$), ($Cr^{2+}$) and [Cr] from scheme 4.**

| Time | ($Cr^{3+}$), wt% | | ($Cr^{2+}$), wt% | | [Cr], wt% | |
|---|---|---|---|---|---|---|
| (mins) | Obsd. | Calc. | Obsd. | Calc. | Obsd. | Calc. |
| 0 | 3.42 | 3.42 | 0.00 | 0.00 | 0.00 | 0.00 |
| 15 | 2.40 | 2.40 | 0.51 | 0.60 | 0.17 | 0.14 |
| 25 | 1.93 | 1.96 | 0.75 | 0.69 | 0.24 | 0.25 |
| 35 | 1.66 | 1.64 | 0.65 | 0.73 | 0.36 | 0.35 |
| 45 | 1.42 | 1.40 | 0.83 | 0.75 | 0.38 | 0.42 |
| 60 | 1.10 | 1.14 | 0.85 | 0.77 | 0.46 | 0.50 |
| 80 | 0.92 | 0.94 | 0.76 | 0.78 | 0.54 | 0.56 |
| 120 | 0.76 | 0.75 | 0.70 | 0.80 | 0.60 | 0.62 |

Fig. 4.10 shows a plot of the calculated rate curves from scheme 4 and the observed values of run AS1. As can be seen from the figure, the ($Cr^{3+}$), ($Cr^{2+}$) and [Cr] curves show satisfactory fits on the observed values within experimental error. This is depicted in the values of the sum of squares of deviations which are the

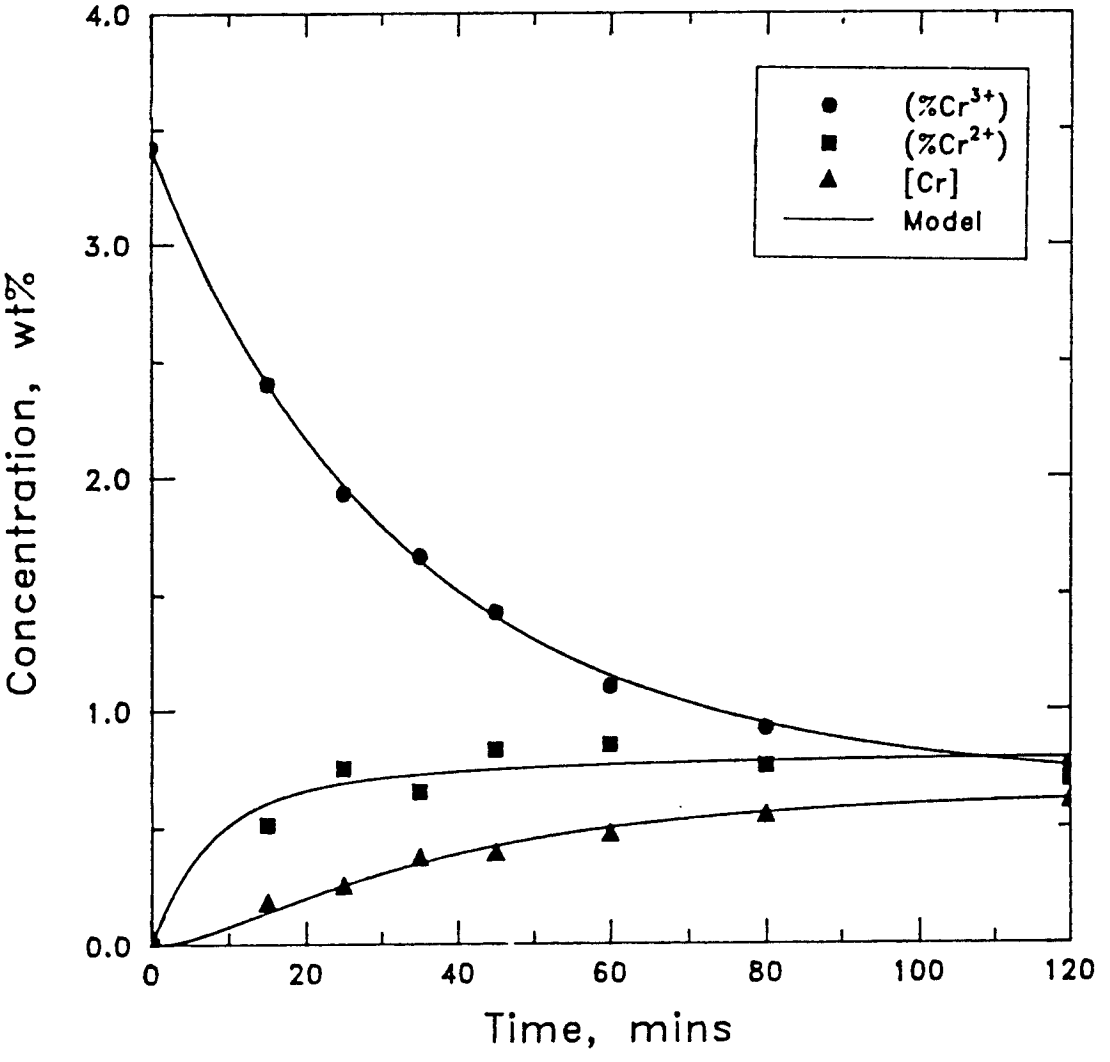


$k_1 = 0.0238\ cm.min^{-1}$. $k_2 = 0.0198\ cm.min^{-1}$.
$k_3 = 0.0760\ cm.min^{-1}$. $k_4 = 0.0313\ cm.min^{-1}$.

Sums of squares of deviations are:
$Cr^{3+} = 0.004$, $Cr^{2+} = 0.042$, $Cr_{Met.} = 0.006$.

Fig. 4.10 Time variation in concentration of ($Cr^{3+}$), ($Cr^{2+}$) and [Cr]. The curves are calculated from scheme 4 and the points are observed values from run AS1.

lowest compared to schemes 1,2 and 3 as shown in Table 4.7.

**Table 4.7: Sums of squares of deviations for schemes 1, 2, 3 and 4.**

| Scheme | $(Cr^{3+})$ | $(Cr^{2+})$ | [Cr] |
|---|---|---|---|
| 1 | 0.301 | 0.303 | 0.087 |
| 2 | 0.210 | 0.298 | 0.065 |
| 3 | 0.301 | 0.051 | 0.027 |
| 4 | 0.004 | 0.042 | 0.006 |

From the above, one can assume that the reduction of $Cr_2O_3$ from slag follows a first-order, consecutive, reversible, two-stage reaction scheme.

### 4.5.2.5 First-order consecutive reversible two-stage reaction scheme with varying slag height.

In the treatment of the model, so far, the height of slag is assumed constant throughout an experimental run. However, this was not the case, as the volume of slag, and therefore the height, reduced each time the slag was sampled. This meant that each time interval had a different slag height. In order to incorporate this into the model, the expressions showing the variation of the chromium species with time were obtained by considering that at t = 0, $(Cr^{3+})$, $(Cr^{2+})$ and [Cr] all can have non-zero values. The expressions obtained were applied to individual time intervals between experimental points, each starting at t = 0. The final concentrations of the chromium species from the previous time interval become the initial concentrations for the following interval. In this case the solutions to the differential equations used are those obtained from scheme 4 but using the conditions at t = 0, $(Cr^{3+}) = (Cr^{3+})_o$, $(Cr^{2+}) = (Cr^{2+})_o$ and $[Cr] = [Cr]_o$, where $(Cr^{3+})_o$, $(Cr^{2+})_o$ and $[Cr]_o$ are the initial concentrations of $(Cr^{3+})$, $(Cr^{2+})$ and [Cr], respectively. The solutions are then applied to individual time intervals between experimental points each starting at t = 0.

### 4.5.2.5 First-order consecutive reversible two-stage reaction scheme with varying slag height.

In the treatment of the model, so far, the height of slag is assumed constant throughout an experimental run. However, this was not the case, as the volume of slag, and therefore the height, reduced each time the slag was sampled. This meant that each time interval had a different slag height. In order to incoporate this into the model, the expressions showing the variation of the chromium species with time were obtained by considering that at t = 0, $(Cr^{3+})$, $(Cr^{2+})$ and [Cr] all can have non-zero values. The expressions obtained were applied to individual time intervals between experimental points, each starting at t = 0. The final concentrations of the chromium species from the previous time interval become the initial concentrations for the following interval. In this case the solutions to the differential equations used are those obtained from scheme 4 but using the conditions at t = 0, $(Cr^{3+}) = (Cr^{3+})_o$, $(Cr^{2+}) = (Cr^{2+})_o$ and $[Cr] = [Cr]_o$, where $(Cr^{3+})_o$, $(Cr^{2+})_o$ and $[Cr]_o$ are the initial concentrations of $(Cr^{3+})$, $(Cr^{2+})$ and [Cr], respectively. The solutions are then applied to individual time intervals between experimental points each starting at t = 0.

Using conventional methods for solving differential equations as in scheme 4 for the case when the initial concentrations of the chromium species are non-zero is laborious and cumbersome. Instead the method of Frost and Pearson[54] is used. The method is made easier by using matrix notation throughout the calculation[53].

Using the diferential equations in scheme 4 and by putting $d(Cr^{3+})/dt = (Cr^{3+})$ etc. and $K_1 = k_1/h$ etc. we have the following equations:

$$(Cr^{3+}) + K_1 (Cr^{3+}) - K_2 (Cr^{2+}) = 0 \qquad (4.44)$$

$$(Cr^{2+}) - K_1 (Cr^{3+}) + K_2 (Cr^{2+}) + K_3 (Cr^{2+}) - K_4 [Cr] = 0 \qquad (4.45)$$

$$[Cr] - K_3 (Cr^{2+}) + K_4 [Cr] = 0 \qquad (4.46)$$

The rate constant matrix becomes:

$$K = \begin{pmatrix} K_1 & K_2 & 0 \\ -K_1 & K_2 + K_3 & -K_4 \\ 0 & -K_3 & K_4 \end{pmatrix} \qquad (4.47)$$

Then the secular equation becomes

$$\begin{vmatrix} K_1 - m_r & -K_2 & 0 \\ -K_1 & K_2 + K_3 - m_r & -K_4 \\ 0 & -K_3 & K_4 - m_r \end{vmatrix} = 0 \qquad (4.48)$$

which when expanded becomes

$$-m_r^3 + m_r^2(K_1 + K_2 + K_3 + K_4) - m_r(K_1K_3 + K_2K_4 + K_1K_4) = 0 \qquad (4.49)$$

The three solutions for $m_r$ are:

$$m_1 = 0$$

$$m_2 = \frac{1}{2}(p + q) \qquad (4.50)$$

$$m_3 = \frac{1}{2}(p - q)$$

where $p = (K_1 + K_2 + K_3 + K_4)$ and

$$q = \sqrt{p^2 - 4(K_1K_3 + K_2K_4 + K_1K_4)}$$

The coefficients B can be deduced by setting $B_{1r} = 1$. In matrix form, this may be written as

$$B = \begin{pmatrix} 1 & 1 & 1 \\ \dfrac{K_1}{K_2} & \dfrac{(K_1 - m_2)}{K_2} & \dfrac{(K_1 - m_3)}{K_2} \\ \dfrac{K_1 K_3}{K_2 K_4} & \dfrac{K_3(K_1 - m_2)}{K_2(K_4 - m_2)} & \dfrac{K_3(K_1 - m_3)}{K_2(K_4 - m_3)} \end{pmatrix} \quad (4.51)$$

or in abbreviated form as

$$B = \begin{pmatrix} 1 & 1 & 1 \\ B_{21} & B_{22} & B_{23} \\ B_{31} & B_{32} & B_{33} \end{pmatrix} \quad (4.52)$$

The determinant of the matrix B is then given by

$$|B| = B_{22}B_{33} + B_{23}B_{31} + B_{21}B_{32} - B_{31}B_{22} - B_{32}B_{23} - B_{33}B_{21} \quad (4.53)$$

The mechanics of the solution for the coefficients Q in Frost and Pearson's treatment[54] can be made more routine by using matrix notation and methods throughout. Let us define the following matrices by equations (4.54), (4.55) and (4.56):

$$A = \begin{pmatrix} (Cr^{3+}) \\ (Cr^{2+}) \\ [Cr] \end{pmatrix} \quad (4.54)$$

$$A_o = \begin{pmatrix} (Cr^{3+})_o \\ (Cr^{2+})_o \\ [Cr]_o \end{pmatrix} \tag{4.55}$$

$$E = \begin{pmatrix} 1 & 0 & 0 \\ 0 & \exp(-m_2 t) & 0 \\ 0 & 0 & \exp(-m_3 t) \end{pmatrix} \tag{4.56}$$

Where $A_o$ is a matrix representing the conditions at t = 0 (the method will accomodate another selection of initial conditions). Then the desired matrix A can be shown to be given by

$$A = B\,E\,B^{-1}\,A_o \tag{4.57}$$

The explicit solution of this equation then gives the desired dependence of the chromium species on time and rate constants for the case when the species have non-zero concentration values at time t = 0. The solutions are given by expressions in equations (4.58), (4.59) and (4.60).

$$(Cr^{3+}) = \frac{1}{|B|} \left\{ (Cr^{3+})_o \left[ (B_{22}B_{33} - B_{23}B_{32}) \right.\right.$$

$$+ (B_{31}B_{23} - B_{21}B_{33}) \exp(-m_2 t) + (B_{21}B_{32} - B_{31}B_{22})$$

$$\exp(-m_3t) \Big] + (Cr^{2+})_o \Big[ (B_{32} - B_{33}) + (B_{33} - B_{31}) \exp(-m_2t) + (B_{31} - B_{32}) \exp(-m_3t) \Big] + [Cr]_o \Big[ (B_{23} - B_{22}) + (B_{21} - B_{23}) \exp(-m_2t) + (B_{22} - B_{21}) \exp(-m_3t) \Big] \Big\} \quad (4.58)$$

$$(Cr^{2+}) = \frac{1}{|B|} \Big\{ (Cr^{3+})_o \Big[ B_{21} (B_{22}B_{33} - B_{23}B_{32}) + B_{22} (B_{31}B_{23} - B_{21}B_{33}) \exp(-m_2t) + B_{23} (B_{21}B_{32} - B_{31}B_{22}) \exp(-m_3t) \Big] + (Cr^{2+})_o \Big[ B_{21} (B_{32} - B_{33}) + B_{22}(B_{33} - B_{31}) \exp(-m_2t) + B_{23} (B_{31} - B_{32}) \exp(-m_3t) \Big] + [Cr]_o \Big[ B_{21} (B_{23} - B_{22}) + B_{22} (B_{21} - B_{23}) \exp(-m_2t) + B_{23} (B_{22} - B_{21}) \exp(-m_3t) \Big] \Big\} \quad (4.59)$$

$$[Cr] = \frac{1}{|B|} \Big\{ (Cr^{3+})_o \Big[ B_{31} (B_{22}B_{33} - B_{23}B_{32}) + B_{23} (B_{31}B_{23} - B_{21}B_{33}) \exp(-m_2t) + B_{33} (B_{21}B_{32} - B_{31}B_{22}) \exp(-m_3t) \Big] + (Cr^{2+})_o \Big[ B_{31} (B_{32} - B_{33}) + B_{32} (B_{33} - B_{31}) \exp(-m_2t) + B_{33} (B_{31} - B_{32}) \exp(-m_3t) \Big] + [Cr]_o \Big[ B_{31} (B_{23} - B_{22}) + B_{32} (B_{21} - B_{23}) \exp(-m_2t) + B_{33} (B_{22} - B_{21}) \exp(-m_3t) \Big] \Big\} \quad (4.60)$$

The concentrations of the chromium species from the equations above were calculated using the computer programs shown in appendices D and E. The programs use the actual slag height in each time interval. The program in appendix D determines the rate constants for a particular set of data by minimising the sums of squares of deviations between the observed and predicted concentrations as discussed in section 4.5.2.1, while that in appendix E calculates the variation in the concentrations of the chromium species and the comparison is made with the same set of data used in determining the rate constants.

In order to see whether the concentrations of the chromium species are sensitive to changes in the height of slag, the concentrations of $(Cr^{3+})$, $(Cr^{2+})$ and [Cr] were calculated from the equations above (varying slag height) using rate constants determined from the program in appendix D for run AS1.

Fig. 4.11 shows the calculated rate curves using the case of varying slag height (dashed lines) and constant slag height (solid lines - Fig. 4.10). The difference in the two sets of curves shown in Fig. 4.11 is such that the slight sensitivity of the chromium species due to changes in slag height becomes insignificant when one takes account of the error in the observed values.

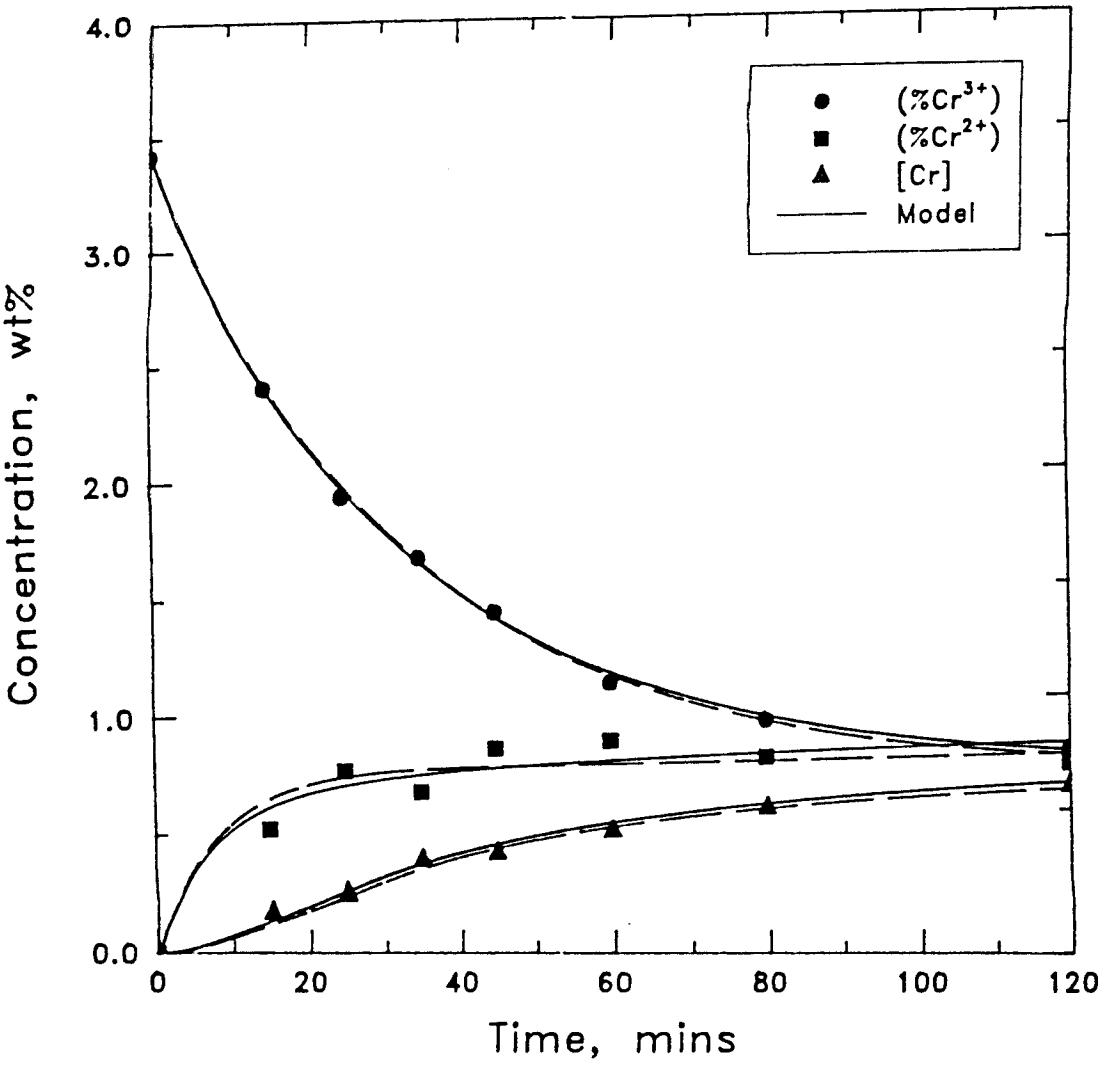


Fig. 4.11 Time variation in concentration of $(Cr^{3+})$, $(Cr^{2+})$ and [Cr]. The points are from run AS1, dashed lines are for varying slag height and solid lines are for constant slag height ( Fig. 4.10).

Tables 4.8 and 4.9 show the least sums of squares of deviations obtained for the chromium species and the rate constants, respectively, for the case of constant and varying slag height. From tables 4.8 and 4.9, it is clear that the differences in the total and individual sums of squares of deviations of the chromium species for the two cases are marginal. The rate constants do not show any marked difference, except for the forward rate constant of the second stage, $k_3$, which decreases when the varying slag height is taken into account. This is attributable to the way in which the concentration of [Cr] is determined. The determination of [Cr] is by mass balance of the chromium in the slag. This assumes that the difference in the chromium content of the slag at the beginning and end of a run (constant slag height) or time interval (varying slag height) goes in the metal and that there is no loss to the atmosphere. Since the concentration of [Cr] is dependent on the weight of the slag, a reduction in the weight would lead to lower values of [Cr] and therefore, a reduction in forward rate constant, $k_3$.

**Table 4.8 Minimum sums of squares of deviations for the case of constant and varying slag height from run AS1.**

| Slag height | Sums of squares of deviations | | | |
|---|---|---|---|---|
| | $(Cr^{3+})$ | $(Cr^{2+})$ | [Cr] | Total |
| Constant | 0.004 | 0.042 | 0.006 | 0.052 |
| Varying | 0.005 | 0.045 | 0.004 | 0.054 |

**Table 4.9 Rate constants for the case of constant and varying slag height from run AS1.**

| Slag height | Rate constants, $cm.min^{-1}$ | | | |
|---|---|---|---|---|
| | $k_1$ | $k_2$ | $k_3$ | $k_4$ |
| Constant | 0.0238 | 0.0198 | 0.0761 | 0.0312 |
| Varying | 0.0239 | 0.0215 | 0.0609 | 0.0226 |

However, the model where the changes in the height of the slag due to sampling are taken into account is considered to present a better picture of the events occurring during an experimental run and is, therefore, applied in the ensuing paragraphs.

### 4.5.3 Testing of the model

It has been established from the foregoing paragraphs that the reduction of $Cr_2O_3$ from slag by carbon in molten iron follows a consecutive reversible first-order two-stage reaction scheme. The model has been modified to take account of the decrease in the weight of slag during an experimental run due to sampling. To ascertain the fact that the reduction of $Cr_2O_3$ from slag follows a consecutive reaction scheme above, the model was further applied to data:

(1) for an initial concentration of $Cr_2O_3$ in slag of 8 wt% with an Ar atmosphere at 1470°C (run AS2);

(2) for an initial concentration of $Cr_2O_3$ in slag of 10 wt% with an Ar atmosphere at 1470°C (run AS3);

(3) for an initial concentration of $Cr_2O_3$ in slag of 5 wt% with a CO atmosphere at 1470°C (run AS5);

(4) for an initial concentration of $Cr_2O_3$ in slag of 5 wt% with CO atmosphere at 1500°C[37].

(5) and for an initial concentration of $Cr_2O_3$ in slag of 5 wt% at 1625°C and reduction by silicon dissolved in molten iron[38].

The variation in concentration of the chromium species with time were calculated as in the preceeding paragraphs for the sets of data above, using combinations of rate constants giving least sums of squares of deviations. Tables 4.10 and 4.11 show the calculated and observed concentrations of the chromium species for runs AS2 and AS3, respectively. The plots of the calculated rate curves of ($Cr^{3+}$), ($Cr^{2+}$) and [Cr] with the corresponding observed values for runs AS2 and AS3 are shown in Figs. 4.12 and 4.13, respectively. As can be seen from the figures, the calculated rate curves fit the observed results satisfactorily.

The average rate constants for the three sets of data, runs AS1, AS2 and AS3, were obtained by minimisation of the sums of squares of deviations of the chromium species, as discussed ealier, on all the three sets of data at the same time using the computer program in appendix F. The average rate constants obtained are shown in Table 4.12 together with those of the individual runs.

The concentrations of the chromium species were calculated for runs AS1, AS2 and AS3 using the program in appendix D and the average rate constants. Fig. 4.14 shows a plot of the calculated rate curves using average rate constants (solid lines) and those from individual

**Table 4.10: Observed and calculated concentrations for ($Cr^{3+}$), ($Cr^{2+}$) and [Cr] from run AS2.**

| Time | ($Cr^{3+}$), wt% | | ($Cr^{2+}$), wt% | | [Cr], wt% | |
|---|---|---|---|---|---|---|
| (mins) | Obsd. | Calc. | Obsd. | Calc. | Obsd. | Calc |
| 0 | 5.47 | 5.47 | 0.00 | 0.00 | 0.00 | 0.00 |
| 16 | 4.08 | 4.13 | 0.88 | 0.86 | 0.15 | 0.16 |
| 25 | 3.64 | 3.48 | 0.81 | 1.01 | 0.29 | 0.30 |
| 35 | 2.93 | 2.86 | 1.05 | 1.06 | 0.41 | 0.44 |
| 45 | 2.25 | 2.36 | 1.13 | 1.07 | 0.55 | 0.55 |
| 60 | 1.77 | 1.79 | 1.10 | 1.07 | 0.66 | 0.67 |
| 80 | 1.31 | 1.29 | 1.13 | 1.06 | 0.74 | 0.78 |
| 110 | 0.96 | 0.94 | 1.01 | 1.06 | 0.81 | 0.83 |

**Table 4.11: Observed and calculated concentrations for ($Cr^{3+}$), ($Cr^{2+}$) and [Cr] from run AS3.**

| Time | ($Cr^{3+}$), wt% | | ($Cr^{2+}$), wt% | | [Cr], wt% | |
|---|---|---|---|---|---|---|
| (mins) | Obsd. | Calc. | Obsd. | Calc. | Obsd. | Calc. |
| 0 | 6.84 | 6.84 | 0.00 | 0.00 | 0.00 | 0.00 |
| 15 | 5.16 | 5.21 | 0.85 | 0.99 | 0.27 | 0.21 |
| 25 | 4.38 | 4.43 | 0.91 | 1.12 | 0.49 | 0.41 |
| 35 | 3.64 | 3.78 | 1.11 | 1.15 | 0.64 | 0.58 |
| 45 | 3.30 | 3.26 | 1.20 | 1.15 | 0.71 | 0.71 |
| 60 | 2.70 | 2.67 | 1.22 | 1.15 | 0.85 | 0.86 |
| 80 | 2.20 | 2.16 | 1.20 | 1.14 | 0.98 | 0.99 |
| 120 | 1.74 | 1.70 | 1.74 | 1.13 | 1.07 | 1.09 |

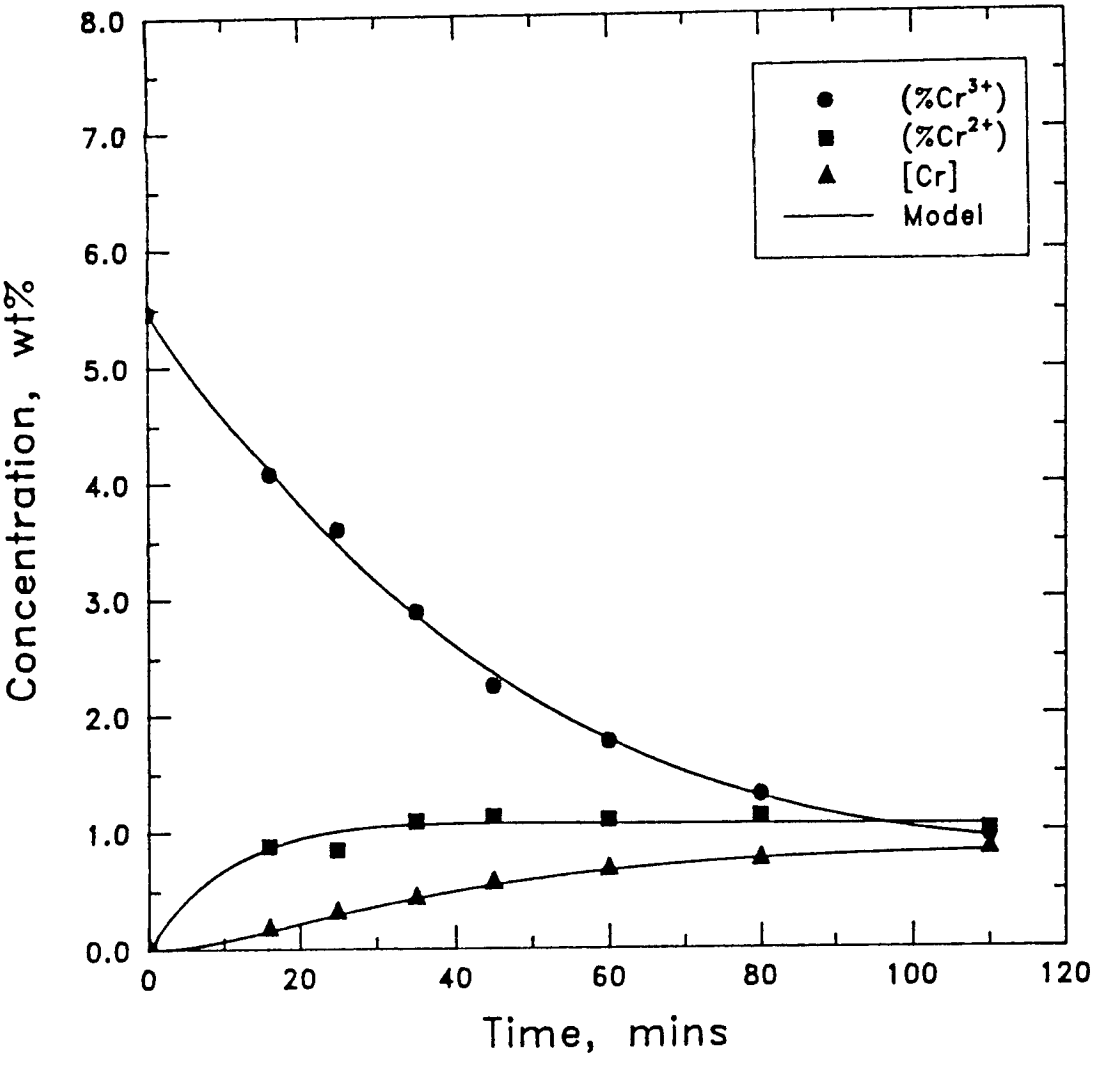


$k_1 = 0.0171\ cm.min^{-1}$. $k_2 = 0.0124\ cm.min^{-1}$.
$k_3 = 0.0551\ cm.min^{-1}$. $k_4 = 0.0159\ cm.min^{-1}$.

Sums of squares of deviations are:
$Cr^{3+} = 0.031$, $Cr^{2+} = 0.038$, $Cr_{Met.} = 0.001$.

Fig. 4.12 Time variation in concentration of ($Cr^{3+}$), ($Cr^{2+}$) and [Cr] for run AS2.

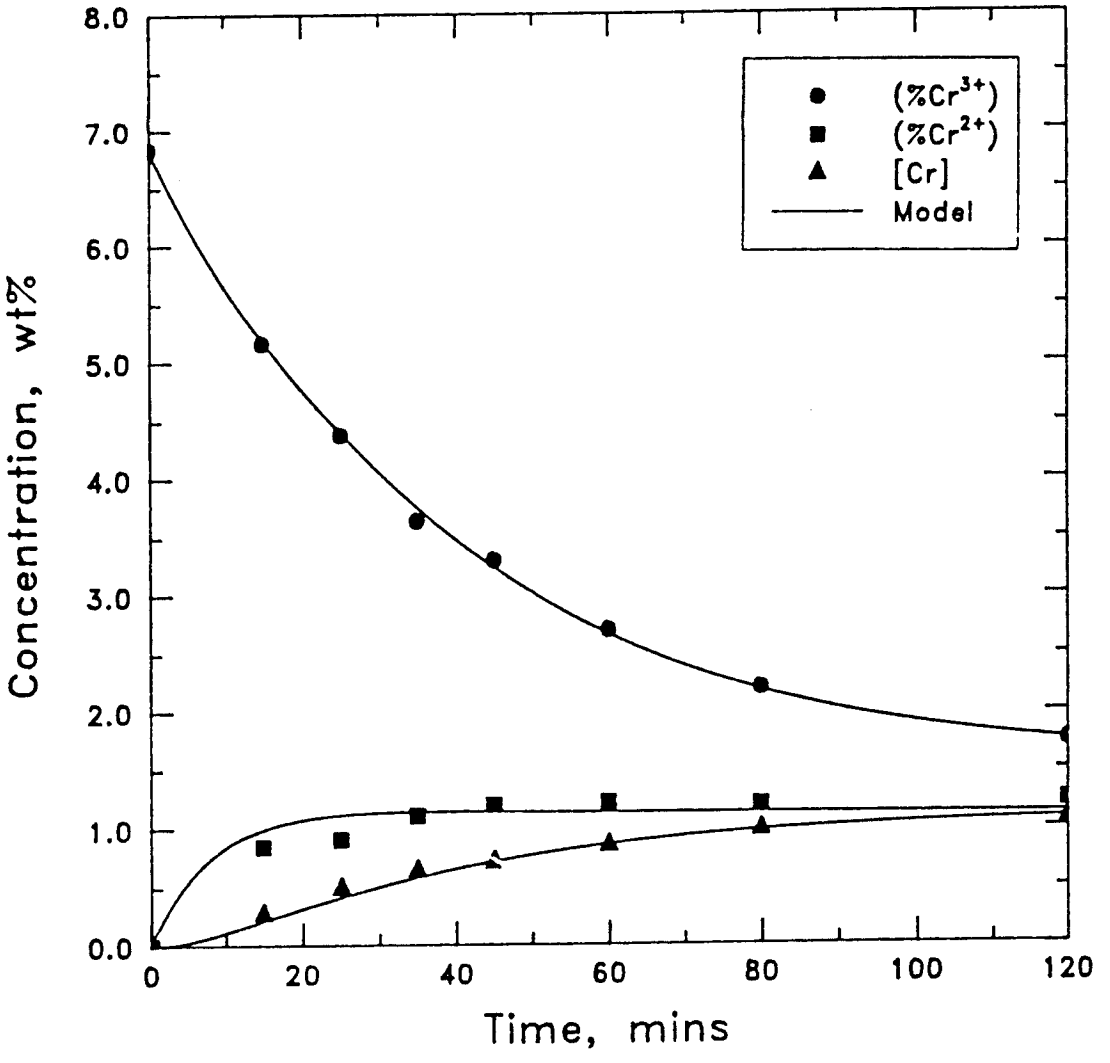


$k_1 = 0.0194\ cm.min^{-1}$. $k_2 = 0.0271\ cm.min^{-1}$.
$k_3 = 0.0665\ cm.min^{-1}$. $k_4 = 0.0180\ cm.min^{-1}$.

Sums of squares of deviations are:
$Cr^{3+} = 0.020$, $Cr^{2+} = 0.092$, $Cr_{Met.} = 0.012$.

Fig. 4.13 Time variation in concentration of ($Cr^{3+}$), ($Cr^{2+}$) and [Cr] for run AS3.

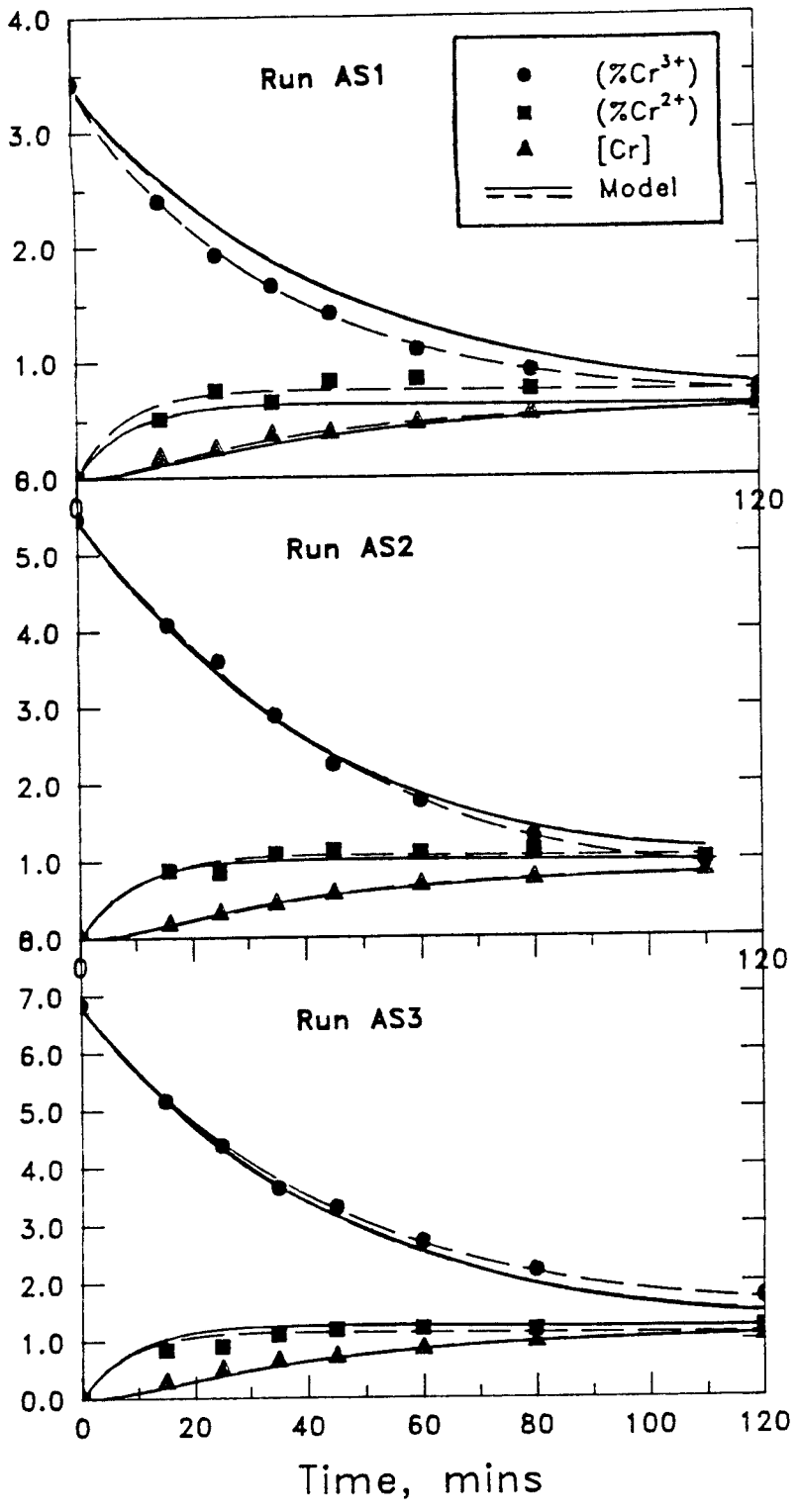


Fig. 4.14 Comparison of rate curves using average (solid lines) and individual (dashed lines) rate constants for runs AS1, AS2 and AS3.

**Table 4.12: Rate constants for runs AS1, AS2 and AS3. Average rate constants obtained by minimisation on all three sets of data.**

| Run | Rate constants, $cm.min^{-1}$ | | | |
|---|---|---|---|---|
| | $k_1$ | $k_2$ | $k_3$ | $k_4$ |
| Average | 0.0186 | 0.0191 | 0.0602 | 0.0173 |
| AS1 | 0.0239 | 0.0215 | 0.0609 | 0.0226 |
| AS2 | 0.0171 | 0.0124 | 0.0551 | 0.0159 |
| AS3 | 0.0188 | 0.0250 | 0.0649 | 0.0174 |

sets of data (dashed lines) for the runs above. The figure shows that the difference in the curves in each run is marginal.

*The sums of squares of deviations of the chromium species* from the individual sets of data and those obtained by use of the average rate constants in each case are shown in Table 4.13. The table shows that the sums of squares of deviations are worse off when the average rate constants are applied in all cases. This is due to the fact that the average rate constants are a compromise of the three sets of data and as such the fits obtained by use of the average rate constants are not expected to be as good as those obtained by minimisation of the sums of squares of deviations of the chromium species of the individual sets of data.

**Table 4.13 Sums of squares of deviations of $(Cr^{3+})$, $(Cr^{2+})$ and [Cr] for runs AS1, AS2 and AS3 using individual and average rate constants.**

| Individual | $(Cr^{3+})$ | $(Cr^{2+})$ | [Cr] |
|---|---|---|---|
| AS1 | 0.005 | 0.045 | 0.004 |
| AS2 | 0.031 | 0.038 | 0.001 |
| AS3 | 0.020 | 0.092 | 0.012 |
| Average | $(Cr^{3+})$ | $(Cr^{2+})$ | [Cr] |
| AS1 | 0.287 | 0.130 | 0.012 |
| AS2 | 0.101 | 0.062 | 0.002 |
| AS3 | 0.180 | 0.166 | 0.020 |

A plot of the forward rate constants for the first and second stages, $k_1$ and $k_3$, respectively, as a function of the initial concentration of $Cr_2O_3$ in slag for the three runs is shown in Fig. 4.15. The lines in the figure represent the average rate constants obtained above. The figure shows that the rate constants for these runs are identical to within experimental error. The general first-order theory which states that the reaction rate is proportional to the concentration of the reactant is thus satisfied since the rate constants for runs AS1, AS2 and AS3 in which 5, 8 and 10 wt% $Cr_2O_3$ were initially added to the slag are identical. This shows that the mechanism

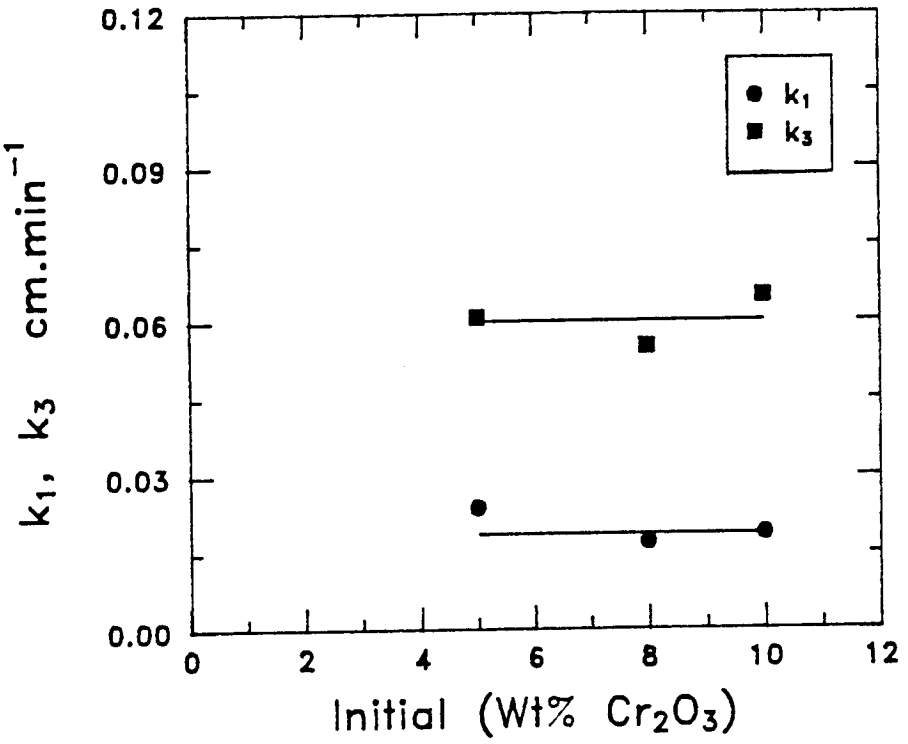


Fig. 4.15 Effect of $Cr_2O_3$ concentration on the forward rate constants, $k_1$ and $k_3$.

of reduction of $Cr_2O_3$ does not change with increase in concentration. Supporting evidence comes from the results of Robison and Pehlke[31] as already discussed in section 4.4.

The calculated and corresponding observed values for run AS5 carried out under CO are shown in Table 4.14. Fig. 4.16 shows a plot of the calculated rate curves for $(Cr^{3+})$, $(Cr^{2+})$ and [Cr] with the corresponding observed values for run AS5. The calculated curves fit the observed values satisfactorily. Comparison of the rate constant values of runs AS1 and AS5, Table 4.15, shows that there is no marked difference in the forward rate constant for the first-stage, $k_1$, between the two runs. However, the forward rate constant for the second stage , $k_3$, is lower for run AS5 compared to that of run AS1. This is in accord with the finding in section 4.3 that the furnace atmosphere does not affect the rate of reduction of $(Cr^{3+})$ in carbon monoxide and argon atmospheres. An argon atmosphere, however, seems to lead to lower $(Cr^{2+})$ by increasing the rate of reduction by a factor of about 1.4. The rate constants for the reverse reactions between the two cases, $k_2$ and $k_4$, do not vary much and have a small influence on the shape of the curve for the intermediate product, as investigated by Lowry et al[58].

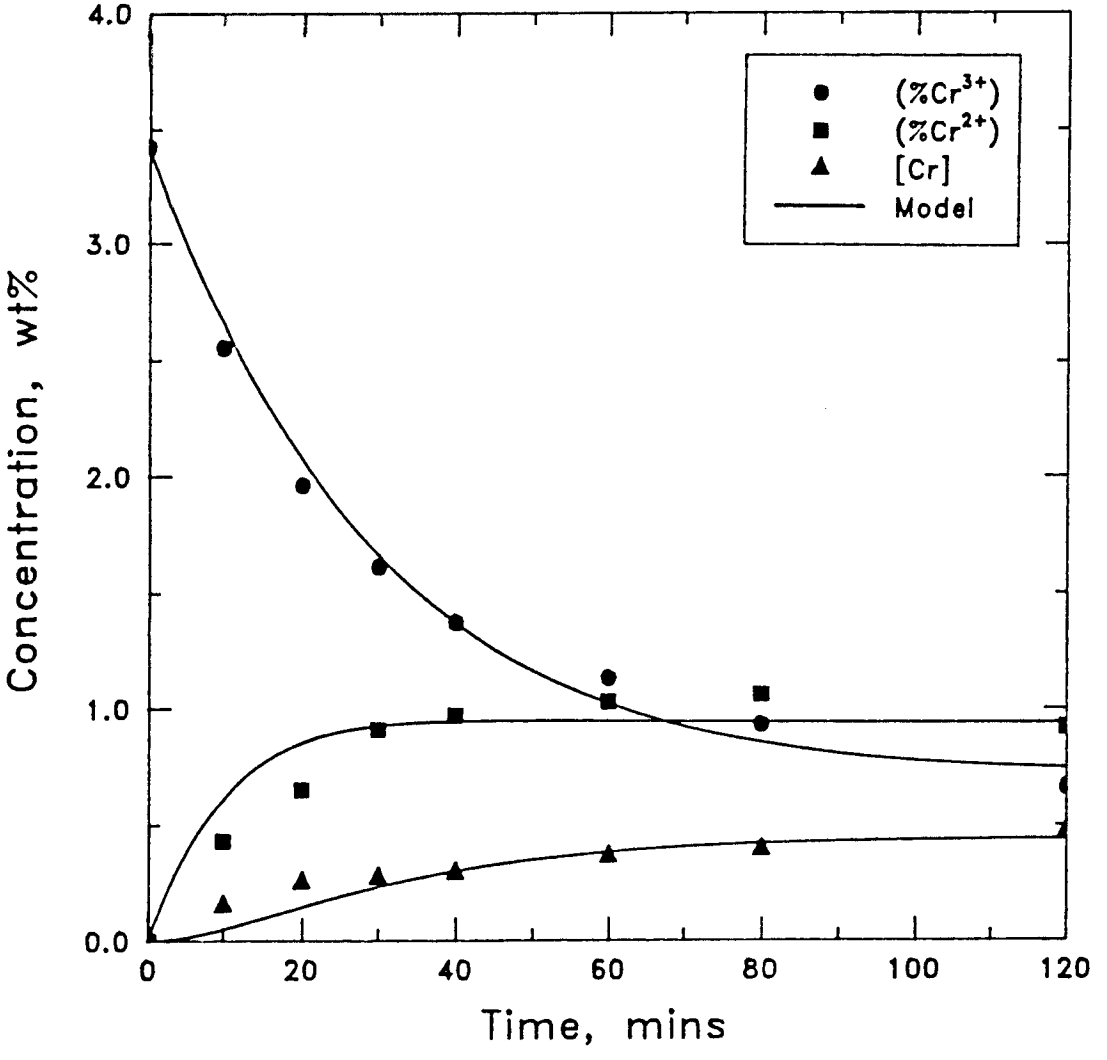


$k_1 = 0.0248\ cm.min^{-1}$. $k_2 = 0.0191\ cm.min^{-1}$.
$k_3 = 0.0434\ cm.min^{-1}$. $k_4 = 0.0233\ cm.min^{-1}$.

Sums of squares of deviations are:
$Cr^{3+} = 0.052$, $Cr^{2+} = 0.094$, $Cr_{Met.} = 0.024$.

Fig. 4.16 Time variation in concentration of ($Cr^{3+}$), ($Cr^{2+}$) and [Cr] for run AS5.

**Table 4.14: Observed and calculated concentrations for ($Cr^{3+}$), ($Cr^{2+}$) and [Cr] from run AS5.**

| Time (mins) | ($Cr^{3+}$), wt% | | ($Cr^{2+}$), wt% | | [Cr], wt% | |
|---|---|---|---|---|---|---|
| | Obsd. | Calc. | Obsd. | Calc. | Obsd. | Calc. |
| 0 | 3.42 | 3.42 | 0.00 | 0.00 | 0.00 | 0.00 |
| 10 | 2.49 | 2.66 | 0.49 | 0.60 | 0.15 | 0.05 |
| 20 | 1.91 | 2.07 | 0.70 | 0.85 | 0.25 | 0.15 |
| 30 | 1.61 | 1.66 | 0.91 | 0.93 | 0.27 | 0.23 |
| 40 | 1.37 | 1.37 | 1.07 | 0.95 | 0.29 | 0.30 |
| 60 | 1.13 | 1.02 | 1.03 | 0.95 | 0.36 | 0.38 |
| 80 | 0.93 | 0.85 | 1.06 | 0.95 | 0.39 | 0.42 |
| 120 | 0.66 | 0.74 | 0.92 | 0.94 | 0.47 | 0.44 |

**Table 4.15: Rate constants for runs AS1 and AS5**

| Run No. | $k_1$ | $k_2$ | $k_3$ | $k_4$ |
|---|---|---|---|---|
| | | $cm.min^{-1}$ | | |
| AS1 | 0.0239 | 0.0215 | 0.0609 | 0.0226 |
| AS5 | 0.0248 | 0.0191 | 0.0434 | 0.0233 |

The calculated and corresponding observed values for data from Anyakwo[37] in which 5 wt% $Cr_2O_3$ was initially added to the slag are shown in Table 4.16. The run was carried out under CO and at a temperature of 1500°C as opposed to 1470°C used in this study. Other experimental conditions were similar to those used in this study.

**Table 4.16: Observed and calculated concentrations for ($Cr^{3+}$), ($Cr^{2+}$) and [Cr] for 5 wt% $Cr_2O_3$ initial content in slag[37].**

| Time | ($Cr^{3+}$), wt% | | ($Cr^{2+}$), wt% | | [Cr], wt% | |
|---|---|---|---|---|---|---|
| (mins) | Obsd. | Calc. | Obsd. | Calc. | Obsd. | Calc. |
| 0 | 3.42 | 3.42 | 0.00 | 0.00 | 0.00 | 0.00 |
| 10 | 2.10 | 2.24 | 0.60 | 0.83 | 0.24 | 0.12 |
| 20 | 1.57 | 1.61 | 0.93 | 0.96 | 0.31 | 0.28 |
| 30 | 1.23 | 1.23 | 1.07 | 0.95 | 0.36 | 0.39 |
| 40 | 1.06 | 1.00 | 1.04 | 0.93 | 0.41 | 0.47 |
| 60 | 0.79 | 0.77 | 0.96 | 0.90 | 0.51 | 0.55 |
| 80 | 0.66 | 0.68 | 0.94 | 0.88 | 0.54 | 0.58 |
| 120 | 0.61 | 0.63 | 0.64 | 0.88 | 0.62 | 0.52 |

Fig. 4.17 shows a plot of the calculated rate curves of the chromium species with the corresponding observed values for this run. Again one sees that the calculated rate curves fit the observed values satisfactorily. The rate constant values obtained for this run are shown in Table 4.17 together with those of run AS5, carried out under CO but at 1470°C.

The forward rate constant values, $k_1$ and $k_3$, from ref (37) are higher than those obtained for run AS5. The increase in the rate constant values is in accord with the finding that the rate of $Cr_2O_3$ reduction increases with increase in temperature[31,37].

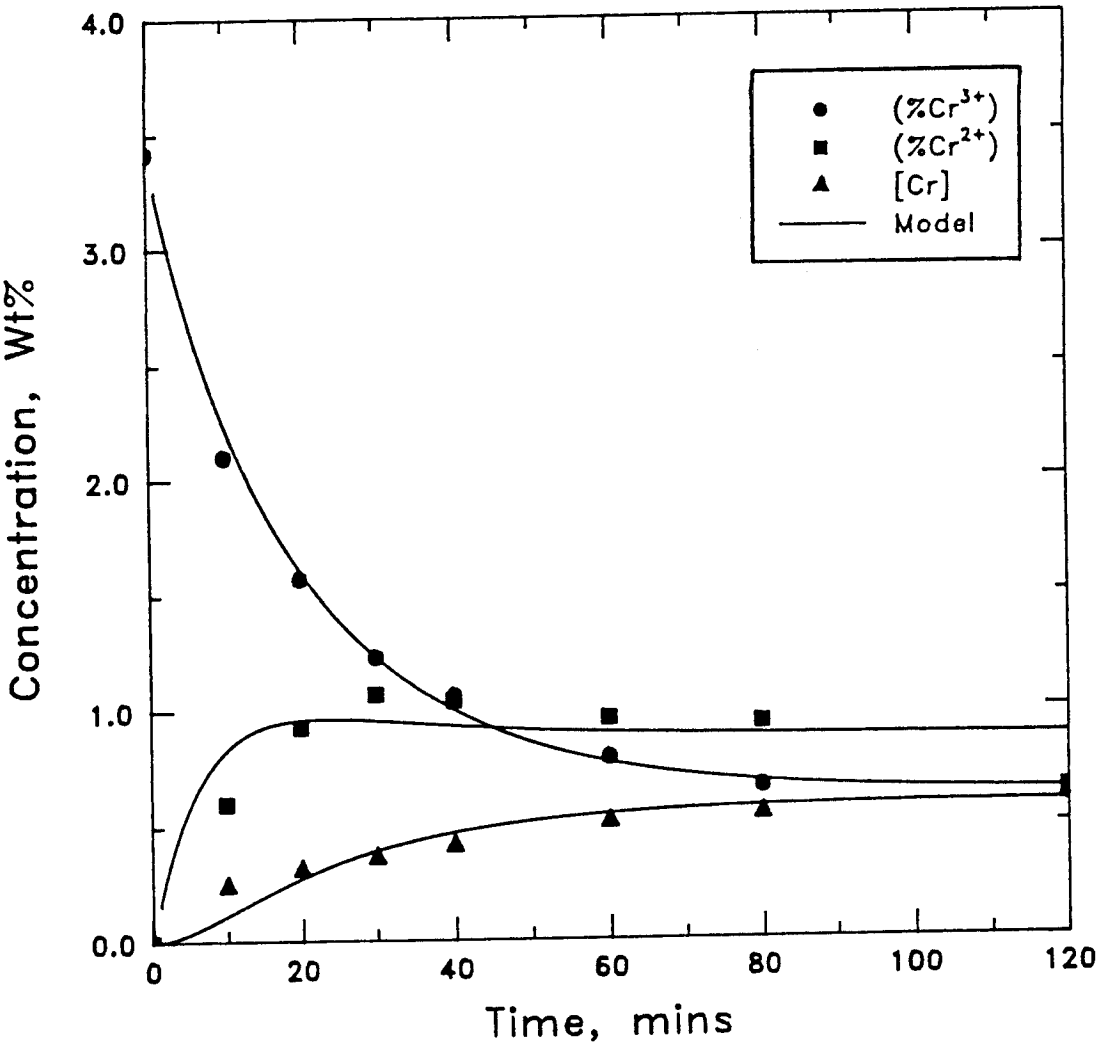


$k_1$ = 0.0441 $cm.min^{-1}$. $k_2$ = 0.0318 $cm.min^{-1}$.
$k_3$ = 0.0667 $cm.min^{-1}$. $k_4$ = 0.0307 $cm.min^{-1}$.

Sums of squares of deviations are:
$Cr^{3+}$ = 0.025, $Cr^{2+}$ = 0.145, $Cr_{Met.}$ = 0.026.

Fig. 4.17 Time variation in concentration of $(Cr^{3+})$, $(Cr^{2+})$ and [Cr] for 5 wt% $Cr_2O_3$ in slag (data from ref. 37).

**Table 4.17: Rate constants for a run from ref(37) and for run AS5.**

| Run No. | $k_1$ | $k_2$ | $k_3$ | $k_4$ |
|---|---|---|---|---|
| | | $cm.min^{-1}$ | | |
| Ref(37) | 0.0441 | 0.0318 | 0.0667 | 0.0307 |
| AS5 | 0.0248 | 0.0191 | 0.0434 | 0.0233 |

The calculated and observed concentrations for data obtained from the results of Robison[38] are shown in Table 4.18. The run was carried out in a zirconia crucible, 127 mm high and 60 mm in diameter at 1625°C. Reduction was by silicon dissolved in molten iron. The charge was 600 g of iron-alloy, containing 10 wt% Cr and 1 wt% Si and 200 g slag of the composition 45% CaO, 35% $SiO_2$, 10% MgO and 10% $Al_2O_3$ to which 5 wt% $Cr_2O_3$ was added. Fig. 4.18 shows a plot of the calculated rate curves of the chromium species with the corresponding observed values from Ref(38). Since the slag sample weights taken at each time interval were not recorded in Ref(38), a model which assumes a constant slag height was used. The difference in the concentrations of the chromium species obtained from this model and that where the variation in slag height is taken into account is very small as discussed in section 4.5.2.5.

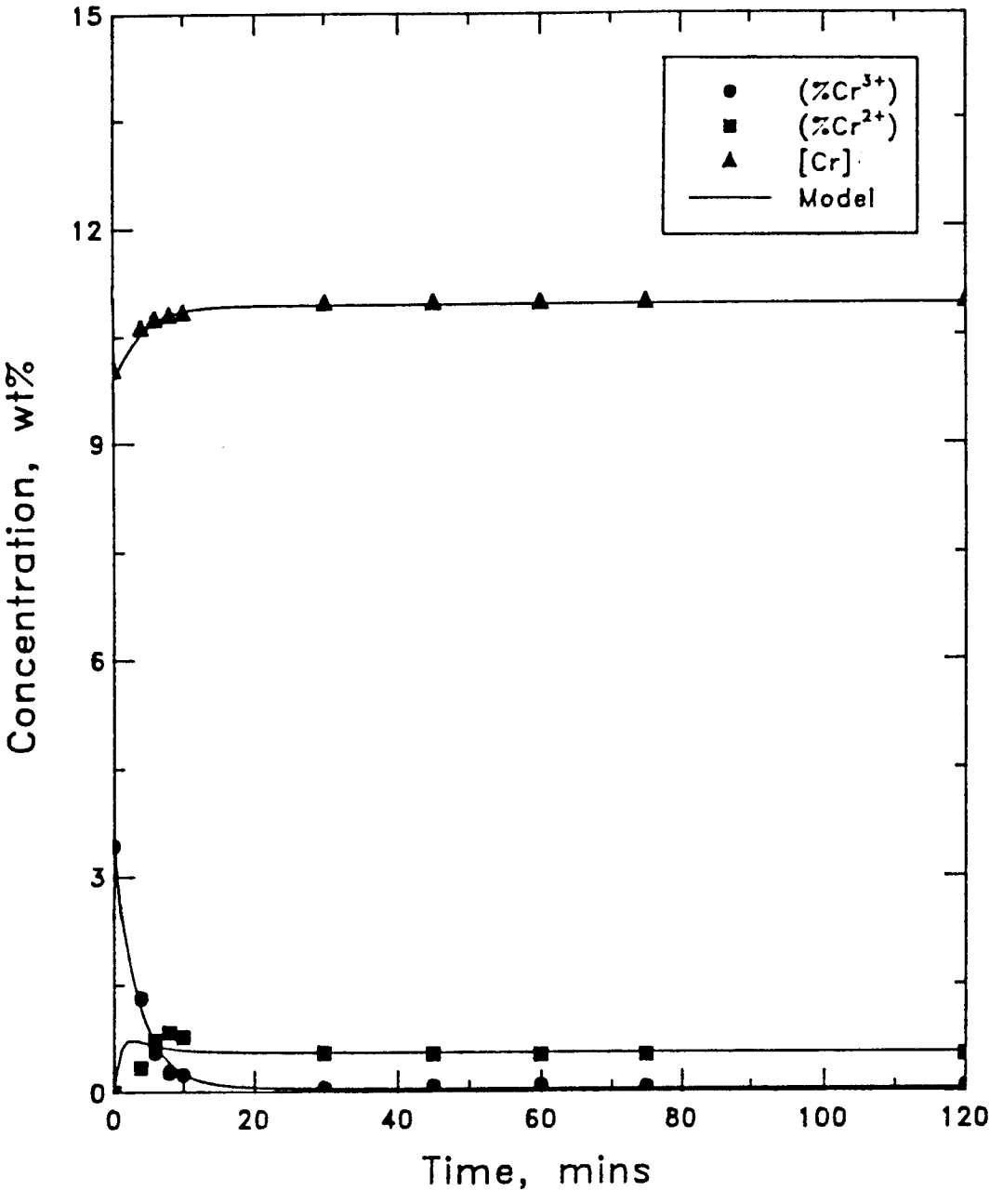


$k_1 = 0.7817\ cm.min^{-1}$. $k_2 = 0.0645\ cm.min^{-1}$.
$k_3 = 2.3702\ cm.min^{-1}$. $k_4 = 0.4591\ cm.min^{-1}$.

Sums of squares of deviations are:
$Cr^{3+} = 0.064$, $Cr^{2+} = 0.226$, $Cr_{Met.} = 0.009$.

Fig. 4.18 Time variation in concentration of ($Cr^{3+}$), ($Cr^{2+}$) and [Cr] for 5 wt% $Cr_2O_3$ in slag and reduction by silicon in metal (data from ref. 38).

A satisfactory fit of the calculated curves on the observed values can be seen from the figure. The rate constants obtained are much higher than those from the present study. This could probably be due to the large interfacial area encountered in Ref(38) as a result of a large crucible used (about twice in height and diameter as those used in this study) and the high temperature, 1625$^{o}$C.

The testing of the model above provides further evidence that the reduction of $Cr_2O_3$ from slag by carbon or silicon dissolved in molten iron follows a first-order, consecutive, reversible, two-stage reaction scheme.

As pointed out earlier, the reduction of $Cr_2O_3$ from slag involves complex reactions. There is a possibility that $(Cr^{3+})$ may be reduced directly to form [Cr], this reduction taking place simultaneously with that through the intermediate, especially in cases where conditions are such that there is an increase in the slag/metal contact area as when surface-active elements are added to the metal. Surface-active elements cause a reduction in the interfacial tension between metal and slag leading to metal emulsification, in which tiny metal droplets scatter in the slag thereby increasing the slag/metal contact area for the reactions to take place. In such cases, it is possible to have a direct reaction between

**Table 4.18: Observed and calculated concentrations for ($Cr^{3+}$), ($Cr^{2+}$) and [Cr] from Ref(38).**

| Time (mins) | ($Cr^{3+}$), wt% | | ($Cr^{2+}$), wt% | | [Cr], wt% | |
|---|---|---|---|---|---|---|
| | Obsd. | Calc. | Obsd. | Calc. | Obsd. | Calc. |
| 0 | 3.42 | 3.42 | 0.00 | 0.00 | 10.00 | 10.00 |
| 4 | 1.30 | 1.15 | 0.34 | 0.69 | 10.59 | 10.52 |
| 6 | 0.55 | 0.68 | 0.72 | 0.64 | 10.71 | 10.69 |
| 8 | 0.27 | 0.41 | 0.83 | 0.60 | 10.77 | 10.80 |
| 10 | 0.24 | 0.25 | 0.77 | 0.58 | 10.80 | 10.85 |
| 30 | 0.05 | 0.05 | 0.54 | 0.55 | 10.93 | 10.93 |
| 45 | 0.08 | 0.05 | 0.53 | 0.54 | 10.93 | 10.93 |
| 60 | 0.09 | 0.04 | 0.52 | 0.54 | 10.93 | 10.93 |
| 75 | 0.07 | 0.04 | 0.52 | 0.54 | 10.93 | 10.93 |
| 120 | 0.07 | 0.04 | 0.52 | 0.54 | 10.93 | 10.93 |

($Cr^{3+}$) and [Cr] in the metal phase. This would require a model which includes a third route where ($Cr^{3+}$) is directly reduced to [Cr] to study the kinetics of the reduction reactions. This model could also be applied to cases where $CaF_2$ is added to the slag. $CaF_2$ in slags, like the one used in this study, reduces the viscosity and this makes it possible for easy mixing of the slag and metal during CO bubling. These conditions increase the slag/metal contact area and would favour a direct reduction of ($Cr^{3+}$) to [Cr] to take place simultaneously with that through the intermediate, ($Cr^{2+}$). A discussion of the model which takes account of a direct reaction between ($Cr^{3+}$) and [Cr] is discussed in the next section.

### 4.5.4 Scheme 5: First-order consecutive reversible two-stage reactions with $(Cr^{3+})$ directly forming [Cr] and varying slag height.

Using this scheme the reactions can be represented as

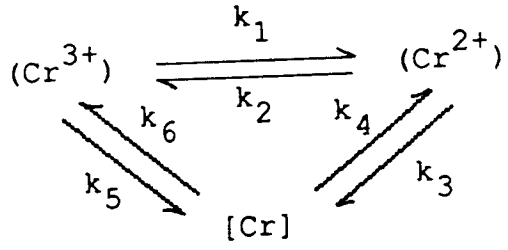


(4.61)

The differential equations are:

$$\frac{d(Cr^{3+})}{dt} = \frac{k_2}{h}(Cr^{2+}) + \frac{k_6}{h}[Cr] - \frac{k_1}{h}(Cr^{3+}) - \frac{k_5}{h}(Cr^{3+}) \quad (4.62)$$

$$\frac{d(Cr^{2+})}{dt} = \frac{k_1}{h}(Cr^{3+}) + \frac{k_4}{h}[Cr] - \frac{k_2}{h}(Cr^{2+}) - \frac{k_3}{h}(Cr^{2+}) \quad (4.63)$$

$$\frac{d[Cr]}{dt} = \frac{k_3}{h}(Cr^{2+}) + \frac{k_5}{h}(Cr^{3+}) - \frac{k_4}{h}[Cr] - \frac{k_6}{h}[Cr] \qquad (4.64)$$

By writing $d(Cr^{3+})/dt = (Cr^{3+})$ etc. and $K_1 = k_1/h$ etc. we have the following equations

$$(Cr^{3+}) + (K_1 + K_5)(Cr^{3+}) - K_2(Cr^{2+}) - K_6[Cr] = 0 \qquad (4.65)$$

$$(Cr^{2+}) - K_1(Cr^{3+}) + (K_2 + K_3)(Cr^{2+}) - K_4[Cr] = 0 \qquad (4.66)$$

$$[Cr] - K_5(Cr^{3+}) - K_3(Cr^{2+}) + (K_4 + K_6)[Cr] = 0 \qquad (4.67)$$

The rate constant matrix becomes

$$K = \begin{pmatrix} K_1 + K_5 & -K_2 & -K_6 \\ -K_1 & K_2 + K_3 & -K_4 \\ -K_5 & -K_3 & K_4 + K_6 \end{pmatrix} \qquad (4.68)$$

The secular equation[54] is

$$\begin{vmatrix} K_1 + K_5 - m_r & -K_2 & -K_6 \\ -K_1 & K_2 + K_3 - m_r & -K_4 \\ -K_5 & -K_3 & K_4 + K_6 - m_r \end{vmatrix} = 0 \qquad (4.69)$$

Expanding equation (4.69) gives

$$-m_r^3 + m_r^2 (K_1 + K_2 + K_3 + K_4 + K_5 + K_6) - m_r (K_1K_3 + K_2K_4 + K_1K_4 + K_3K_5 + K_2K_5 + K_3K_6 + K_2K_6 + K_1K_6 + K_4K_5) = 0 \qquad (4.70)$$

The three solutions for $m_r$ are:

$$m_1 = 0$$

$$m_2 = \frac{1}{2} (p + q) \qquad (4.71)$$

$$m_3 = \frac{1}{2} (p - q)$$

where $p = (K_1 + K_2 + K_3 + K_4 + K_5 + K_6)$ and

$$q = [\, p^2 - 4 (K_1K_3 + K_2K_4 + K_1K_4 + K_3K_5 + K_2K_5 + K_3K_6 + K_2K_6 + K_1K_6 + K_4K_5 ) \,]^{1/2}$$

As described by Lewis et al[53], the coefficients B can be deduced by setting $B_{3r} = 1$ and solving the equation

$$\sum_{j=1}^{n} (K_{ij} - I_{ij}m)\, B_j = 0 \qquad (4.72)$$

In this particular case, in contrast to the case illustrated by Frost and Pearson[54] setting $B_{1r} = 1$ leads to some infinities of other B values[53]. Solving equation (4.72) gives the expressions for the B coefficients:

$$B_{11} = \frac{(K_4 + K_6)\, D - K_3[\,(K_4 + K_6)\,(K_1 + K_5) - K_5K_6\,]}{K_5\, D} \qquad (4.73)$$

$$B_{12} = \left\{ (K_4 + K_6 - m_2)(D - K_3m_2) - K_3\,[\,(K_4 + K_6 - m_2)\,(K_1 + K_5 - m_2) - K_5K_6\,] \right\} \Big/ K_5\,(D - K_3m_2) \qquad (4.74)$$

$$B_{13} = \left\{ (K_4 + K_6 - m_3)(D - K_3m_3) - K_3\,[\,(K_4 + K_6 - m_3)\,(K_1 + K_5 - m_3) - K_5K_6\,] \right\} \Big/ K_5\,(D - K_3m_3) \qquad (4.75)$$

$$B_{21} = \frac{(K_4 + K_6)\ (K_1 + K_5)\ -\ K_5K_6}{D} \qquad (4.76)$$

$$B_{22} = \frac{(K_4 + K_6 - m_2)(K_1 + K_5 - m_2) - K_5K_6}{D\ -\ K_3m_2} \qquad (4.77)$$

$$B_{23} = \frac{(K_4 + K_6 - m_3)(K_1 + K_5 - m_3) - K_5K_6}{D\ -\ K_3m_3} \qquad (4.78)$$

where $D = K_2K_5 + K_1K_3 + K_3K_5$. In matrix form the coefficients B can be written as

$$B = \begin{pmatrix} B_{11} & B_{12} & B_{13} \\ B_{21} & B_{22} & B_{23} \\ 1 & 1 & 1 \end{pmatrix} \qquad (4.79)$$

of which the determinant is

$$|B| = B_{11}B_{22} + B_{12}B_{23} + B_{13}B_{21} - B_{22}B_{13} - B_{23}B_{11} - B_{12}B_{21} \qquad (4.80)$$

When the following matrices are defined as in section 4.5.2.5

$$A = \begin{pmatrix} (Cr^{3+}) \\ (Cr^{2+}) \\ [Cr] \end{pmatrix} \qquad A_o = \begin{pmatrix} (Cr^{3+})_o \\ (Cr^{2+})_o \\ [Cr]_o \end{pmatrix}$$

$$E = \begin{pmatrix} 1 & 0 & 0 \\ 0 & \exp(-m_2 t) & 0 \\ 0 & 0 & \exp(-m_3 t) \end{pmatrix}$$

the desired matrix A can be shown to be given by

$$A = B\,E\,B^{-1}\,A_o$$

The explicit solution of this equation then gives the desired dependence of the concentration on time and rate constants. The final solutions are given by equation (4.81), (4.82) and (4.83) below:

$$(Cr^{3+}) = \frac{1}{|B|}\Big\{ (Cr^{3+})_o \big[ B_{11}(B_{22} - B_{23}) + B_{12}(B_{23} - B_{21})\exp(-m_2 t) + B_{13}(B_{21} - B_{22})\exp(-m_3 t) \big] + (Cr^{2+})_o \big[ B_{11}(B_{13} - B_{12}) + B_{12}(B_{11} - B_{13})\exp(-m_2 t) + B_{13}(B_{12} - B_{11})\exp(-m_3 t) \big] + [Cr]_o \big[ B_{11}(B_{12}B_{23} - B_{22}B_{13}) + B_{12}(B_{21}B_{13} - B_{11}B_{23})\exp(-m_2 t) + B_{13}(B_{11}B_{22} - B_{21}B_{12})\exp(-m_3 t) \big] \Big\} \qquad (4.81)$$

$$(Cr^{2+}) = \frac{1}{|B|} \left\{ (Cr^{3+})_o \left[ B_{21} (B_{22} - B_{23}) + B_{22} \right.\right.$$

$$(B_{23} - B_{21}) \exp(-m_2 t) + B_{23} (B_{21} - B_{22}) \exp(-m_3 t) \left.\right]$$

$$(Cr^{2+})_o \left[ B_{21} (B_{13} - B_{12}) + B_{22} (B_{11} - B_{13}) \exp(-m_2 t) \right.$$

$$\left. + B_{23} (B_{12} - B_{11}) \exp(-m_3 t) \right] + [Cr]_o \left[ B_{21} (B_{12}B_{23} \right.$$

$$\left. - B_{22}B_{13}) + B_{22} (B_{21}B_{13} - B_{11}B_{23}) \exp(-m_2 t) + B_{23} \right.$$

$$\left. (B_{11}B_{22} - B_{21}B_{12}) \exp(-m_3 t) \right] \left.\right\} \qquad (4.82)$$

$$[Cr] = \frac{1}{|B|} \left\{ (Cr^{3+})_o \left[ (B_{22} - B_{23}) + (B_{23} - B_{21}) \right.\right.$$

$$\exp(-m_2 t) + (B_{21} - B_{22}) \exp(-m_3 t) \left.\right] + (Cr^{2+})_o$$

$$\left[ (B_{13} - B_{12}) + (B_{11} - B_{13}) \exp(-m_2 t) + (B_{12} - B_{11}) \right.$$

$$\exp(-m_3 t) \left.\right] + [Cr]_o \left[ (B_{12}B_{23} - B_{22}B_{13}) + (B_{21}B_{13} \right.$$

$$\left. - B_{11}B_{23}) \exp(-m_2 t) + (B_{11}B_{22} - B_{21}B_{12}) \exp(-m_3 t) \right] \left.\right\}$$

(4.83)

The concentrations of the chromium species were calculated from this scheme using the computer programs shown in appendices G and H for runs AS1, AS2, AS3 and AS5. The program in appendix G computes the six rate constants giving minimum sums of squares of deviations

for the chromium species and for a particular set of *data, that in appendix H calculates the concentrations of* the chromium species with time using the rate constants obtained from the program in appendix G.

Figs 4.19, 4.20, 4.21 and 4.22 show concentration-time curves for runs AS1, AS2, AS3 and AS5, respectively, with the corresponding observed results using scheme 5. Table 4.19 shows a comparison of the sums of squares of deviations of the chromium species from the above runs using schemes 4 and 5.

**Table 4.19: Comparison of sums of squares of deviations for schemes 4 and 5.**

| Run No. | $(Cr^{3+})$ | $(Cr^{2+})$ | [Cr] |
|---|---|---|---|
| | Scheme 4 | | |
| AS1 | 0.005 | 0.045 | 0.004 |
| AS2 | 0.031 | 0.038 | 0.001 |
| AS3 | 0.020 | 0.092 | 0.012 |
| AS5 | 0.052 | 0.094 | 0.024 |
| | Scheme 5 | | |
| AS1 | 0.005 | 0.022 | 0.001 |
| AS2 | 0.028 | 0.033 | 0.001 |
| AS3 | 0.036 | 0.023 | 0.006 |
| AS5 | 0.031 | 0.010 | 0.004 |

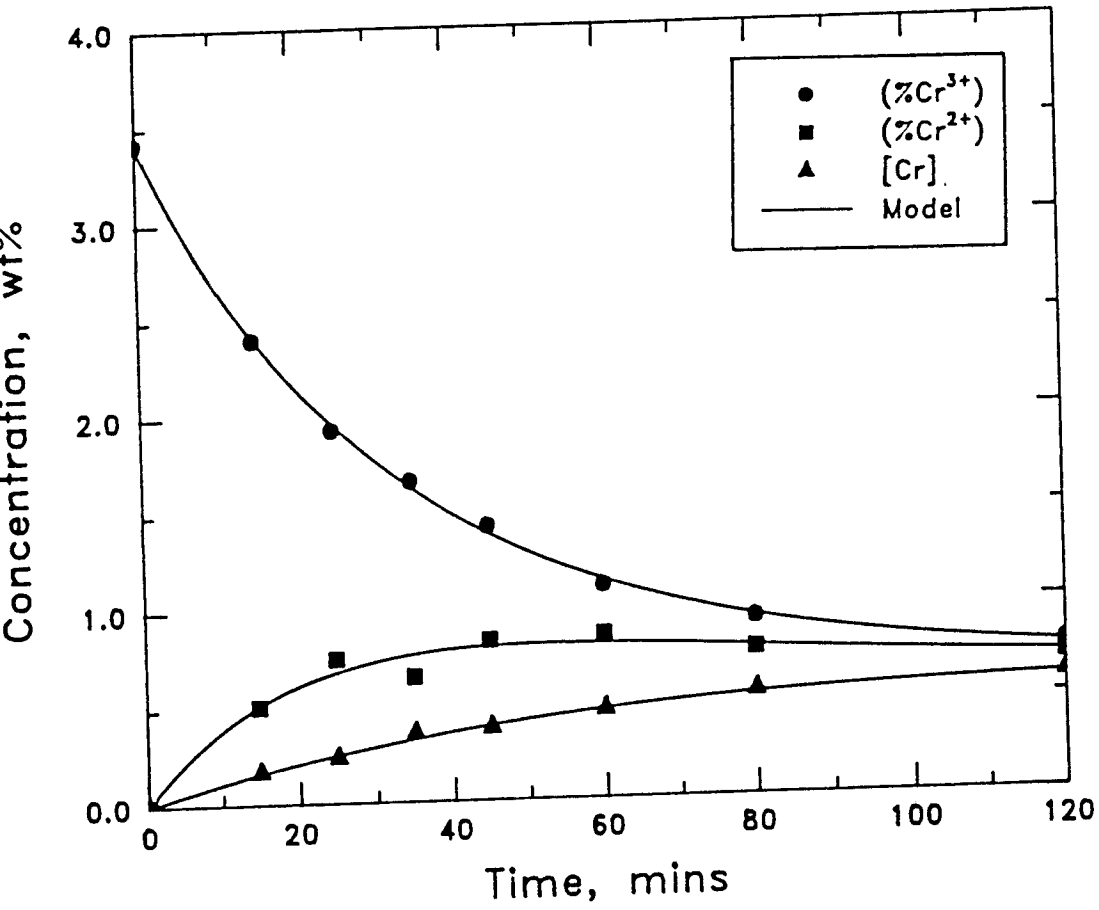


$k_1 = 0.0130\ cm.min^{-1}$. $k_2 = 0.0134\ cm.min^{-1}$.
$k_3 = 0.0142\ cm.min^{-1}$. $k_4 = 0.0045\ cm.min^{-1}$.
$k_5 = 0.0094\ cm.min^{-1}$. $k_6 = 0.0029\ cm.min^{-1}$.

Sums of squares of deviations are:

$Cr^{3+} = 0.005$, $Cr^{2+} = 0.022$, $Cr_{Met.} = 0.001$.

Fig. 4.19 Time variation in concentration of $(Cr^{3+})$, $(Cr^{2+})$ and [Cr] for run AS1 using scheme 5.

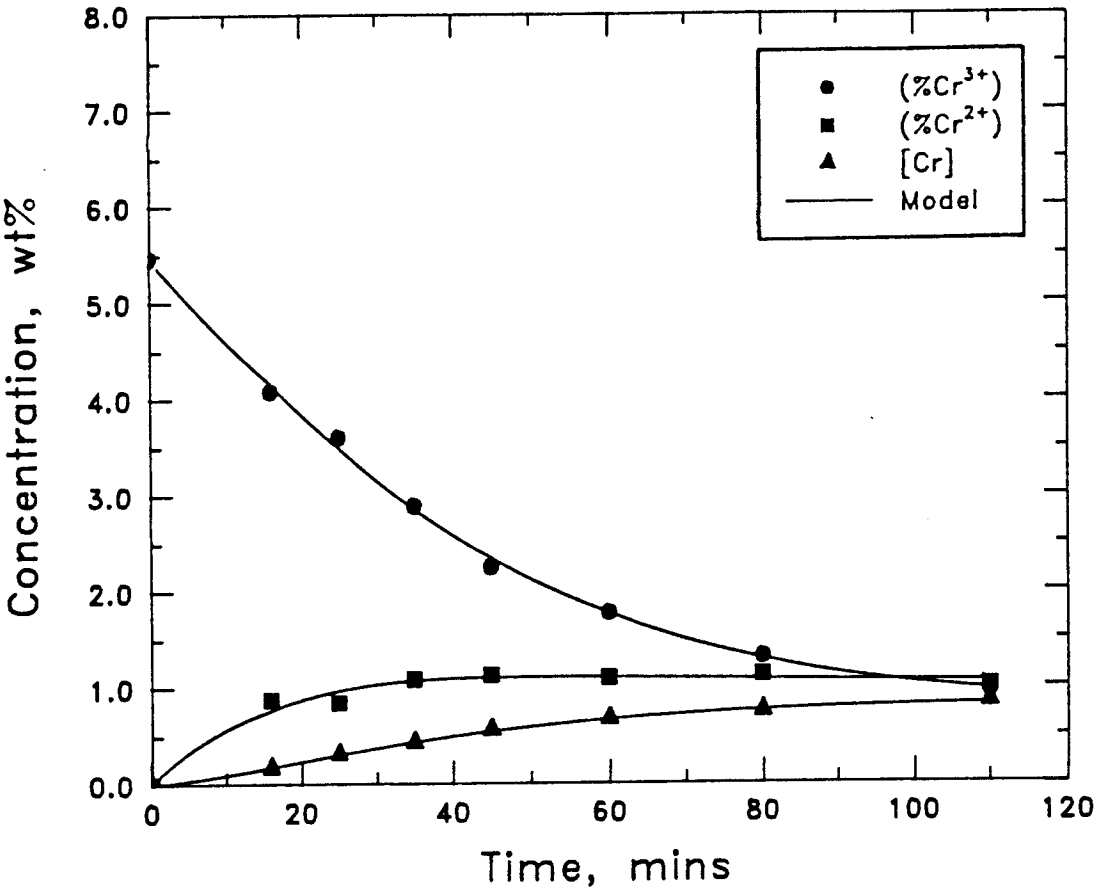


$k_1 = 0.0126$ cm.min$^{-1}$. $k_2 = 0.0043$ cm.min$^{-1}$.
$k_3 = 0.0396$ cm.min$^{-1}$. $k_4 = 0.0098$ cm.min$^{-1}$.
$k_5 = 0.0031$ cm.min$^{-1}$. $k_6 = 0.0023$ cm.min$^{-1}$.

Sums of squares of deviations are:
$Cr^{3+} = 0.028$, $Cr^{2+} = 0.033$, $Cr_{Met.} = 0.001$.

Fig. 4.20 Time variation in concentration of ($Cr^{3+}$), ($Cr^{2+}$) and [Cr] for run AS2 using scheme 5.

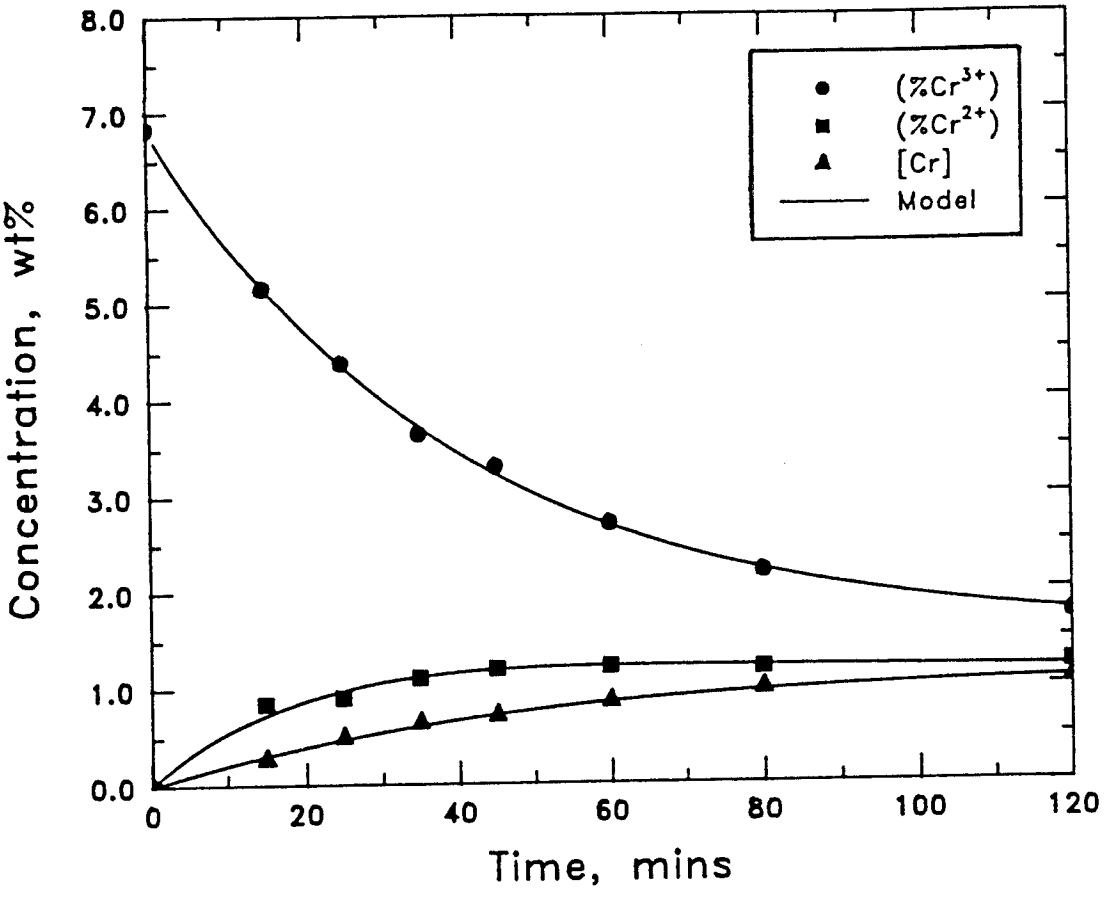


$k_1 = 0.0093\ cm.min^{-1}$. $k_2 = 0.0239\ cm.min^{-1}$.
$k_3 = 0.0121\ cm.min^{-1}$. $k_4 = 0.0067\ cm.min^{-1}$.
$k_5 = 0.0090\ cm.min^{-1}$. $k_6 = 1.34 \times 10^{-8}$

Sums of squares of deviations are:
$Cr^{3+} = 0.036$, $Cr^{2+} = 0.023$, $Cr_{Met.} = 0.006$.

Fig. 4.21 Time variation in concentration of ($Cr^{3+}$), ($Cr^{2+}$) and [Cr] for run AS3 using scheme 5.

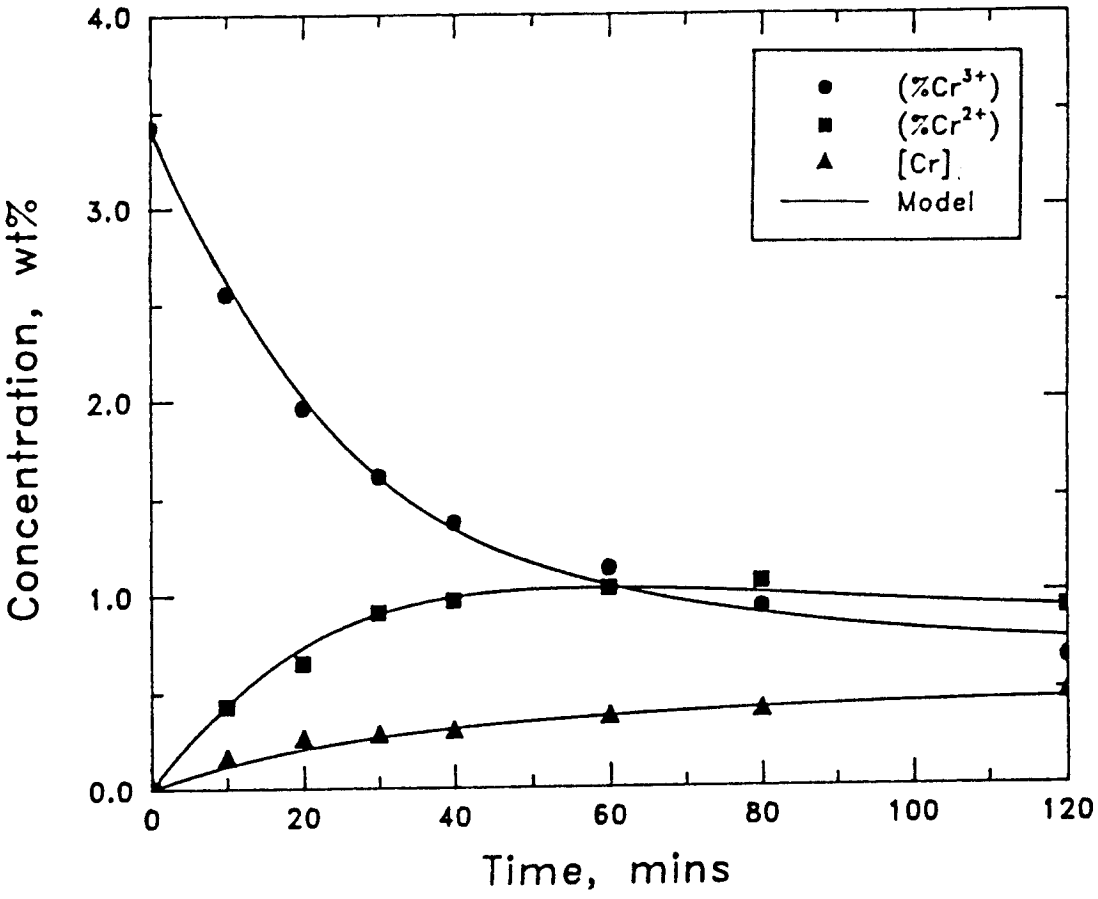


$k_1 = 0.0139\ cm.min^{-1}$. $k_2 = 0.0193\ cm.min^{-1}$.
$k_3 = 0.0000\ cm.min^{-1}$. $k_4 = 0.0038\ cm.min^{-1}$.
$k_5 = 0.0109\ cm.min^{-1}$. $k_6 = 0.0000\ cm.min^{-1}$.

Sums of squares of deviations are:

$Cr^{3+} = 0.031$, $Cr^{2+} = 0.010$, $Cr_{Met.} = 0.004$.

Fig. 4.22 Time variation in concentration of $(Cr^{3+})$, $(Cr^{2+})$ and [Cr] for run AS5 using scheme 5.

Assuming a direct reduction of $(Cr^{3+})$ to [Cr] to be taking place simultaneously with that through the intermediate, gives better fits for the runs above than when it is assumed absent, as shown by a reduction in the sums of squares of deviations of the chromium species, Table 4.19. However, the rate constants obtained do not account for what was physically taking place in the system. For example, the rate constants for run AS5 indicate that there was transfer of chromium from the metal to the slag. This is not possible since there was no chromium in the metal at the beginning of the run and as such the metal acted as a sink for chromium. The rate constants also suggest that reduction was mainly by direct reduction of $(Cr^{3+})$ to [Cr]. This is contrary to the evidence from other investigators[20,31,37] and indeed from this study that the reduction of $Cr_2O_3$ takes place mainly through the intermediate, $(Cr^{2+})$, as the change of colour of the slag from light green to deep blue confirms the reduction of $(Cr^{3+})$ to $(Cr^{2+})$. In view of this, the rate constants $k_3$ and $k_4$ are expected to be higher than Fig. 4.22 suggest. Also, the rate constants $k_5$ and $k_6$ are expected to be less than those of $k_3$ and $k_4$.

The ambigous rate constants obtained using scheme 5 are due to the fact that the program for determining rate constants is allowed to vary six interrelated constants

independently whilst minimising the sums of squares of deviations. This gives a statiscally significant result that does not fit the chemical constraints in the system. A reduction in the number of rate constants to vary will give more meaningful results. To achieve this, $k_2$, $k_4$ and $k_6$ were derived as dependent variables on $k_1$, $k_3$ and $k_5$, respectively. Consider scheme 5 again as

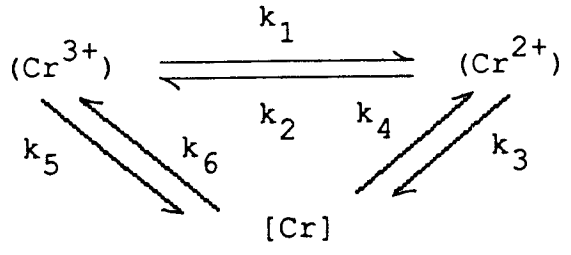


The reactions can be considered to be approaching equilibrium, as an approximation, as shown by the levelling of the curves at longer times. Then the rate constants are related from the equilibrium constants as

$$K_1' = \frac{k_1}{k_2} = \frac{(Cr^{2+})}{(Cr^{3+})} \qquad (4.84)$$

$$K_2' = \frac{k_3}{k_4} = \frac{[Cr]}{(Cr^{2+})} \qquad (4.85)$$

$$K_3' = \frac{k_5}{k_6} = \frac{[Cr]}{(Cr^{3+})} \qquad (4.86)$$

where $K_1'$, $K_2'$ and $K_3'$ are the equilibrium constants for the first, second and third stages, respectively. The equilibrium constants are determined from the concentrations of the chromium species where the curves start to level off and are considered to be constant throughout an experimental run. Then $k_2$, $k_4$ and $k_6$ are governed by the following relations:

$$k_2 = \frac{k_1}{K_1'} \tag{4.86}$$

$$k_4 = \frac{k_3}{K_2'} \tag{4.87}$$

$$k_6 = \frac{k_5}{K_3'} \tag{4.88}$$

Consideration of the above relations in scheme 5 reduces the number of independent variables to three. This was incoporated in the model by modifying the program in appendix G so that only $k_1$, $k_3$ and $k_5$ were varied during the loops to arrive at the minimum sums of squares of deviations of the chromium species. The rate constants, $k_2$, $k_4$ and $k_6$ were determined from the relations above and the equilibrium constants $K_1'$, $K_2'$ and $K_3'$ were determined from the concentrations of the chromium species at longer times, where the curves level off, in

each run. It was hoped that by reducing the number of rate constants to vary in the model, reasonable values of the rate constants could be obtained.

Rate curves for runs AS1 and AS5 were calculated using a modified model incoporating the above relations and are shown in Figs. 4.23 and 4.24, respectively. Observation of the figures show that the values of the rate constants, $k_3$ and $k_4$, are very small in both cases which is contrary to what is physically supposed to be happening in the system. The goodness of fits is worse when three rate constants are varied in the program, as shown by an increase in the sums of squares of deviations. Incoporation of the relations between the rate constants in the model still gives ambigous values of the rate constants.

In an effort to improve the fits, only the first 60 minutes of reaction were fitted. This is thought valid because the mechanism of reduction is thought to change at longer times, since silica reduction also takes place. This is supported by the results of Anyakwo[37] who found the reduction of ($Cr^{3+}$) and ($Cr^{2+}$) to take place in two stages, a fast initial stage and a slower second stage. The reduction of slag chromium, which is predominantly (CrO) at longer times, is thought to be taking place concurrently with silica reduction and as such the

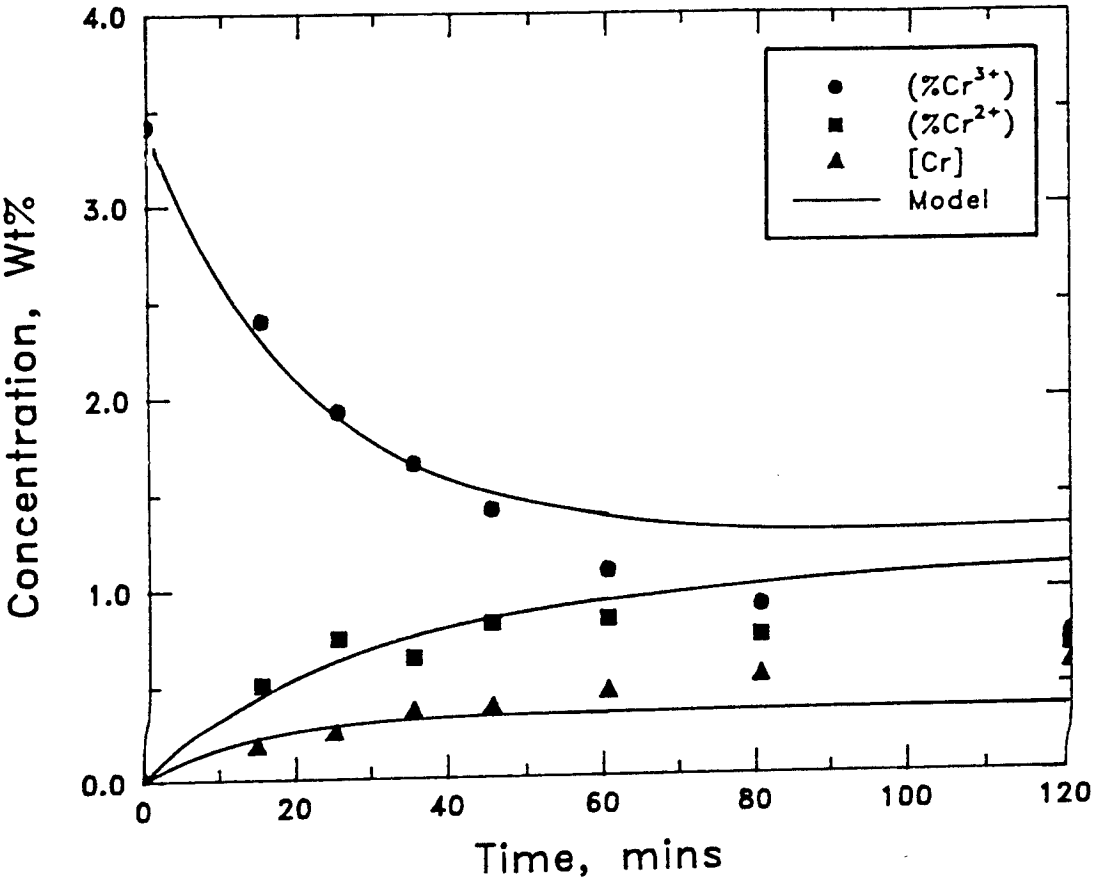


$k_1 = 0.0101$ cm.min$^{-1}$. $k_2 = 0.0110$ cm.min$^{-1}$.
$k_3 = 3.04 \times 10^{-7}$. $k_4 = 3.54 \times 10^{-7}$.
$k_5 = 0.0181$ cm.min$^{-1}$. $k_6 = 0.0229$ cm.min$^{-1}$.

Sums of squares of deviations are:

$Cr^{3+} = 0.550$, $Cr^{2+} = 0.255$, $Cr_{Met.} = 0.120$.

Fig. 4.23 Time variation in concentration of ($Cr^{3+}$), ($Cr^{2+}$) and [Cr] for run AS1 using scheme 5 with equilibrium constant relations.

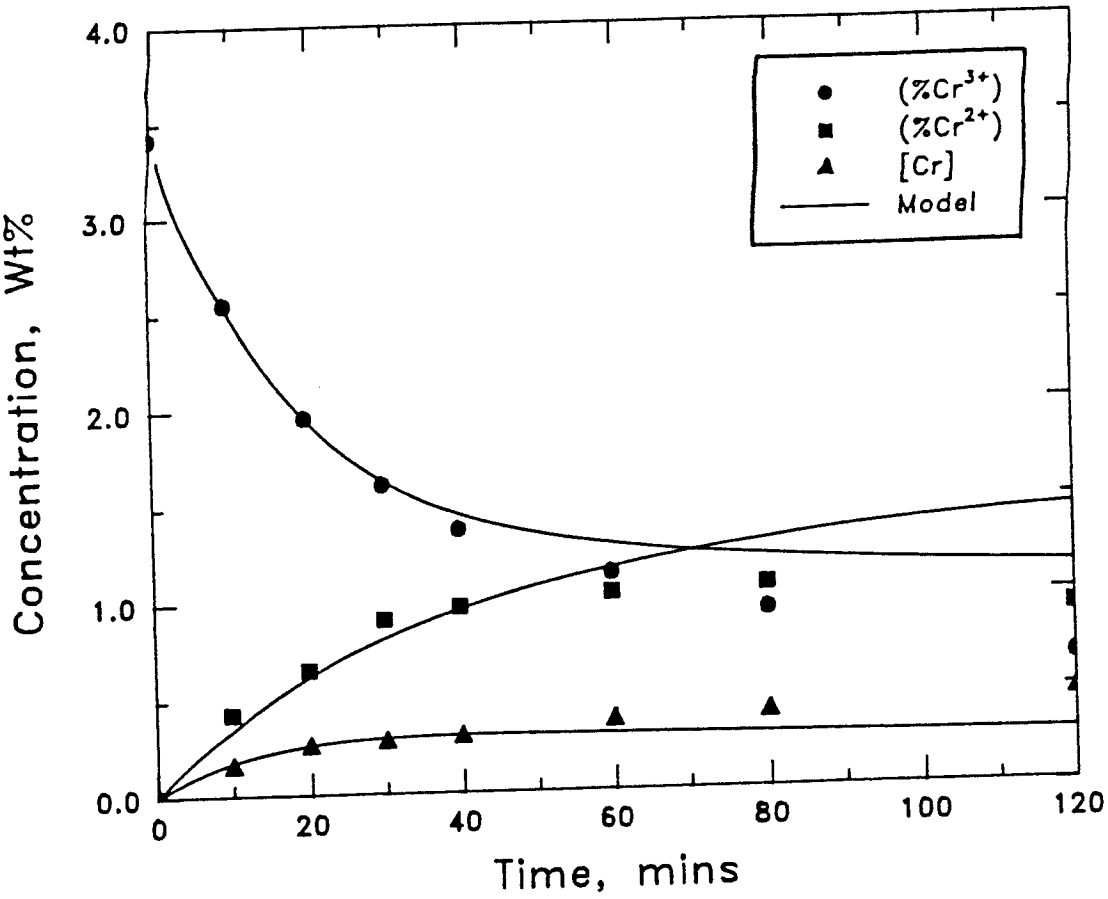


$k_1 = 0.0109\ cm.min^{-1}$. $k_2 = 0.0078\ cm.min^{-1}$.
$k_3 = 2.98 \times 10^{-7}$. $k_4 = 5.82 \times 10^{-8}$.
$k_5 = 0.0189\ cm.min^{-1}$ .$k_6 = 0.0265\ cm.min^{-1}$ .

Sums of squares of deviations are:

$Cr^{3+} = 0.336$, $Cr^{2+} = 0.369$, $Cr_{Met.} = 0.059$.

Fig. 4.24 Time variation in concentration of $(Cr^{3+})$, $(Cr^{2+})$ and [Cr] for run AS5 using scheme 5 with equilibrium constant relations.

mechanism of reduction at longer times will be different. This could introduce errors in the determination of rate constants. To eliminate this problem, the curves were calculated up to 60 minutes, beyond which the mechanism of reduction is thought to change. The calculated rate curves for runs AS1 and AS5, up to 60 minutes, are shown in Figs. 4.25 and 4.26, respectively. The figures show that there is an improvement in the fits, as shown by a reduction in the sums of squares of deviations of the chromium species. Calculating the curves to 45 minutes further improves the fits as shown in Figs 4.27 and 4.28 but the general trend of the rate constants does not show any improvement, as very small values for $k_3$ and $k_4$ are obtained which do not make any metallurgical sense as to what is physically happening in the system.

To ascertain whether scheme 5 could best be applied to cases where the direct reduction of $(Cr^{3+})$ to [Cr] is thought to be favoured, such as when a surface-active element like sulphur is added to the system, rate curves were calculated for runs AS11, AS12 and AS13 in which 0.05, 0.10 and 0.30 wt%S were added to metal, respectively. The curves were calculated up to 60 minutes to eliminate the error introduced by commencement of a slower second stage of reactions at longer times[37]. Figs. 4.29, 4.30 and 4.31 show the calculated rate curves with the corresponding observed values for

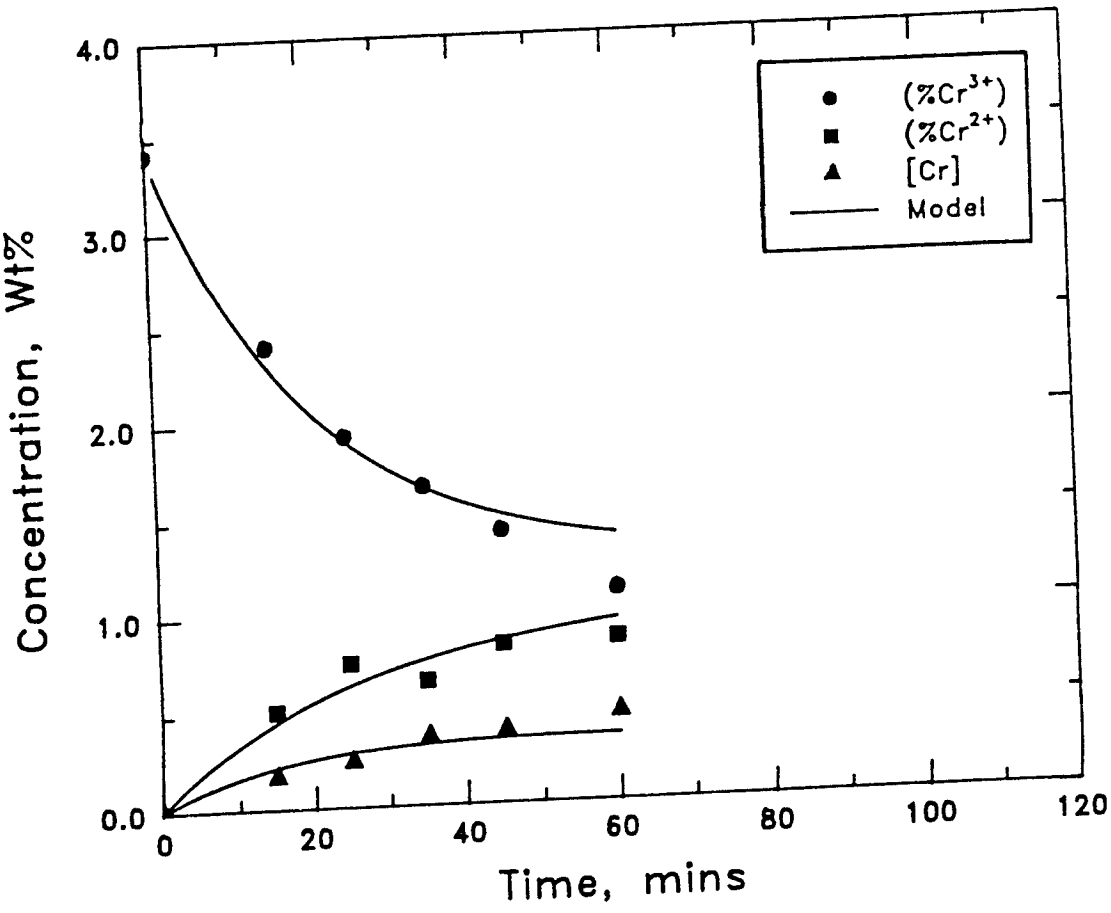


$k_1 = 0.0106\ cm.min^{-1}$. $k_2 = 0.0116\ cm.min^{-1}$.
$k_3 = 3.03 \times 10^{-7}$. $k_4 = 3.54 \times 10^{-7}$.
$k_5 = 0.0170\ cm.min^{-1}$. $k_6 = 0.0216\ cm.min^{-1}$.

Sums of squares of deviations are:
$Cr^{3+} = 0.100$, $Cr^{2+} = 0.041$, $Cr_{Met.} = 0.019$.

Fig. 4.25 Time variation in concentration of $(Cr^{3+})$, $(Cr^{2+})$ and [Cr] for run AS1 using scheme 5 with equilibrium constant relations and fitting the first 60 minutes of reaction.

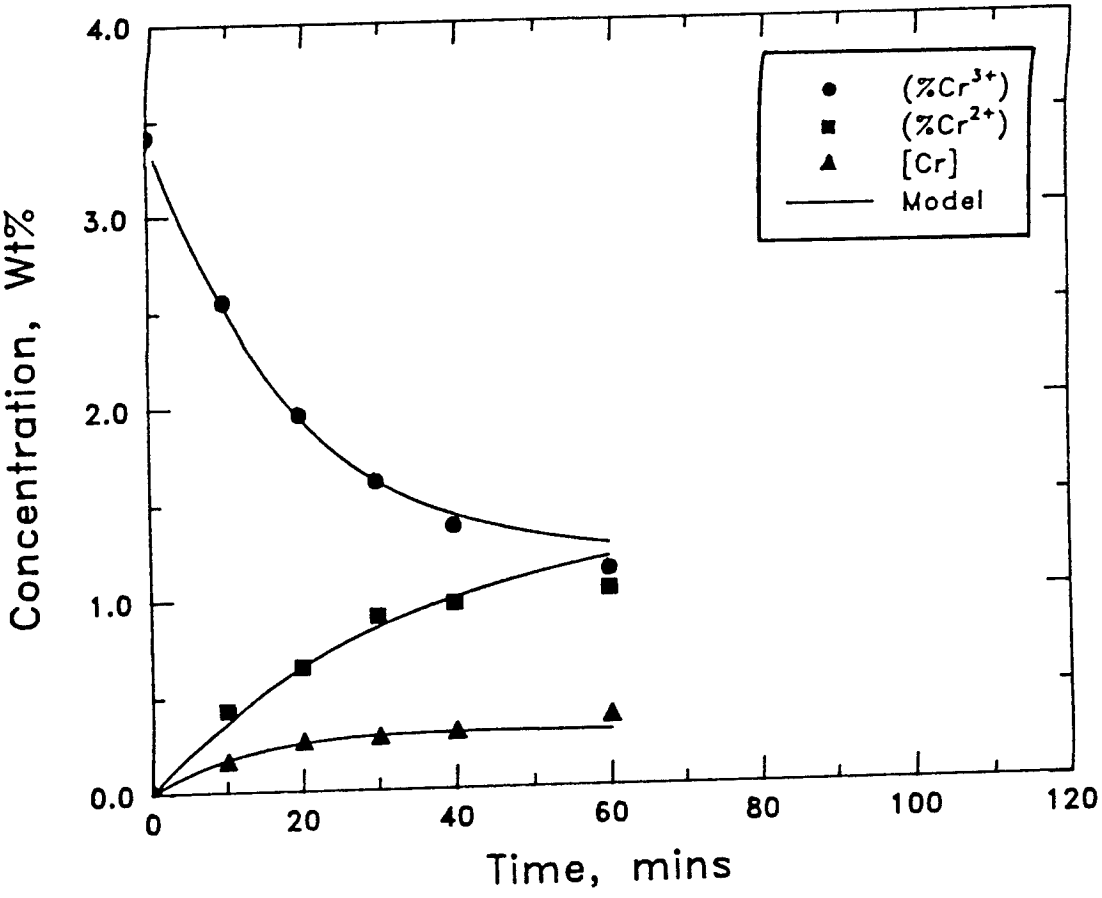


$k_1 = 0.0116\ cm.min^{-1}$. $k_2 = 0.0083\ cm.min^{-1}$.
$k_3 = 4.49 \times 10^{-7}$. $k_4 = 8.78 \times 10^{-8}$.
$k_5 = 0.0183\ cm.min^{-1}$ .$k_6 = 0.0257\ cm.min^{-1}$ .

Sums of squares of deviations are:

$Cr^{3+} = 0.018$, $Cr^{2+} = 0.041$, $Cr_{Met.} = 0.006$.

Fig. 4.26 Time variation in concentration of $(Cr^{3+})$, $(Cr^{2+})$ and [Cr] for run AS5 using scheme 5 with equilibrium constant relations and fitting the first 60 minutes of reaction.

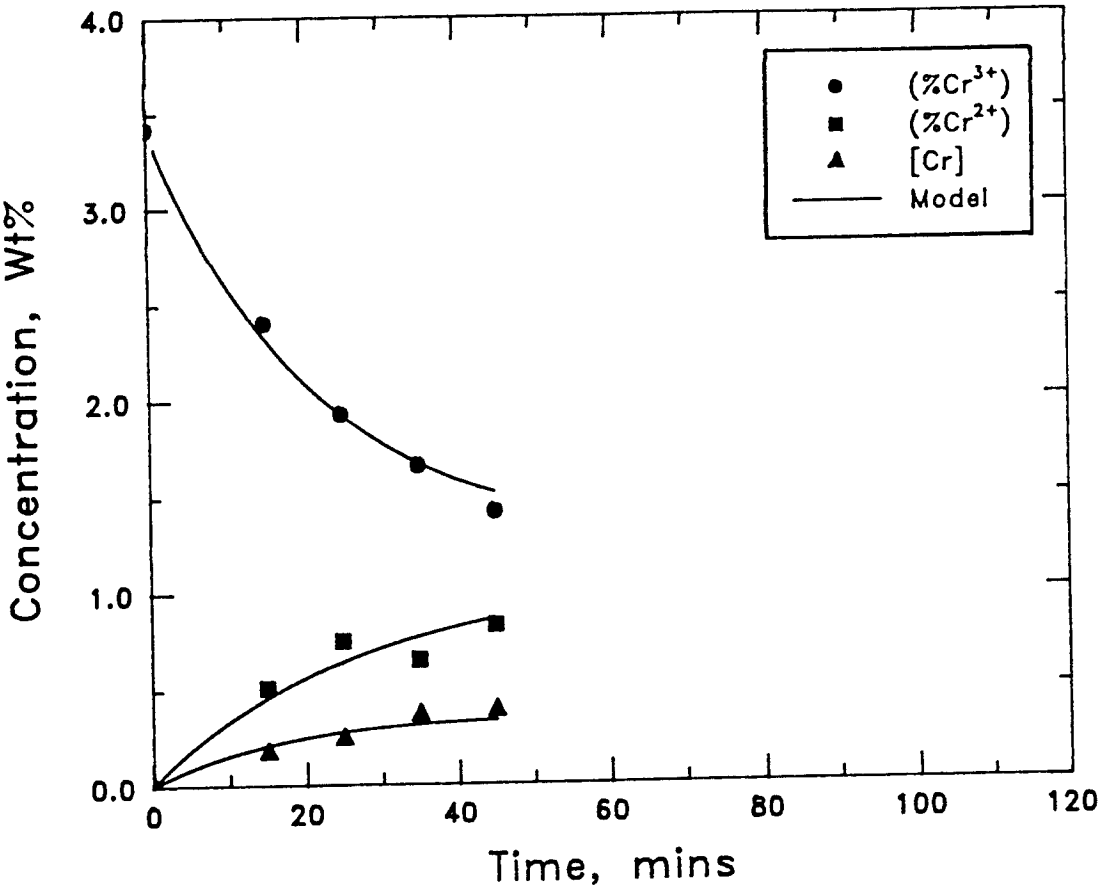


$k_1 = 0.0107\ cm.min^{-1}$. $k_2 = 0.0116\ cm.min^{-1}$.
$k_3 = 4.80 \times 10^{-7}$. $k_4 = 5.60 \times 10^{-7}$.
$k_5 = 0.0160\ cm.min^{-1}$. $k_6 = 0.0203\ cm.min^{-1}$.

Sums of squares of deviations are:

$Cr^{3+} = 0.015$, $Cr^{2+} = 0.031$, $Cr_{Met.} = 0.007$.

Fig. 4.27 Time variation in concentration of ($Cr^{3+}$), ($Cr^{2+}$) and [Cr] for run AS1 using scheme 5 with equilibrium constant relations and fitting the first 45 minutes of reaction.

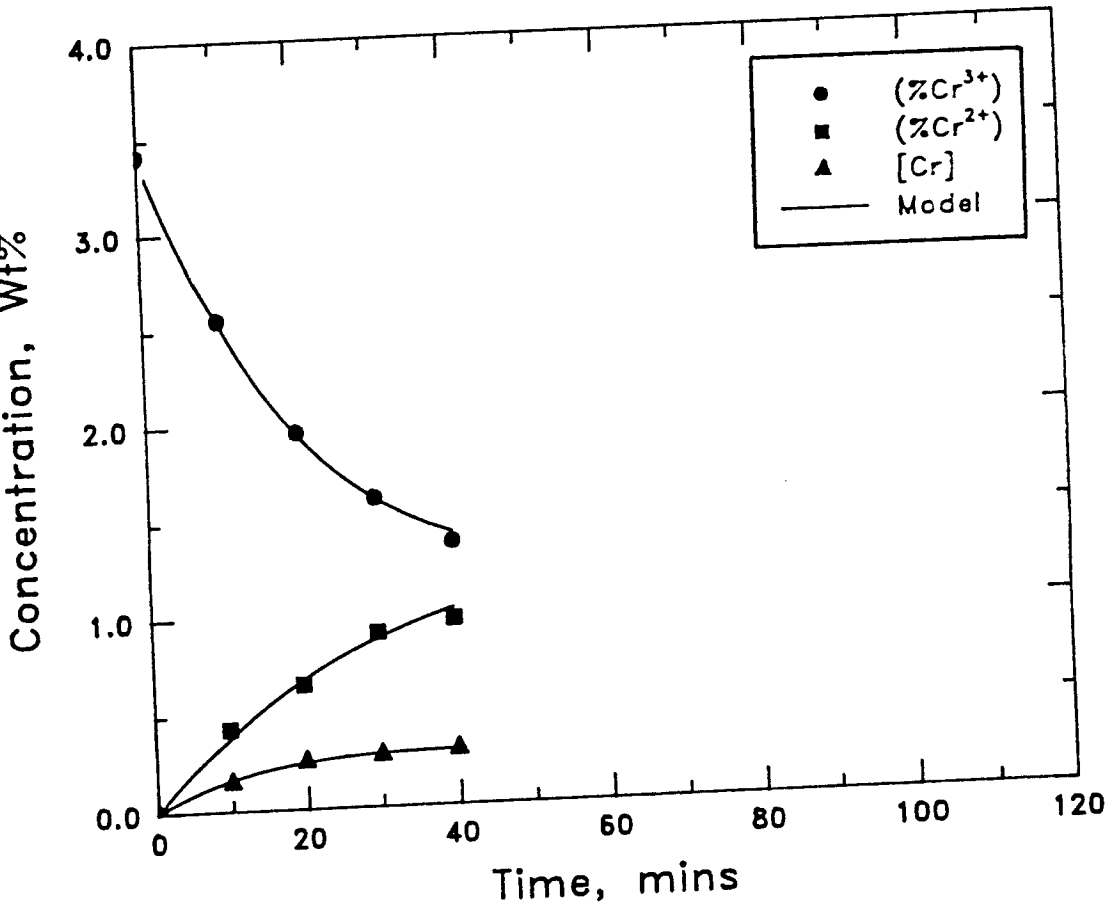


$k_1 = 0.0120\ cm.min^{-1}$. $k_2 = 0.0086\ cm.min^{-1}$.
$k_3 = 2.37 \times 10^{-7}$. $k_4 = 4.63 \times 10^{-7}$.
$k_5 = 0.0174\ cm.min^{-1}$. $k_6 = 0.0244\ cm.min^{-1}$.

Sums of squares of deviations are:
$Cr^{3+} = 0.002$, $Cr^{2+} = 0.007$, $Cr_{Met.} = 0.001$.

Fig. 4.28 Time variation in concentration of $(Cr^{3+})$, $(Cr^{2+})$ and [Cr] for run AS5 using scheme 5 with equilibrium constant relations and fitting the first 40 minutes of reaction.

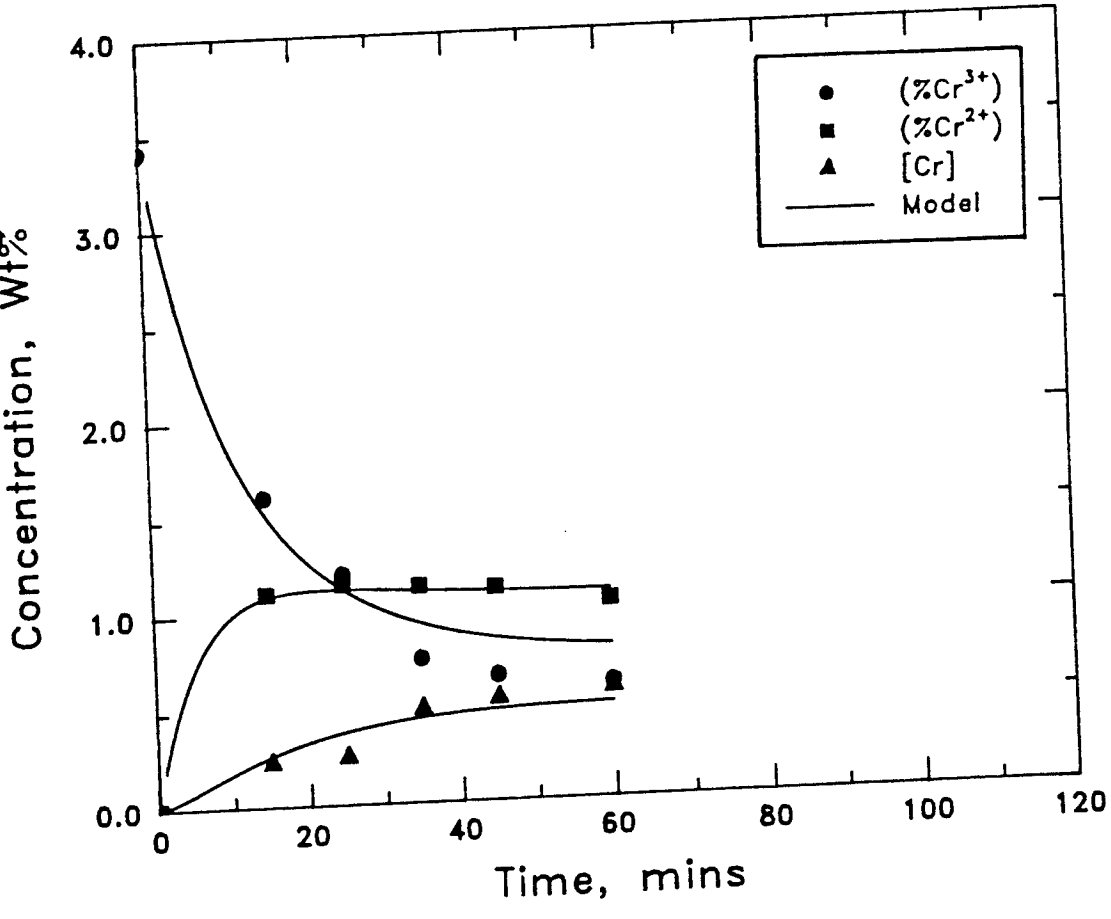


$k_1 = 0.0556\ cm.min^{-1}$. $k_2 = 0.0397\ cm.min^{-1}$.
$k_3 = 0.0582\ cm.min^{-1}$. $k_4 = 0.0398\ cm.min^{-1}$.
$k_5 = 0.0087\ cm.min^{-1}$. $k_6 = 0.0043\ cm.min^{-1}$.

Sums of squares of deviations are:

$Cr^{3+} = 0.122$, $Cr^{2+} = 0.004$, $Cr_{Met.} = 0.029$.

Fig. 4.29 Time variation in concentration of $(Cr^{3+})$, $(Cr^{2+})$ and [Cr] for run AS11 using scheme 5 with equilibrium constant relations and fitting the first 60 minutes of reaction.

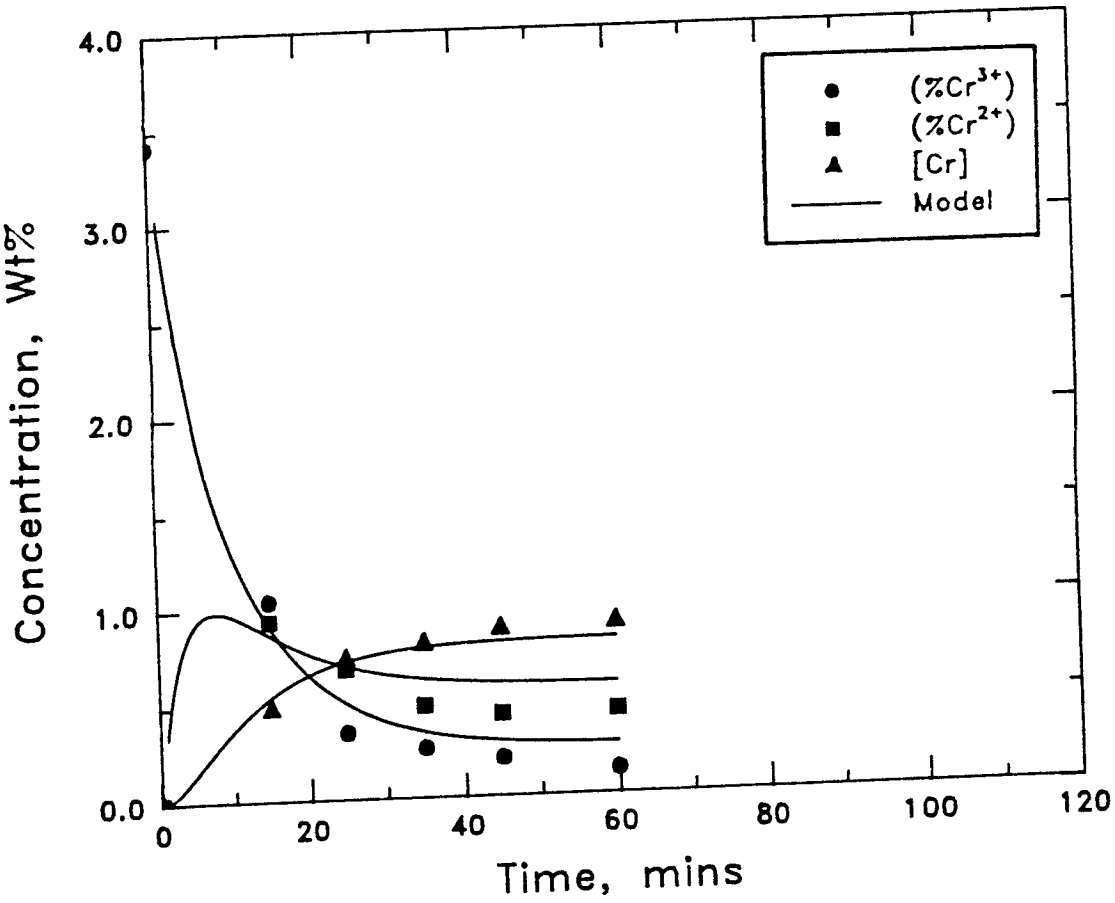


$k_1 = 0.1059\ cm.min^{-1}$. $k_2 = 0.0481\ cm.min^{-1}$.
$k_3 = 0.1487\ cm.min^{-1}$. $k_4 = 0.0334\ cm.min^{-1}$.
$k_5 = 1.23 \times 10^{-6}$. $k_6 = 1.88 \times 10^{-7}$.

Sums of squares of deviations are:
$Cr^{3+} = 0.074$, $Cr^{2+} = 0.071$, $Cr_{Met.} = 0.013$.

Fig. 4.30 Time variation in concentration of $(Cr^{3+})$, $(Cr^{2+})$ and [Cr] for run AS12 using scheme 5 with equilibrium constant relations and fitting the first 60 minutes of reaction.

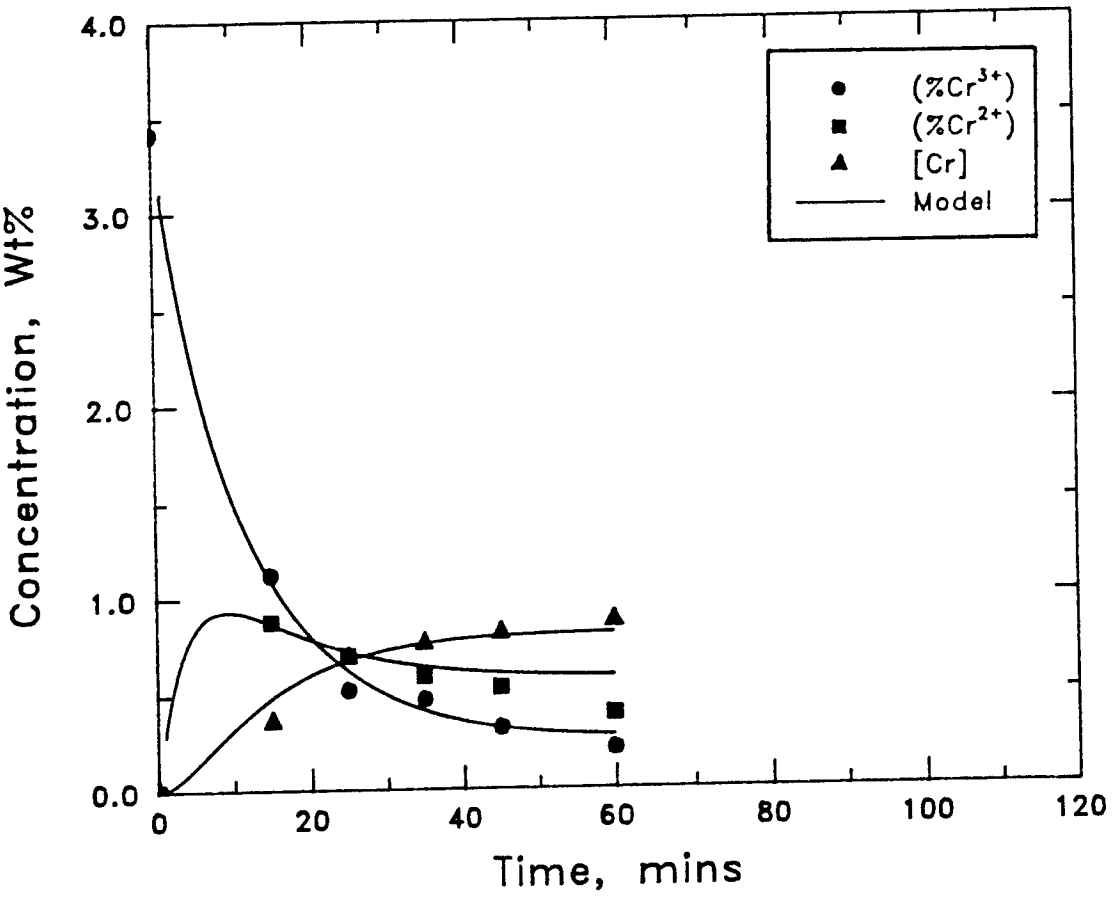


$k_1 = 0.0861\ cm.min^{-1}$. $k_2 = 0.0391\ cm.min^{-1}$.
$k_3 = 0.1379\ cm.min^{-1}$. $k_4 = 0.0309\ cm.min^{-1}$.
$k_5 = 2.03 \times 10^{-7}$. $k_6 = 3.11 \times 10^{-8}$.

Sums of squares of deviations are:
$Cr^{3+} = 0.019$, $Cr^{2+} = 0.045$, $Cr_{Met.} = 0.019$.

Fig. 4.31 Time variation in concentration of $(Cr^{3+})$, $(Cr^{2+})$ and [Cr] for run AS13 using scheme 5 with equilibrium constant relations and fitting the first 60 minutes of reaction.

runs AS11, AS12 and AS13, respectively. Contrary to expectations, the values of the rate constants, $k_5$ and $k_6$, are small in run AS11 and even smaller in runs AS12 and AS13 where higher levels of sulphur were added. Since the direct reduction of $(Cr^{3+})$ to [Cr] is expected to be favoured under these conditions, it should be shown by an increase in the values of $k_5$ in all cases, but this was not the case, as shown by the values obtained.

## 4.6 Summary

In the preceding paragraphs, a first-order, consecutive, reversible, two-stage reaction model for the reduction of $Cr_2O_3$ from slag by carbon or silicon dissolved in molten iron has been developed. It has been established that there is very little difference in the calculated curves obtained for the chromium species between the model where the height of the slag is assumed constant and the one where the actual slag height in each time interval is used. However, the model where the actual slag height in each time interval is taken into account in the calculation is considered to present a better picture of the events occurring during an experimental run and is applied in the kinetic analysis of the system. The model has been tested on data obtained using different $Cr_2O_3$ concentrations in slag and those from other

investigators[37,38], and this has shown to give further evidence that the reduction of $Cr_2O_3$ from slag follows a consecutive reaction model above.

A model for the reduction of $Cr_2O_3$ which includes an extra route where $(Cr^{3+})$ directly reduces to [Cr] and involving six rate constants has been developed. This has been shown to give better fits than the model having four rate constants i.e no direct reduction of $(Cr^{3+})$ to [Cr]. However, the rate constants obtained from the model with six rate constants do not make any metallurgical sense as to what is physically happening in the system. In view of this, a model which employs four rate constants is considered adequate to help in the interpretation of results from the reduction of $Cr_2O_3$ from slag by carbon or silicon dissolved in molten iron and is, therefore, applied in the next chapter.